Doctoral Thesis

Upscaling of mixing-limited chemical reactions from pore to continuum scale using the dispersive lamella concept

Author:
Lazaro J. Perez Fonseca

Advisor:
Dr. **Marco Dentz**

Advisor:
Dr. **Juan J. Hidalgo**

Tutor:
Prof. **Maarten Saaltink**

Institute of Enviromental Assessment and Water Research (IDAEA)

Spanish National Research Council (CSIC)

Department of Civil and Environmental Engineering, Program of Geotechnical Engineering, Universitat Politècnica de Catalunya (UPC)

April, 2019
Barcelona, Spain

This thesis was funded by the European Research Council (ERC) through the Project MHetScale (617511).

Abstract

Reactive transport modeling is an important tool for the analysis of coupled physical, chemical, and biological processes in Earth systems. Observed reactive transport in heterogeneous porous media shows a different behavior than the established transport laws for homogeneous media. Natural aquifers exhibit physical and chemical heterogeneities at all scales, which leads to reaction and transport dynamics that cannot be explained by traditional reactive models based on the advection-dispersion-reaction equation (ADRE). In particular, the behavior discrepancy is traced back to the nonuniform nature of flow velocity fields, complex spatial concentration distributions, and the degree of mixing between reactants. The role and contribution of these factors is key to provide accurate predictions of chemical reactions. The complexity of the task lies in the enormous range of spatial and temporal scales that reactants find in natural porous media. Hence, the complete characterization of the fate of chemical reactions requires that models accounts for the basic mechanisms that govern the mixing and reaction dynamics.

In this thesis, we present a novel methodology for the simulation of homogeneous chemical reactions. The proposed methodology is a random walk particle tracking approach (RWPT) coupled with reactions that simulates bimolecular chemical reactions, and is equivalent to the ADRE. Reactions among particles are determined by a reaction probability given in terms of the reaction rate coefficient, the total number of particles, and an interaction radius that describes a well-mixed support volume at which all particles have the same probability to react. The method is meshless and free of numerical dispersion. The developed RWPT approach is validated against analytical solutions for different flow scenarios under slow and fast reaction kinetics.

We focus on the impact of the mixing degree between chemical species and its role in the global reaction behavior. We first consider a reactive displacement in a Poiseuille flow through a pore channel, this system allow us to quantify the impact of the interaction of interface deformation and diffusion on mixing and reactive transport. We observe overestimation of the global reaction efficiency by the use of the Taylor dispersion coefficient at preasymptotic times, when the system is characterized by incomplete mixing. Next, we observe features of incomplete mixing in a synthetic porous medium. Results show that macroscopic predictions using the hydrodynamic dispersion coefficient overestimates the amount of reac-

tion. In addition, we analize the bimolecular reactive transport in a laboratory experiment, where we find that the amount of reaction is affected by the amount of mixing due to difusion, the amount of mixing due to spreading and the degree of heterogeneity of the flow field. The contributions of these factors induces that ADRE estimation of the total reaction product fails.

In order to characterize incomplete mixing and provide an explicit relation between fluid deformation and its impact on the temporal evolution of the chemical reactivity, we develop the dispersive lamella approach based on the concept of effective dispersion which accurately predicts the full evolution of the product mass. Specifically, the approach captures the impact of interface deformation and diffusive coalescence. Using this methodology, we quantify the impact of flow heterogeneities on the amount of fluid mixing in a pore channel, where we observe three temporal regimes based on the production rate of the product mass. In addition, the dispersive lamella predictions capture the kinetics of the reaction in a synthetic porous medium. Results reveal that reaction behavior is controlled by the interface front between the to reactants. In the pore-scale experimental visualization, the dipersive lamella results show that reaction is controlled by the deformed mixing interface at early times, and for fingering coalescence at late times.

Resumen

Los modelos de transporte reactivo son una herramienta importante para el análisis de procesos físicos, químicos y biológicos en los sistemas terrestres. Los procesos de transporte reactivo observados en medios porosos heterogéneos muestra un comportamiento diferente al de las leyes de transporte establecidas para medios homogéneos. Los acuíferos exhiben heterogeneidades físicas y químicas a todas las escalas, lo que conduce a dinámicas de transporte y reacción que no pueden explicarse mediante modelos de transporte reactivo tradicionales basados en la ecuación advección-dispersión-reacción (ADRE). En particular, la discrepancia de este comportamiento se remonta a la naturaleza no uniforme de los campos de velocidad de flujo, a complejas distribuciones de concentración espacial y al grado de mezcla entre los reactivos. El papel y la contribución de estos factores es clave para proporcionar predicciones precisas de las reacciones químicas. La complejidad de la tarea radica en la enorme gama de escalas espaciales y temporales que los reactivos encuentran en los medios porosos naturales. Por lo tanto, la caracterización completa del destino de las reacciones químicas requiere que los modelos determinen los mecanismos básicos que gobiernan la dinámica de mezcla y reacción.

En esta tesis, presentamos una metodología para la simulación de reacciones químicas de una sola fase. La metodología propuesta es un "random walk particle tracking" (RWPT) acoplado con reacciones que simula reacciones químicas bimoleculares, y es equivalente a la ADRE. Las reacciones entre partículas están determinadas por una probabilidad de reacción en términos del coeficiente de velocidad de reacción, el número total de partículas y el radio de interacción que describe un volumen de mezcla completa en el que todas las partículas tienen la misma probabilidad de reaccionar. El método no utiliza malla y es libre de dispersión numérica. El RWPT desarrollado se valida frente a soluciones analíticas para diferentes escenarios de flujo con cinéticas de reacción lenta y rápida.

Además estudiamos el impacto del grado de mezcla entre las diferentes especies químicas y su papel en el comportamiento global de la reacción. Primero consideramos un desplazamiento reactivo en un flujo de Poiseuille a través de un canal de poro, este sistema nos permite cuantificar el impacto de la interfaz de deformación y difusión en la mezcla y el transporte reactivo. Y observamos la sobreestimación de la eficiencia global de reacción mediante el uso del coeficiente de dispersión de Taylor en tiempos preasintóticos, cuando el sistema se caracter-

iza por una mezcla incompleta. A continuación, observamos el grado de mezcla de los reactivos en un medio poroso sintético. Los resultados muestran que las predicciones macroscópicas que utilizan el coeficiente de dispersión hidrodinámica sobreestiman la cantidad de reacción. Además, analizamos el transporte reactivo en un experimento de laboratorio, donde encontramos que la cantidad de reacción se ve afectada por la cantidad de mezcla debida a la difusión, la cantidad de mezcla debida a la extension de la interfaz y el grado de heterogeneidad del campo de flujo. La contribución de estos factores induce que la estimación de la masa total del producto de reacción por parte de la ADRE falle.

Con el fin de caracterizar la mezcla incompleta y proporcionar una relación explícita entre la deformación del fluido y su impacto en la evolución temporal de la reactividad química, desarrollamos el método de la lamela dispersiva basado en el concepto de dispersión efectiva que predice con precisión la evolución de la masa total del producto de la reacción. Específicamente, el método capta el impacto de la deformación de la interfaz y la coalescencia difusiva. Usando esta metodología, cuantificamos el impacto de las heterogeneidades de flujo en el grado de mezcla de reactivos en un canal de poro, donde observamos tres regímenes temporales basados en la tasa de producción de la masa del producto. Además, la predicción de las lamelas dispersivas capturan la cinética de la reacción en el medio poroso sintético estudiado. Los resultados revelan que la reacción está controlada por la interfaz de mezcla entre los reactivos. En la visualización experimental a escala de poro, los resultados de las lamelas dipersivas muestran que la reacción está controlada por la interfaz de mezcla deformada en los primeros tiempos, y para la fusión de los “fingers” en los últimos tiempos.

Resum

Els models de transport reactiu són una eina important per l'anàlisi de processos físics, químics i biològics en els sistemes terrestres. Els processos de transport reactiu observats en medis porosos heterogenis mostren un comportament diferent al de les lleis de transport establertes per homogenis. Els aqífers són heterogenis a totes les escales, tan físicament com químicament. Això produeix dinàmiques de transport i reaccion que no es poden explicar amb models de transport reactiu tradicionals basats en l'equació advecció-dispersió-reacció (ADRE). Concretament, a discrepància d'aquest comportament es remunta a la naturalesa no uniforme dels camps de velocitat de flux, a complexes distribucions de concentració espacial i al grau de barreja entre els reactius. El paper i la contribució d'aquests factors s clau per a proporcionar prediccions precises de les reaccions químiques. La complexitat de la tasca rau en l'enorme gamma d'escales espacials i temporals que els reactius troben en els mitjans porosos naturals. Per tant, la caracterització completa de la destinació de les reaccions químiques requereix que els models determinin els mecanismes bàsics que governen la dinàmica de mescla i reacció.

En aquesta tesi, presentem una metodologia per a la simulació de reaccions químiques d'una sola fase. La metodologia proposada s un"random walk particle tracking" (RWPT) acoblat amb reaccions que simulen reaccions químiques bimoleculars, i s equivalent a la ADRE. Les reaccions entre partícules estan determinades per una probabilitat de reacció en termes del coeficient de velocitat de reacció, el nombre total de partícules i el radi d'interacció que descriu un volum de mescla completa en el qual totes les partícules tenen la mateixa probabilitat de reaccionar. El mètode no utilitza malla i no mostra dispersió numèrica. El RWPT desenvolupat es valida comparant-lo amb solucions analítiques per a diferents escenaris de flux amb cinètiques de reacció lenta i ràpida.

A ms, hem estudiat l'impacte del grau de barreja entre les diferents espècies químiques i el seu paper en el comportament global de la reacció. Primer considerem un desplaament reactiu en un flux de Poiseuille a travs d'un canal de pors, aquest sistema ens permet quantificar l'impacte de la interfície de deformació i difusió en la barreja i el transport reactiu. I observem la sobreestimació de l'eficiència global de reacció mitjanant l's del coeficient de dispersió de Taylor en temps pre-asimptòtics, quan el sistema es caracteritza per una barreja incompleta. A continuació, observem el grau de barreja dels reactants en un medi porós

sintètic. Els resultats mostren que les prediccions macroscòpiques que utilitzen el coeficient de dispersió hidrodinàmica sobreestimen la quantitat de reacció. A ms, analitzem el transport reactiu en un experiment de laboratori, on trobem que la quantitat de reacció es veu afectada per la quantitat de mescla deguda a la difusió, la quantitat de barreja deguda a l'extensió de la interfície i el grau d'heterogenetat del camp de flux. La contribució d'aquests factors produeix que l'estimació de la massa total del producte de reacció per part de la ADRE falli.

Per tal de caracteritzar la barreja incompleta i proporcionar una relació explicita entre la deformació del fluid i el seu impacte en l'evolució temporal de la reactivitat química, desenvolupem el mètode de la lamella dispersiva basat en el concepte de dispersió efectiva que prediu amb precisió l'evolució de la massa total del producte de la reacció. Específicament, el mètode capta l'impacte de la deformació de la interfície i la coalescència difusiva. Usant aquesta metodologia, quantifiquem l'impacte de les heterogenetats de flux en el grau de barreja de reactants en un canal de pors, on observem tres règims temporals basats en la taxa de producció de la massa del producte. A ms, la predicció de les lamelles dispersives capturen la cinètica de la reacció en el medi porós sintètic estudiat. Els resultats revelen que la reacció està controlada per la interfície de barreja entre els reactants. A la visualització experimental a escala de pors, els resultats de les lamelles dispersives mostren que la reacció està controlada per la interfície de mescla deformada en els temps inicials, i per la fusió dels "fingers" en els temps finals.

Acknowledgements

I would like to express my deep gratitude to my advisors, Dr. Marco Dentz and Dr. Juan J. Hidalgo.

To Marco, for giving me the opportunity that this PhD has represented for me, for your excellent guidance that I received throughout these years, and for your sincere support and encouragement along the PhD.

To Juan, for guiding me, on one hand, and for letting me grow on my own, on the other hand, for your advices and availability in every moment to solve my doubts, and for all the motivation through all these years.

I am truly thankful for the wise guidance that I received from my advisors and for their suggestions to overcome all the challenges that I have encountered along the path.

I am also grateful to Dr. Alessandro Comolli and Dr. Vivien Hakoun, who reviewed this thesis, as well as my examiners Dr. Pietro de Anna, Dr. Joaquín Jímenez-Martínez, and Dr. Daniel Fernández García, and all the anonymous referees who reviewed my publications.

A special thanks to my MhetScale family: Alessandro, Alec, Filippo and Tomas. I have to sincerely thank you all for the awesome working atmosphere, for the discussions in the weekly meetings, and, most of all, for sharing the good and the bad days. I am deeply grateful to Alessandro who was the first to welcome me and be there everytime I needed a friend (although still waiting for your personal computer), to Alec for his help and contribution in the completion of my thesis, for being my friend and being there when I needed someone to consult or talk to, and for all the great and funny travel memories that we share (we did it homie!), to my colleague Filippo for the stimulating discussions and for all the maluma laughs with and without wine (still cannot believe that your daughter's name is Lazzara), to Tomas for his constant help to solve doubts and celebrated working code motivation (Tomas, my code works too!).

Tengo que dar las gracias a todos los compañeros del grupo de Hidrogeología, a los que han estado siempre, a los que ya se han ido y a los que he encontrado durante el camino. Gracias por los buenos momentos que hemos vivido dentro y fuera de la oficina. En particular, agradecer a los que han compartido despacho

conmigo, a Silvia por escucharme siempre y a Mar por los buenos momentos y las risas en el despacho.

Mi más sincero agradecimiento a Alejandra, “china” no hay palabras que expresen toda mi gratitud hacia ti. Tu apoyo y confianza incondicional en mi son parte de tesis. Gracias por sacarme una sonrisa en los momento ms difciles (“Never Fade”), y por poner cordura en los ms inverosmiles (“Precious Little Diamond”). Gracias y un millón de gracias.

Por último, quiero agradecer a mi familia. Esta tesis está dedicada a mis padres y mi hermano y Elvira, sus esfuerzos en mi educación y confianza en mi es un honor. Solo tengo sentimientos de agradecimiento por su amor y apoyo a lo largo de toda mi vida. Gracias papá por ser un ejemplo. Gracias mamá por darme la vida.

Table of Contents

List of Figures

List of Tables

CHAPTER 1

Introduction

1.1 Motivation

Geological media exhibit heterogeneities in their physical and chemical properties. The rigorous treatment of each physical and chemical variation in space and in time is a crucial challenge in several branches of science and engineering. This task is, however, anything but trivial. Heterogeneity in geological media exists from micro (pore) to kilometric (regional) scale. Heterogeneity modifies locally the dispersive motion of solutes, inducing concentration contrasts which affect the reaction progress of the migrating fluids. The resulting chemical reaction dynamics are very different from the ones observed under well-mixed equilibrium conditions (Kapoor et al., 1998; Raje and Kapoor, 2000; Gramling et al., 2002; Willingham et al., 2008; de Anna et al., 2014b) and the ones predicted by the classical transport laws established for homogeneous media (Steefel and Lasaga, 1994; Steefel et al., 2005; Li et al., 2006; Dentz et al., 2011b).

Variations of mixing front and reactive interface dynamics, which alters the reaction efficiency, are often encountered in a wide variety of natural and engineered systems. Examples include mineral dissolution of primary phases in water-rock interaction in carbonates (Wintsch et al., 1995; Renard et al., 1998) and magmatic systems (Koyaguchi and Woods, 1996), modification of the viscosity ratio at the reactive interface in CO_2 sequestration (Gérard and De Wit, 2009) and oil recovery (Hornof and Baig, 1995), and spatial fiber sorption variations in artificial cementitious composites (Zhou et al., 2012). In biology, variations in the mixing front topology affecting the the kinetics of the reaction have been observed in intracellular pathways (Carlotti et al., 1999; Pogson et al., 2006), in formation of lipids at the air/fluid interface in the lungs (Oosterlaken-Dijksterhuis et al., 1992; Serrano and Pérez-Gil, 2006), and many others (Petrungaro et al., 2018).

In groundwater hydrology, flow heterogeneities modify the topology of the reactive fronts which alters the degree of mixing and the reaction dynamics. The

impact of mixing interface deformation and the degree of mixing of reactants on chemical reactions has been observed in diverse studies. For instance, at the pore scale incomplete mixing of reactants have been identified as a major cause of failure of deterministic models (Kapoor et al., 1998; Willingham et al., 2008; de Anna et al., 2014a,b; Jiménez-Martínez et al., 2015). Interface deformation and concentration fluctuations have led to reduced reaction efficiency at Darcy scale (Raje and Kapoor, 2000; Gramling et al., 2002; Rolle et al., 2009), and discrepancies between estimated and observed reaction rates at the field scale (Roberts et al., 1986; Borden et al., 1997), The direct solution of reactive models is not feasible, since it would require a complete knowledge of the medium heterogeneity and vast computational resources. For this reason, several attempts have been made in the last decades to characterize mixing and chemical reactions in porous media. These include perturbation models (Luo et al., 2008), non-local adaptable models (Edery et al., 2009, 2010; Willmann et al., 2010; Bolster et al., 2012), and models with time-dependent rate coefficients (Sanchez-Vila et al., 2010).

The next section summarizes the state of the art of the modeling of fluid mixing and chemical reactions in heterogeneous porous media. A detailed state of the art specific for the topics of every chapter can be found in the respective introductory sections.

1.2 State of the art

Reactive transport evaluates the complex coupling of solute transport in heterogeneous media, across different scales, and the chemical transformations that occur on a local level. Reactive transport modeling can be described in the framework of the classical advection-dispersion-equation (ADE) coupled to a chemical reaction equation to form the advection-dispersion-reaction equation (ADRE).

In the literature, several approaches have been proposed to describe and predict fluid mixing and chemical reactions in porous media in the context of reactive transport. These approaches can be classified as Eulerian, which solve the ADRE directly, and Lagrangian. Eulerian models are in the form of a partial differential equation that accounts for the interconnection of the transport and the reaction. The key feature in the model characterization to an observational level is some form of averaging of the medium and transport properties, and the chemical concentrations (Battiato and Tartakovsky, 2011; Porta et al., 2012b). The Lagrangian approach treats the transport of a solute mass via a number of representative particles, i.e. it is based on the study of particles undergoing transitions that include the displacement due to advective heterogeneity of the medium and the diffusion/dispersion term. This approach avoids solving the transport equation directly and therefore is free of numerical dispersion and artificial oscillations. Lagrangian models include random walk particle tracking (RWPT) (Andrews and Bray, 2004; Ding et al., 2013; Zhang et al., 2013; Alhashmi et al., 2015, 2016; Sole-Mari and Fernàndez-Garcia, 2018) and continuous time random walks (CTRW) (Edery et al., 2009, 2010). In this thesis we use the RWPT approach to describe and predict mixing and chemical reactions. In Chapter 4 we

present a detailed description of the RWPT modeling approach. The RWPT approach enables development of efficient numerical tools to model a variety of reactive transport scenarios that accounts for mixing, reaction and transport (Benson and Meerschaert, 2008; Rahbaralam et al., 2015; Alhashmi et al., 2016). Chemical reaction is treated by considering that the particles pairs react according to some probabilistic rules when particles are within an interaction distance. The definition of the interaction distance is still subject to debate (see Chapter 4). For instance, fast kinetic reactions have been properly simulated by applying simplistic reaction rules based on proximity between reactant particles (Edery et al., 2009, 2010), conditional probabilities that accounts for reactant particles located at the same volume (co-located) (Benson and Meerschaert, 2008; Ding et al., 2013; Paster et al., 2014; Hansen et al., 2014), or kernel density estimators associated to two potentially reactive particles (Rahbaralam et al., 2015; Schmidt et al., 2017; Sole-Mari and Fernàndez-Garcia, 2018), among other reaction implementations (Berkowitz et al., 2016).

It is well known that medium heterogeneity, which manifests itself in different forms and different scales, alters the degree of mixing between reactants. Experimental work have addressed different aspects of how the mixing degree of reactants impact chemical reactions in porous media. The visualization techniques has been often evaluated experimentally through the Beer-Lambert law and colorimetry techniques applied to the light that traveled through glass beads representing porous media (Gramling et al., 2002; Jiménez-Martínez et al., 2015). Experimental work generally quantifies mixing studying irreversible homogeneous bimolecular chemical reactions using different set-ups to account for medium heterogeneity. This type of reaction, among the simplest reactions, allows to study in detail the impact of the fundamental mechanisms of flow and mixing degree. Data from column experiments from bimolecular chemical reactions have shown the inadequacy of the ADRE model (Gramling et al., 2002; Oates and Harvey, 2006; Edery et al., 2015) which overpredicts significantly the production rate of product mass. Other experimental studies have observed segregation phenomena of reactants in homogeneous media and verified that the efficiency of the reaction is reduced compared to the one predicted for a Darcy scale porous media (Raje and Kapoor, 2000; Monson and Kopelman, 2004). However an increased reaction behavior, caused by enhanced mixing, has been reported in heterogeneous flows where experimental results exhibit product mass evolutions faster than classical ADRE predictions (Rolle et al., 2009; de Anna et al., 2014b; Jiménez-Martínez et al., 2015). In these systems, the medium properties play a major role in determining the reactants mixing degree, and thus chemical reactions (Willingham et al., 2008). These studies highlight that mixing phenomena cannot be represented in terms of large scale transport theories that describes averaged solute concentration fields.

Prediction of mixing and spreading of solutes are often addresed in reactive transport models. Despite the limitations of ADRE models to predict chemical reactions shown by laboratory experiments, a significant body of previous studies applied modifications to the ADRE to describe and predict fluid-fluid reactive

transport. Examples include continuum scale models using fitting parameters and time-dependent reaction rates to estimate the amount of pore-scale mixing (Sanchez-Vila et al., 2010), numerical and parameter corrections that accounts for the effects of natural heterogeneity on transport (Najafi and Hajinezhad, 2008), and distribution of mixing ratios within support volumes employing calibrated parameters based on the peak concentration of the product Chiogna and Bellin (2013).

While the validity of ADRE models has been discussed in several publications (Battiato et al., 2009; Battiato and Tartakovsky, 2011). Other studies have implemented particle-based methods to characterize chemical reactions to overcome the averaged estimations of the ADRE (Salamon et al., 2006; Alhashmi et al., 2015; Paster et al., 2015). For instance, the RWPT approach coupled to reaction have been used to quantify reactive transport for bimolecular chemical reactions in porous media. Experimental work has been used to validate reactive RWPT models (Ding et al., 2013; Zhang et al., 2013; Alhashmi et al., 2015). Numerical RWPT simulations have demonstrated that reactants are not perfectly mixed and diffusion is a limiting process (Benson and Meerschaert, 2008; Paster et al., 2014; Rahbaralam et al., 2015), higher advective heterogenety favors mixing in higher-velocity mobile regions (Alhashmi et al., 2016; Sole-Mari and Fernàndez-Garcia, 2018).

The impact of incomplete mixing processes on the kinetics of the reaction is still an open issue. Recently, a new approach for the effective characterization of mixing has been introduced for 2-dimensional problems. This method is based on the concept of lamellae, or diffusive strips (Ranz, 1979; Villermaux, 2012). Lamellae are enlogated structures that are naturally formed by the action of advection. The spatial fluctuations in the flow velocity causes deformation of the reactive fronts that may be viewed as a collection of stretched diffusive strips. Under the lamellae assumptions, mixing can be estimated by predicting the evolution of the interface between reacting species process, which depends on two temporal regimes. At early times, the length of the mixing interface grows linearly in time at some rate and the evolution of the interface thickness can be predicted (Duplat et al., 2010; de Anna et al., 2014a; Borgne et al., 2014). In the long time regime, after compression and diffusive growth equilibrate, the different strips of the interface can no longer be independent and they interact via diffusion, and coalescence becomes the key process (Duplat and Villermaux, 2008). The lamellar representation of mixing is a powerful approach to quantify impact of flow heterogeneities on reactants mixing.

1.3 Open questions

Despite the remarkable progress in the understanding of fluid mixing and chemical reactions, some important questions are still open. These refer to

1. the role of flow heterogeneity and its impact on mixing-induced chemical reactions;

2. the influence of the mixing degree between reactants, and its quantification in terms of effective rate laws;

3. the characterization of the aspects of mixing limitations on fast chemical reactions;

4. the upscaling and implementation of complex heterogeneities and chemical processes in the RWPT methodology.

This thesis, as part of the ERC project MHetScale, aims to address these open issues and to describe reactive mixing at pore scale.

1.4 Objectives

The main objective of the thesis is to quantify the mixing process at pore scale and relate it to the medium heterogeneity by means of the study of bimolecular chemical reactions in porous media.

On the basis of the mentioned open questions, we set the following specific objectives for this thesis

1. to derive a Lagrangian particle based-method that provides a better understanding of chemical reactions;

2. to quantify the impact of the degree of mixing between reactants underlying in reactive transport in terms of observables such as local and global reaction rates, product formation, and enhanced mixing rates;

3. to use the knowledge obtained from the previous points to characterize mixing behaviors, i.e. mixing temporal scales;

4. to account for different heterogeneity degrees and to quantify their impact on upscaled reactive transport within the proposed stochastic framework.

5. define an effective model that represents the presence of complex flow heterogeneities and quantify chemical reactions;

1.5 Thesis outline

To address these objectives, in the following chapters we consider different heterogeneity scenarios. Most of the chapters are based on papers that are published in peer-reviewed journals. These chapters can be read independently and may therefore present differences in notation as well as repeated concepts. Nevertheless, the chapters are interconnected by the common main objective of quantifying the impact of degree of mixing between reactants in chemical reaction. Therefore, the thesis is structured as follows.

- In Chapter 2, we present the methodology used to simulate reactive transport throughout this thesis. The Chapter details the main four components of the numerical simulations: geometry, flow, transport, and chemical reaction.

- In Chapter 3, we discuss the notion of incomplete mixing of reactants in the context of species segregation and avalaible laboratory data that recognize the role of small-scale fluctuations that affect the kinetics of irreversible chemical reactions. In particular, we study the impact of fluctuations in the concentration that leads to segregation of the reactants and affects the global reaction behavior in a diffusion-controlled reaction.

- In Chapter 4, we validate the proposed reactive RWPT approach to describe bimolecular reactive transport against analytical solutions for different scenarios characterized by slow and fast chemical kinetics under diffusion and heterogeneous advection. In addition, we discuss the concept of the interaction distance between particles, or reaction radius, that acts as a well-mixed reactor. We show the equivalence between the ADRE and our reactive RWPT method.

- In Chapter 5, we study the impact of the interaction of interface deformation and diffusion on mixing and reactive transport. We consider a fast irreversible bimolecular reaction in a Poiseuille flow through a pore channel. We propose the dispersive lamella approach based on the concept of effective dispersion, which accurately predicts the evolution of the product total mass. We demonstrate the substantial difference in predicting the total mass between the use of the effective dispersion coefficient, which captures the features of mixing in heterogeneous flows, and the traditional approaches such as the use of an apparent dispersion coefficient or the lamellae theory.

- In Chapter 6, we investigate the impact of pore structure heterogeneity, interface deformation and incomplete mixing between reactants on a bimolecular irreversible chemical reaction at pore scale. The porous medium used for the reactive transport simulation consists in a 2-dimensional porous medium characterized by a random close packing of equally sized grains. We estimate the full evolution of the global reactivity of the system using the dispersive lamella model to account for the local geometry, interface topology, and flow field at the pore scale. In addition, the developed methodology is applied to the pore-scale experiments reported by Jiménez-Martínez et al. (2015).

- In Chapter 7 presents the general conclusions to the thesis and provides some ideas for future work.

CHAPTER 2

Methodology

We perform numerical simulations to analyze the dynamics that control bimolecular reactive transport in porous media. Our reactive transport methodology consists of four components: geometry, flow, transport, and chemical reaction. This Chapter describes each component in detail.

2.1 Pore scale geometry

We simulate the motion of the reactive species in a 2-dimensional synthetic heterogeneous porous medium. The synthetic porous medium consists of a random packing of equally sized circular grains. Note that the representation of granular obstacles in porous media using circular grains provide several advantages compared to real rock samples. It is possible, for example, to test simple geometries that make it easier to generalize results to multiple porous media while the use of experimentally acquired real images provide representations with a high degree of arbitrariness.

We generate the grains by selecting their position from a uniform distribution. We avoid superposition or overlapping of grains by rejecting the position of a given grain if overlaps a previous placed grain. The algorithm stops when the target porosity is achieved or the maximum number of attempts to place a new grain is exceeded.

We discretize the generated porous medium and we convert it to a binary image, which is composed of regular pixels that represent either void or solid. The discretization level is selected such that radius of grain is divided in at least 15 pixels. The mesh is created from a regular hexahedra mesh compatible with OpenFOAM equivalent to the pixels of the image. We refine the mesh by dividing each hexaedra by 2 in all directions. We use this meshing technique to avoid any averaging or smoothing that often occurs in the course of the standard OpenFOAM meshing procedure (Gjetvaj et al., 2015).

2.2 Flow simulations

To obtain the flow field in the pore space, we solve the incompressible Newtonian flow governed by the Stokes equations

$$\nabla \cdot \mathbf{v} = 0, \tag{2.1}$$

$$-\nabla P + \mu \nabla \mathbf{v} = \rho \left(\frac{\partial \mathbf{v}}{\partial t} + \mathbf{v} \cdot \nabla \mathbf{v} \right), \tag{2.2}$$

where $\mathbf{v}$ is the velocity vector (m s^{-1}), P(kg m s^{-2}) is the pressure, we use water density $\rho = 1000$kg m^{-3}, and μ the dynamic viscosity ($\mu = 10^{-3}$ kg m^{-1} s^{-1}). The single-phase flow field in the pore voids is solved using the steady-state solver for incompressible flow simpleFOAM that belongs to the open-source code OpenFOAM (Weller et al., 1998). We apply a constant pressure boundary condition at the inlet and outlet faces of the image. On the other solid faces, including the void-rock interface, we apply no-slip boundary conditions. The Reynolds number used in all simulations, defined as

$$Re = \frac{\rho \bar{v} L}{\mu} \tag{2.3}$$

where $\bar{v}$ is the mean flow velocity and L is a characteristic length, is less than 1.

2.3 Transport simulations

We simulate the solute transport by following the trajectory of the particles for each time-step Δt by advection and diffusion,

$$\mathbf{x}(t + \Delta t) = \mathbf{x}(t) + \mathbf{v}[\mathbf{x}(t)]\Delta t + \sqrt{2D\Delta t}\boldsymbol{\eta}(t), \tag{2.4}$$

where the $\mathbf{v}(\mathbf{x})$ is the velocity flow field, the $\boldsymbol{\eta}(t)$ are independent distributed Gaussian random variables characterized by $\mathbf{0}$ mean and unit variance, and D ($m^2 s^{-1}$) is the molecular diffusion coefficient.

We use a streamline-based method for the advective step of the particle tracking through the pore voids similar to the methodology presented in Puyguiraud et al. (2019) to track the motion of the particles in three-dimensional porous medium. The streamline-based method incorporates a quadratic velocity interporlation in the voids in contact with the solids to honor the no-slip boundary conditions at the void-solid interface (Mostaghimi et al., 2012). The quadratic interpolation constrasts to the linear interpolation that has been used for particle tracking in Darcy-scale heterogeneous flow fields (Pollock, 1988). The movement of particles by diffusion ($\sqrt{2D\Delta t}\boldsymbol{\eta}(t)$) is based on a random walk, which is a series of random spatial displacements in both directions that are based on the mean diffusive displacement that define the transition of the particles. The diffusive step is usually smaller than the image resolution pixel of the discretized medium. In the case that the diffusive jump is greater than a pixel, we divide the jump in

steps in order to check if intermediate or destination cell is not rock. If that is the case we apply reflection conditions. Otherwise particles might cross a pixel that represents a solid, which is physically incorrect. Particle trajectories are simulated until they leave the porous medium.

2.4 Reaction

We simulate the irreversible reaction

$$A + B \rightarrow C. \tag{2.5}$$

The reaction is a second-order instantaneous chemical reaction.

2.4.1 Reaction methodology

The process to include reactions between particles in a simple algorithm is straightforward and implemented in a MATLAB code using a operator splitting technique.

For every time step Δt, the particles move in the porous medium based on (2.4). After the transport step, we record the position of particles in the domain. Now, we determine the number of particles within a support volume ΔV centered in a B particle. We assume that ΔV is well-mixed, under this assumption the reaction probability is given by

$$P_r = 1 - [1 - p(\Delta t)]^{N_A} \tag{2.6}$$

where N_A is the number of A particles within the well-mixed support volume around the particle B and $p(\Delta t)$ is the probability of a single reaction

$$p(\Delta t) = \frac{k\Delta t}{N_0 \Delta V}, \tag{2.7}$$

where N_0 is the initial number of particles, ΔV $\left[L^d\right]$ is the well-mixed support volume, and k $\left[L^d M^{-1} T^{-1}\right]$ is the reaction rate constant. The details of the derivation of the probability of reaction P_r and the discussion of the meaning and choice of ΔV can be found in Chapter 4. In order to calculate the number of particles within ΔV we use a KD-tree technique (Bentley, 1975) implemented in MATLAB. The KD-tree (short for K-dimensional) is a binary tree for efficient storage of neighbor information to be retrieved by distance searches. All A neighbors of B are sorted in ascending order of distance.

After determination of N_A and P_r, we compare P_r to a random number U uniformly distributed between 0 and 1. If the probability of the reaction P_r is larger than U, we choose the first neighbor, the closest A particle to the B particle, and remove both particles from the simulation. Note that the choice of the first neighbor or any other neighbor does not impact on the results as the B particle have the same probability of reaction P_r with all neighbors present.

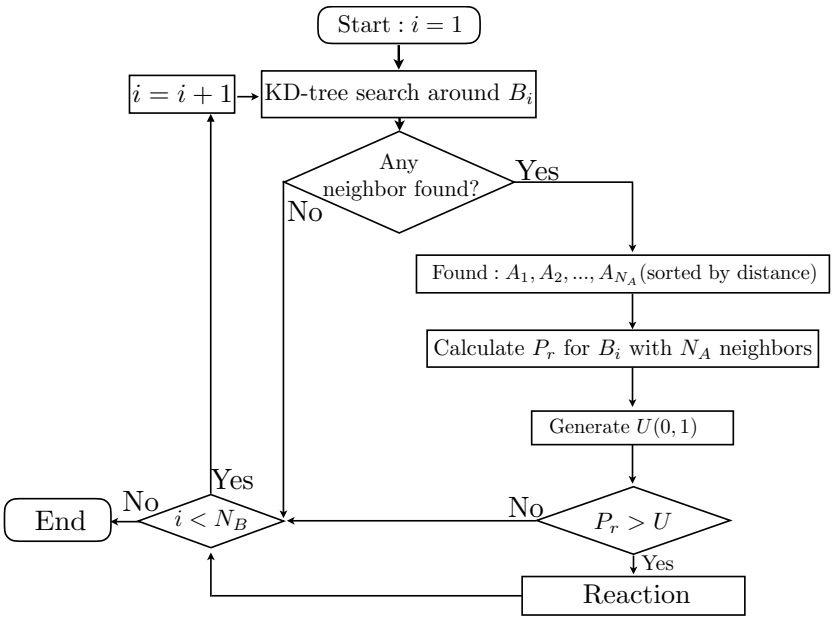

Figure 2.1: Flow chart for implementation of particle reaction in the algorithm.

After removal, a new particle C is generated and placed in the middle position of the initial A and B particle locations. Again, results are not affected by the placement of C wether it is at a intermediate distance, or placed randomly between the reactant particles. The process, illustrated visually in Figure 2.1, is repeated for every transport/reaction time step.

2.4.2 Reaction in experimental visualizations

To simulate the instantaneous chemical reaction (2.5) in laboratory experiments, we use the methodology presented in Gramling et al. (2002). The methodology is a generalized approach to quantify fluid mixing in fast reactions from the conservative concentration fields.

The proposed methodology considers that the spatial distribution of the non-reactive chemical species c_A in time within a homogeneous porous medium can be described by the one-dimensional equation for mass transport

$$\frac{\partial c(x,t)}{\partial t} = D_x \frac{\partial^2 c}{\partial x^2} - v \frac{\partial c}{\partial x} \tag{2.8}$$

where $c(x,t)$ is the concentration of the chemical species at position x and time t, D_x is the longitudinal hydrodynamic dispersion coefficient, and v the flow velocity. This nonreactive transport equation can be modified to add reactions by adding a term that describes the rate of chemical reaction. For the bimolecular

chemical reaction (2.5) considered, the C product production at any x is equal to the rate of loss of each reactant

$$r_C = -r_A = -r_B. \tag{2.9}$$

Thus, the reactive transport equation for C is

$$\frac{\partial c_C(x,t)}{\partial t} = D_x \frac{\partial^2 c_C}{\partial x^2} - v\frac{\partial c_C}{\partial x} + r_C, \tag{2.10}$$

while the reactive transport equation for A is

$$\frac{\partial c_A(x,t)}{\partial t} = D_x \frac{\partial^2 c_A}{\partial x^2} - v\frac{\partial c_A}{\partial x} - r_A. \tag{2.11}$$

Adding the two reactive equations gives c_{A+C} which represents the combined concentrations of reactant A and product C,

$$\frac{\partial c_{A+C}(x,t)}{\partial t} = D_x \frac{\partial^2 c_{A+C}}{\partial x^2} - v\frac{\partial c_{A+C}}{\partial x}, \tag{2.12}$$

note that c_{A+C} is the total molar concentration of reactant A (Gramling et al., 2002). We now find the expression for the combined concentration of reactant B and product C (c_{B+C}), which is displaced by the inflowing reactant A,

$$c_{B+C} = 1 - c_{A+C}. \tag{2.13}$$

This result assumes that the dispersion coefficient of reactant B is the same for reactant A and product C, and follows directly from the linearity of the advective-dispersive equation (2.8). The schematics of reaction between the two chemical species within a 1D column are shown in figure 2.2. For the instantaneous bi-

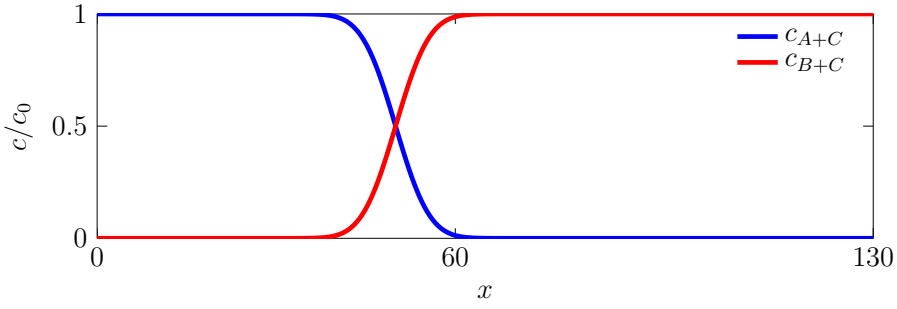

Figure 2.2: Schematics of reaction between the two reactants A and B within a column. The area under the blue curve represents the total A in the medium. This is analogous to B represented by the red curve. We integrate the central area over time to predict all product C in the medium.

molecular reaction (2.5) considered here, the amount of product C is determined

by the concentration of the limiting reactants A and B. Thus, the concentration c_C can be calculated directly from the two known concentrations, c_{A+C} and c_{B+C} as,

$$c_C = \min\left(c_{A+C}, c_{B+C}\right) \tag{2.14}$$

This solution predicts that c_C will be at the mixing interface of reactants A and B, and its concentration peak remains equal to 0.5 as the reactants and product move through the medium. This can be understood by considering that since the reaction is instantaneous both reactants are completely consumed at the advective front. The concentration of the product C is equal to half of the initial concentration of the reactants (Gramling et al., 2002). The reaction will stop once the reactants are completely consumed.

CHAPTER 3

Incomplete mixing and chemical reactions

3.1 Basic considerations

In hydrological systems, mixing of reactants can trigger changes in solution chemistry and a wide variety of chemical transformations that may result in changes in the physical properties of the medium. For instance, mineral precipitation and/or dissolution, alter the medium structure and affect the flow field. Thus, changing the reaction pattern or mixing interface, and producing a feedback on the solute transport.

Here, we summarize the main features of reactive transport that accounts for the impact of solute mixing on fast chemical reactions. The orientation of the discussion is on incomplete mixing of reactants in the context of species segregation and available laboratory that recognize the role of small-scale fluctuations that control fast irreversible chemical reactions.

Reactive transport observations that could treat any combination of transport and geochemical processes are characterized by features that correspond to Fickian models defined by averaged medium and transport properties. Even in simple settings, factors such as pore size distributions, pore geometry, tortuosity, and connectivity play a role on the degree of mixing between reactants and chemical reactions. Translating these observations across scales is where the challenging problem arises.

3.2 Reactants segregation inducing incomplete mixing in diffusion-limited reactions

The study of fluid-fluid mixing processes requires quantitative methods that express goodness of mixing. But the goodness, or degree, of mixing can be affected by fluctuations, which impacts in the way solutes spread, mix and react. Spatial fluctuations in concentrantion fields induces changes in the global behavior of reactive mixtures. The relative influence of the fluctuations in chemical reactions becomes increasingly important in time. At early times, fluctuations about the mean concentration are small and the sytem is barely affected. But reactions consume mass, and as the reactant mean concentrations become smaller, the fluctuations becomes greater which causes isolation of reactants. The concept of isolated, or segregated, reactants was first described by Danckwerts (1952) for a second-order chemical reaction, which describes the importance of some of the factors which affect the efficiency of mixing processes.

Reactants segregation phenomenon, in conjunction with diffusion and reaction, can have repercussions on the global reaction kinetics. This is relevant to reactive tranport models that aim to predict reaction kinetics in heterogeneous porous media. We illustrate the impact of incomplete mixing on chemical reactions studying the example of Ovchinnikov-Zeldovich segregation (Ovchinnikov and Zeldovich, 1978) for purely diffusive problems.

We study the Ovchinnikov-Zeldovich segregation in the course of the diffusion controlled irreversible bimolecular reaction

$$A + B \to 0 \tag{3.1}$$

subject to a heterogeneous initial distribution of the A and B reactants. The two species present, A and B, react kinetically and irreversibly with unitary rate of reaction. The product of the reaction plays no role in the system. It does not produce any change in porosity or permeability.

Traditionally, bimolecular reactive models consider well-mixed chemical systems when the reactants concentrations are spatially homogeneous, in this case the diffusion plays redistributes the reactants without changing the concentrations at a given position. In these conditions, the well-mixed reactive problem is described by

$$\frac{dc_i(t)}{dt} = -kc_A(t)c_B(t)\,; \quad i = A, B; \tag{3.2}$$

where A, B are the reactants. For equal initial concentrations $c_A(t = 0) = c_B(t = 0) = c_0$, an analytical solution (Kang and Redner, 1985) exists for $c_A(t)$ and $c_B(t)$

$$c_i(t) = \frac{c_0}{1 + c_0 kt}\,; \quad i = A, B; \tag{3.3}$$

which implies that the reactant species concentrations decay as $c_{A,B}(t) \sim t^{-1}$ for times greater than the characteristic reaction time scale $\tau_r = 1/(kc_0)$. This decay is characteristic of rate-limited reactions in the well-mixed regime. The kinetic

rate law (3.2) relies explicitly on the assumption of a well-mixed deterministic initial condition.

For purely diffusive mass transfer, i.e. $\mathbf{v}(\mathbf{x}) = 0$, the diffusion-reaction equations for the species A, B and C are given by

$$\frac{\partial c_i(\mathbf{x},t)}{\partial t} = D\nabla^2 c_i(\mathbf{x},t) - kc_A(\mathbf{x},t)c_B(\mathbf{x},t), \tag{3.4}$$

where $i = A, B$ and k is the reaction rate coefficient. Under heterogeneous initial distribution of the chemical species, the $\sim t^{-1}$ behavior changes dramatically (Ovchinnikov and Zeldovich, 1978; Kang and Redner, 1985; Benson and Meerschaert, 2008; de Anna et al., 2011; Rahbaralam et al., 2015). The irreversible reaction leads to the formation of A and B islands, or in other words to the segregation of the chemical species. The kinetics of the reaction are diffusion-controlled now, because reactions between A and B can only occur at the boundaries of the islands.

A random walk particle tracking (RWPT) model combined with a probabilistic rule for the reaction was implemented to illustrate reactants segregation in a diffusion-limited 1-D system. The initial particle locations of the chemical species A and B, denoted by x_A and x_B are spreaded uniformly within a domain of size $L = 16$ cm. The initial particle location, such that $0 \leq x_i < \Omega$ where $i = A, B$, is chosen from a uniform distribution. In the numerical model, transport and reaction dictated by pure diffusion. The equation that governs the diffusive motion of particles belonging to the A and B species is the Langevin equation (Risken, 1996)

$$x_i(t + \Delta t) = x_i(t) + \sqrt{2D\Delta t}\xi(t), \quad i = A, B; \tag{3.5}$$

where $x(t)$ is the location of a particle at time t, D is the diffusion coefficient and $\xi(t)$ is Gaussian white noise characterized by zero mean and unit variance.

Reaction is modeled during each time step. For a given B particle, we search for A particles that are located within a well-mixed volume $\Delta V = 2r$, for which the interaction radius $r = \sqrt{24D\Delta t}$. For each of the B particles the reaction probability (P_r) depends on the number of $N_A[x(t)]$ of A particles within ΔV centered at the position $x(t)$ of the B particle.

$$P_r = 1 - \exp\left[-p(\Delta t)N_A[x(t)]\right] \tag{3.6}$$

where $p(\Delta t) = k\Delta t(N_0\Delta V)$ is the chemical probability for a single reaction event, and N_0 is the total number of particles. Once the reaction probability P_r for the A and B particle is known, a random number U, uniformly distributed on $[0, 1]$, is generated. The reaction occurs if $P_r > U$. We remove the A and B particles from the system if they react.

For the diffusion-limited example illustrated here, we set the reaction rate to $k = 20$ cm/s, the diffusion coefficient is $D = 10^{-4}$ cm^2/s, with a time step $\Delta t = 10^{-2}$ s. Figure 3.1 shows the spatial concentration segregation of both reactants at $t = 200$ s. At late times, we find reactants isolated pockets, or so-called segregated concentration islands, characterized by $c_A c_B = 0$, the A and B

species do not coexist at the same position. The reaction is limited by how quickly reactants can diffuse across the interfaces of these islands. The global kinetics of the reaction are shown in Figure 3.2, where we plot the mass evolution of reactant A. At early times results are similar to the well-mixed analytical solution (3.3). This happens because at those early times the fluctuations of concentrations are small and the reaction is rate-controlled. For increasing times, the system deviates from the well-mixed solution, as the fluctuations become greater. At these late times, the domain will self-organize into islands of segregated A and B species seen in Figure 3.1. The reactants segregation affects mixing, which

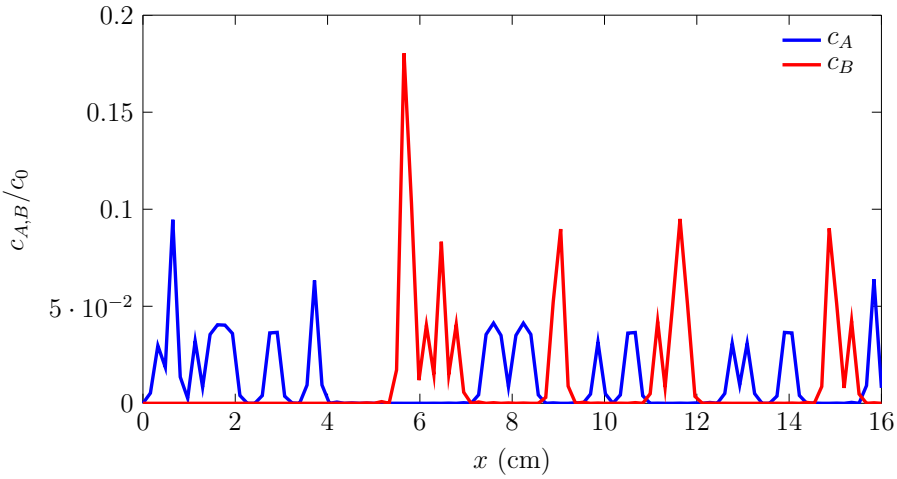

Figure 3.1: Spatial concentration of A (blue line) and B (red line) at $t = 200$s. Emergence of reactants segregation is observed as both reactants cannot coexist at the same position.

in the case of (3.3) solution scales as t^{-1} for late times changes to a scaling of $t^{-d/4}$, where d is the number of dimensions (Ovchinnikov and Zeldovich, 1978; Kang and Redner, 1985). Note that the time at which the reaction change from well-mixed to incomplete mixing regime ($t^{-1/4}$ scaling) depends on the number of initial particles. This occurs because lower numbers of initial particles N_0 enhances particle segregation and therefore earlier deviation from the well-mixed solution.

3.3 Reactants segregation induced by porous medium structure: Experimental reactive fronts

Within the context of incomplete mixing, there are two particularly well-known experimental investigations that account for the segregation effects of reactants concentration and highlight some of the key challenges of upscaling pore-scale

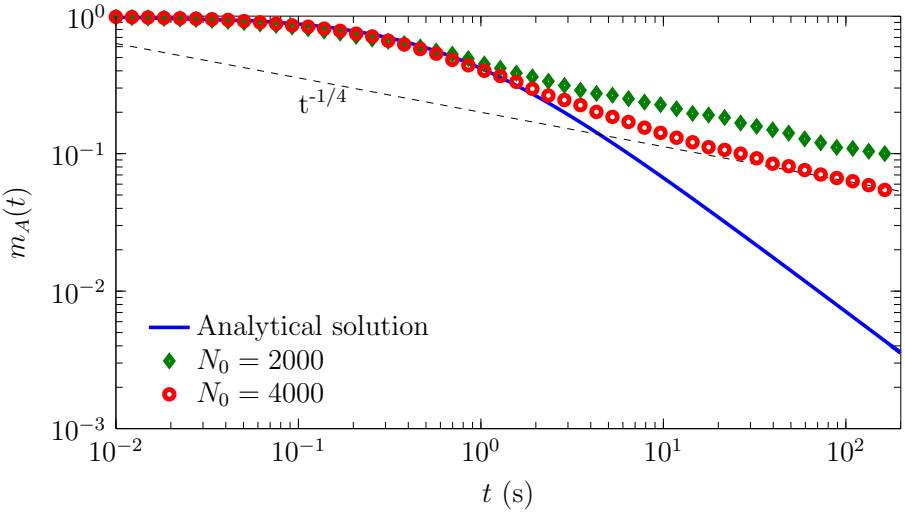

Figure 3.2: Evolution of the reactant A from the RWPT model using $N_0 = 2000$ (green diamonds) and $N_0 = 4000$ (blue circles) compared against analytical solution of the well-mixed system (solid line). The time where reactants segregation causes $m_A(t)$ deviate from the well-mixed solution depends on the initial number of particles N_0 in the system.

reactions to field scales (Gramling et al., 2002; Raje and Kapoor, 2000). Prior to these laboratory experiments, classical reactive transport considerations were based on reaction parameters estimated from traditional batch experiments and transport parameters measured from a porous medium. The assumption was that one could use these parameters together in an ADRE model to predict reactive transport.

Raje and Kapoor (2000) constructed a column filled with glass beads and observed in a solution the displacement of 1,2-naphthoquinone-4-sulfonic acid by aniline, which is a known bimolecular reaction that produces 1,2-naphthoquinone-4-aminobenzene. The authors chose this reaction because is a simple reaction and the effect of segregation of reactants can be important. The authors measured transport parameters from a non-reactive column experiment, and determined the reaction rate under completely well mixed conditions in batch tests. In all experimental runs, the measured parameters predicted almost perfectly the non-reactive transport of reactants (Figure 3.3). Finally, they parameterized an ADRE model with the measured parameters and predicted breakthrough curves of the reaction product that would be produced in the reactive displacement.

They found that the predicted peak product concentration in some cases was almost 40% more than the experimental peak concentration (Figure 3.4). A major conclusion of their work is that the reactive transport model overpredicts the amount of chemical reaction that takes place because the model neglects

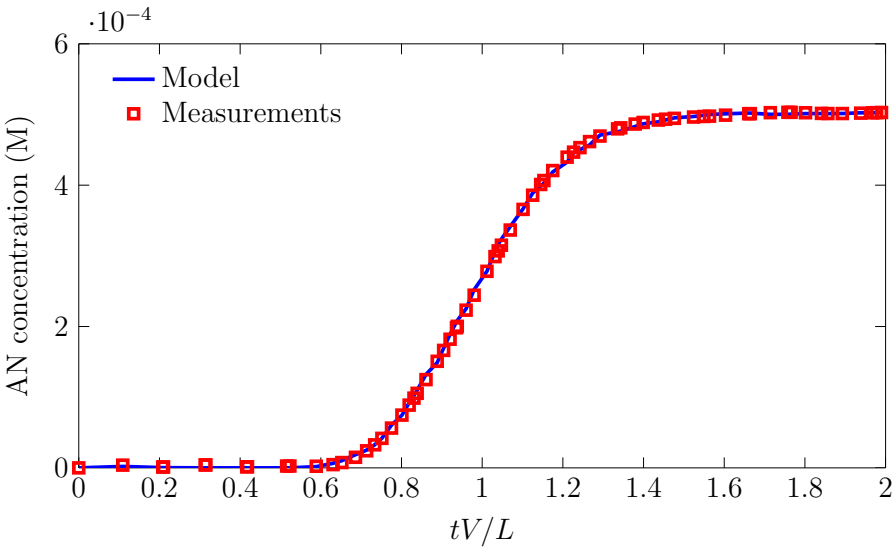

Figure 3.3: Comparison between observed and modeled nonreactive breakthrough curves. Modified from Raje and Kapoor (2000)

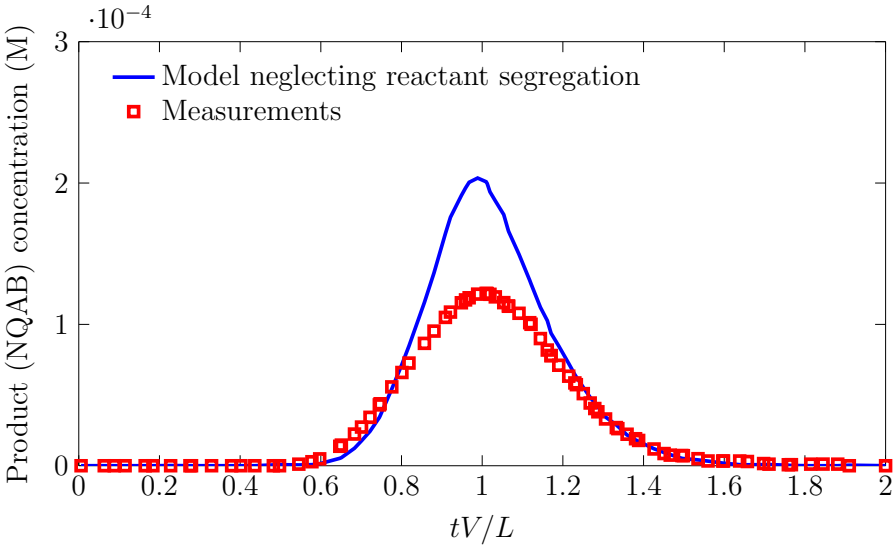

Figure 3.4: Comparisons between experimental results on reactive transport and the reactive transport model. Modified from Raje and Kapoor (2000)

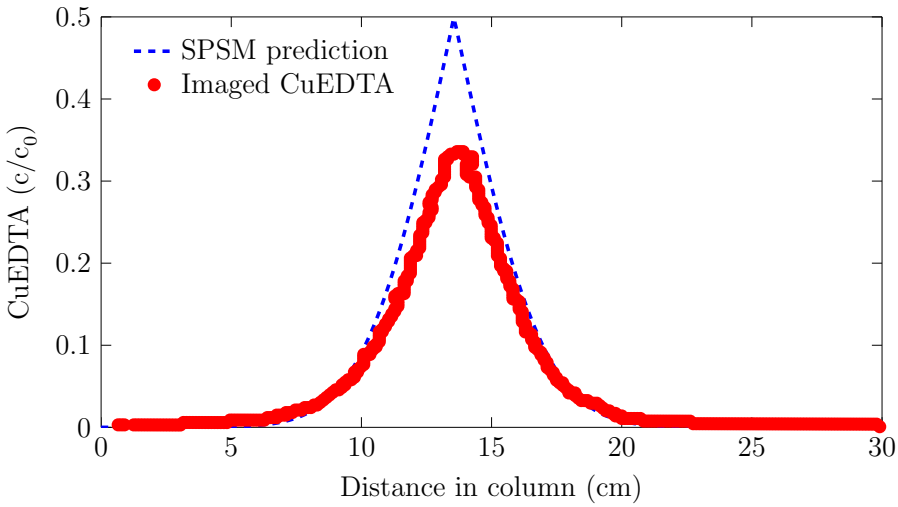

Figure 3.5: Comparison from estimated hydrodynamic dispersion coefficient in the experiment against predicted dispersion of $CuEDTA^{2-}$ in Gramling et al. (2002)

segregation phenomena among reactants.

In a similar setup, Gramling et al. (2002) studied the instantaneous irreversible reaction between $CuSO_4$ and $EDTA^{4-}$, a fluid-fluid colorimetric bimolecular reaction that gives $CuEDTA^{2-}$ as a product. The light intensity of the reaction product was used to construct spatial distributions of concentrations. The authors repeated the experiment three times using different inlet flow rates and measured dispersion coefficients with high confidence using conservative tracer experiments (Figure 3.5). The reaction rate constants were measured from well-mixed batch experiments. In addition, they developed a reactive transport model based on analytical solutions of the ADRE. The model assumption was that the concentration of the reactants was instantaneously consumed in the reaction. Again, mismatches between model predictions and experimental measurements were observed. Their ADRE model significantly overpredicted the spatial distribution and time evolution of $CuEDTA^{2-}$ in the system (Figure 3.6). This discrepancy is traced back to pore-scale velocity fluctuations and incomplete mixing of reactants.

Recently, the mechanisms that lead to incomplete mixing were investigated in further detail by de Anna et al. (2014a). These authors used also a colorimetric bimolecular reaction, but different to the one used by Gramling et al. (2002), to visualize the reaction front and quantify the amount of product produced. Their setup allowed them to visualize transport, mixing and reaction mechanisms in the system by measuring local concentrations with a sensitivity of 3 orders of magnitude. They studied a wide range of Péclet and Damköhler numbers varying

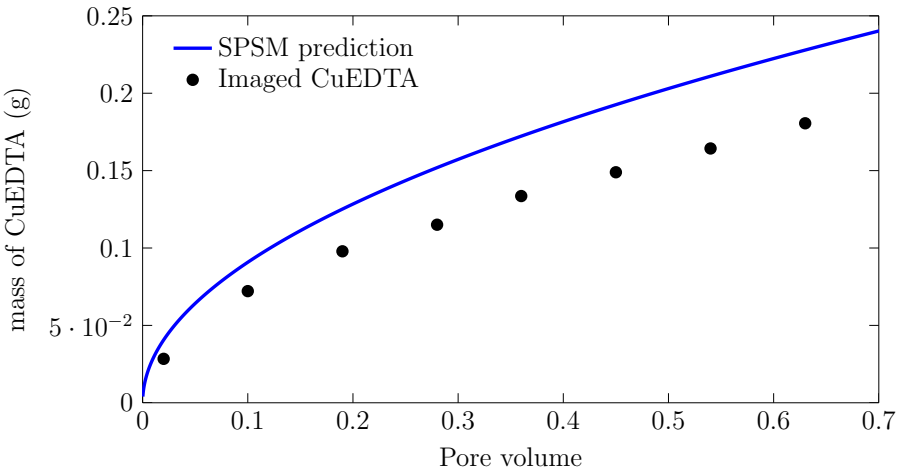

Figure 3.6: Model predictions of total mass of $CuEDTA^{2-}$ formed in the experiment against the observed mass of $CuEDTA^{2-}$. Modified from Gramling et al. (2002)

the flow rate within the cell and the reaction rate. The results revealed complex incomplete mixing dynamics that are not described by simple ADRE models. They identified two regimes where the rate of product mass production evolves faster than the ADRE prediction. So, in addition to Raje and Kapoor (2000) and Gramling et al. (2002) overprediction observations of ADRE models, the authors suggest that ADRE models cannot capture the correct temporal scaling of mass production. Also, de Anna et al. (2014b) experimental observations show that the geometry of the medium, which controls the shape of the mixing interface between reactants, plays an important role by determining the rate of product production.

3.4 Summary and conclusions

The experiments of Raje and Kapoor (2000) and Gramling et al. (2002), which are very simple observations of mixing-controlled chemical reactions in porous media, showed that known dispersion and chemical kinetic parameters estimated from well-mixed conditions are not sufficient to predict reactive transport. The main reason for this is that classical ADRE models assume perfect mixing of chemical reactants over the pore scale, while the observed fluctuations at the pore-scale means that mixing is not perfect between the reactants.

Several reactive transport models have been proposed to account for mixing, reaction and transport. One approach is the reactive RWPT, which represent the reactants by particles. The RWPT method has the potential advantage of being free from numerical dispersion, however an incorrect representation of the

reaction through the number of particles may result not only in loss of accuracy, but also may lead to an improper reproduction of the mixing process. Based on this methodology, we will show how to address these issues in the thesis.

CHAPTER 4

Reactive Random Walk Particle Tracking and Its Equivalence With the Advection-Diffusion-Reaction Equation

Abstract

We present a reactive random walk particle tracking approach to describe bimolecular chemical reactions and show its equivalence with the advection-diffusion-reaction equation. The method is able to efficiently simulate reactions in d-dimensional systems with homogeneous and spatially variable advection. Reactions among particles are determined by the reaction probability that is given in terms of the reaction rate coefficient, the total number of particles and an interaction radius which describes the well-mixed support volume at which all particles have the same probability to interact. The method is meshless and free of numerical dispersion. The method is validated for the bimolecular irreversible chemical reaction $A + B \rightarrow C$ in scenarios characterized by slow and fast chemical kinetics under diffusion and heterogeneous advection and diffusion.

This Chapter is based on the paper "Perez et al. (2019). - Reactive random walk particle tracking and its equivalence with the advection-diffusion-reaction equation. Water Resources Research, 55".

4.1 Introduction

In recent years a variety of particle-tracking methods coupled with reactions have been proposed to model reactive transport in porous media (Berkowitz et al., 2016). Random walk particle tracking (RWPT) models coupled with reactions assume that particle pairs react according to some probabilistic rules when particles are within some reaction radius r. There has been some ambiguity regarding the definition of this reaction radius in the literature. In the following, we will briefly discuss implementations of the reaction radius in reactive random walk particle tracking algorithms for irreversible bimolecular reactions.

Several alternative definitions of r have been used to quantify reactive transport in porous media. For instance, fast kinetic reactions have been properly simulated applying simplistic reaction rules based on proximity between reactant particles (two particles react whenever they are at a distance smaller than r) (Edery et al., 2009, 2010). However, in these models r must be calibrated using empirical data or based on physical properties of the medium as grain or pore size to represent the degree of mixing between reactants. Therefore r cannot represent the same reaction if the medium properties or size changes. The parameter r has been linked to the reaction rate coefficient k, the mass carried by each particle, and the time step Δt (Zhang et al., 2013). This coupling suggest a dependency between the reactants mass and kinetics that overestimates reaction. Other approaches employ a time variable reaction radius $r(t)$ based on kernel density estimators (KDE) (Rahbaralam et al., 2015; Schmidt et al., 2017). However, these reaction algorithms coupled with KDE methods are not without their limitations. If the reactions are simulated as a birth/death process of particles the reaction radius may increase over time. At late times, a finite number of particles combined with an increased r may overestimate the reaction efficiency and oversmooth the spatial distributions of the reacting species. Other approaches employ a collocation probability that depends on the separation distance between reactant particles that may underestimate the reaction kinetics when k is defined through the number of particles (Benson and Meerschaert, 2008; Ding et al., 2013; Hansen et al., 2014; Paster et al., 2014).

Here, we present a reactive RWPT methodology which is fully equivalent to the advection-diffusion reaction equation. The derivation of the equivalence between the two frameworks sheds some light on the meaning of the reaction radius and its choice.

4.2 Reactive random walks

We consider the irreversible bimolecular reaction $A + B \to C$. In the particle, or agent-based modeling approach employed here, the concentrations of A, B and C particles are represented by the number densities

$$c_i(\mathbf{x}, t) = \frac{N_i(\mathbf{x}, t)}{N_0 \Delta V} \quad \text{for} \quad i = A, B, C, \tag{4.1}$$

where $N_i(\mathbf{x}, t)$ is the number of particles belonging to species i in a support volume ΔV located at the position $\mathbf{x}$ at time t and $N_0 \gg 1$ is the total number of particles that are contained in the initial volume V_0. The support volume ΔV is well-mixed, which means that there are no mass transfer limitations on the support scale. This notion and its implications are discussed further below. The definition of concentration considers the limit of large particle numbers $N_0 \to \infty$ such that $N_i(\mathbf{x}, t)/N_0$ remains finite. The molar concentration $\mu_i(\mathbf{x}, t)$, this means number of moles $m_i(\mathbf{x}, t)$ of a species per ΔV is defined by

$$\mu_i(\mathbf{x}, t) = \frac{m_i(\mathbf{x}, t)}{\Delta V}. \tag{4.2}$$

Thus, the relation between the number density $c_i(\mathbf{x}, t)$ and the molar concentration $\mu_i(\mathbf{x}, t)$ is given by

$$\mu_i(\mathbf{x}, t) = m_0 c_i(\mathbf{x}, t), \tag{4.3}$$

where m_0 is the total initial molarity, which means the sum of moles of the species contained in the initial volume V_0. In the following, we first consider reactions in a well mixed reactor. Then, we show the equivalence between reactive random walks and the advection-diffusion reaction equation.

4.2.1 Well-mixed reactor

In the following, we develop the reaction probability for a single particle in a well mixed reactor of volume V_0 without mass transfer limitations. Thus, the species concentrations $c_i(\mathbf{x}, t) = c_i(t)$ are independent of the spatial position and given by

$$c_i(t) = \frac{N_i(t)}{N_0 V_0}, \tag{4.4}$$

where here N_0 here is the total initial number of particles. We focus on the survival and reaction probabilities from the point of view of a B particle. The lack of any mass transfer limitations implies that a B particle has an equal chance to interact with any of the surrounding $N_A(t)$ A particles and there is no memory between successive reaction events. We denote by $p_r(\Delta t)$ the probability for an individual particle-particle interaction to occur in the time Δt. Thus, the probability that a B particle survives an individual reaction event in Δt is $1 - p_r(\Delta t)$. The well-mixed condition implies that the survival probability for a B particle after Δt is

$$P_s(t; \Delta t) = \left[1 - p_r(\Delta t)\right]^{N_A(t)}. \tag{4.5}$$

The reaction probability $P_r(t; \Delta t)$ is accordingly given by

$$P_r(t; \Delta t) = 1 - \left[1 - p_r(\Delta t)\right]^{N_A(t)}. \tag{4.6}$$

The survival probability (4.5) can also be written as the ratio of the number of surviving particles at time $t + \Delta t$ to the number of particles at time t as

$$P_s(t; \Delta t) = \frac{N_B(t + \Delta t)}{N_B(t)}. \tag{4.7}$$

By combining (4.5) and (4.7), we obtain

$$N_B(t + \Delta t) = N_B(t) \left[1 - p_r(\Delta t)\right]^{N_A(t)} \tag{4.8}$$

Reactions between particles occur at a constant rate. Thus, the reaction probability is set to

$$p_r(\Delta t) = \alpha \Delta t \leq 1, \tag{4.9}$$

where α is a rate defined below. Using this definition, we can write

$$N_B(t + \Delta t) = N_B(t) \left[1 - \alpha \Delta t\right]^{N_A(t)} \tag{4.10}$$

In the limit $\Delta t \to 0$, we obtain the rate equation

$$\frac{dN_B(t)}{dt} = -\alpha N_A(t) N_B(t). \tag{4.11}$$

Using definition (4.4) of the species concentrations, we obtain the well known kinetic rate law for the number densities

$$\frac{dc_B(t)}{dt} = -k c_B(t) c_A(t). \tag{4.12a}$$

where k is the reaction rate coefficient. The rate α is thus given in term of k, V_0 and N_0 as

$$\alpha = \frac{k}{N_0 \Delta V}. \tag{4.12b}$$

The equations for the concentration of the A and C species are analogously given by

$$\frac{dc_A(t)}{dt} = -k c_A(t) c_B(t), \qquad \frac{dc_C(t)}{dt} = k c_A(t) c_B(t). \tag{4.12c}$$

Note that the reaction rate coefficient k here is referred to the number densities $c_i(t)$. The reaction rate coefficient with respect to the molar concentrations $\mu_i(t)$ is $k' = k/m_0$. The characteristic reaction time is $\tau_r = 1/kc_0$, where c_0 is a characteristic concentration. For example, for the initial concentrations $c_A(0) = c_B(0) = 1/2V_0 = c_0$, the solution for $c_A(t)$ is

$$c_A(t) = \frac{c_0}{1 + k c_0 t}. \tag{4.13}$$

4.2.2 Reaction under advection and diffusion

The position $\mathbf{x}(t)$ of a B particle under advection and diffusion is described by the Langevin equation (Risken, 1996)

$$\frac{d\mathbf{x}(t)}{dt} = \mathbf{v}[\mathbf{x}(t)] + \sqrt{2D}\boldsymbol{\xi}(t), \tag{4.14}$$

where $\boldsymbol{\xi}(t)$ is a vectorial Gaussian white noise characterized by $\langle\boldsymbol{\xi}(t)\rangle = \mathbf{0}$ and $\langle\xi_i(t)\xi_j(t')\rangle = \delta_{ij}\delta(t-t')$. Note that we use here the notation of the textbook by Risken (1996) and denote the particle position by $\mathbf{x}(t)$ and the position vector in space by $\mathbf{x}$. The former is distinguished from the latter by its argument. The angular brackets denote the white noise average. The density, or concentration of B particles can be written as

$$c_B(\mathbf{x},t) = \langle\delta\left[\mathbf{x}-\mathbf{x}(t)\right]P_s(t)\rangle, \tag{4.15}$$

where $\delta(\mathbf{x})$ is the Dirac delta and $P_s(\mathbf{x},t)$ is the probability of survival of a B particle until time t.

4.2.2.1 Survival probability

The probability of survival until $t+\Delta t$ is given by the probability of survival until time t multiplied by the probability $P_s(t;\Delta t)$ to survive in the time interval $[t, t+\Delta t]$. This means

$$P_s(t+\Delta t) = P_s(t)P_s(t;\Delta t). \tag{4.16}$$

As in the previous section, the probability $P_s(t;\Delta t)$ of survival during Δt in the well-mixed support volume ΔV centered in $\mathbf{x} = \mathbf{x}(t)$ is given by

$$P_s(t;\Delta t) = \left[1 - p_r(\Delta t)\right]^{N_A[\mathbf{x}(t),t]}, \tag{4.17}$$

where $N_A[\mathbf{x}(t),t] = c_A[\mathbf{x}(t),t]N_0\Delta V$ is the number of A particles in the support volume centered in $\mathbf{x}(t)$. Note that the concentration $c_A[\mathbf{x}(t),t]$ is constant over the well mixed support volume, and that the B particle located at $\mathbf{x}(t)$ can react with any of the $N_A[\mathbf{x}(t),t]$ A particles in its vicinity with equal probability within the time interval Δt. The reaction probability during Δt is given accordingly by

$$P_r(t;\Delta t) = 1 - \left[1 - p_r(\Delta t)\right]^{N_A[\mathbf{x}(t),t]}, \tag{4.18}$$

In analogy to (4.9) we set

$$p_r(\Delta t) = \frac{k\Delta t}{N_0\Delta V}. \tag{4.19}$$

where we used expression (4.12b) for the rate α. Inserting the latter into (4.17) and performing the limit $N_0 \to \infty$ gives for the survival probability

$$P_s(t;\Delta t) = \exp(-kc_A[\mathbf{x}(t),t]\Delta t). \tag{4.20}$$

It is assumed that $c_A[\mathbf{x}(t), t]$ is approximately constant during Δt, which is a good approximation if $\Delta t \ll \tau_r$. Note that (4.18) and (4.20) imply that the survival probability $P_s(t; t - t')$ over a time interval $t - t' \gg \Delta t$ is given by

$$P_s(t; t - t') = \exp\left(-k \int_0^{t-t'} dt'' c_A[\mathbf{x}(t - t''), t - t''] \right). \tag{4.21}$$

This expression may be useful in random walk schemes characterized by variable transition times.

4.2.2.2 Kramers-Moyal expansion

In order to derive the governing equation for $c_B(\mathbf{x}, t)$, we expand (4.15) as

$$c_B(\mathbf{x}, t + \Delta t) = \langle \delta[\mathbf{x} - \mathbf{x}(t + \Delta t)] P_s(t + \Delta t) \rangle. \tag{4.22}$$

By noting that

$$\mathbf{x}(t + \Delta t) = \mathbf{x}(t) + \mathbf{v}[\mathbf{x}(t)]\Delta t + \sqrt{2D} \int_t^{t+\Delta t} dt' \boldsymbol{\xi}(t') \tag{4.23}$$

and using relation (4.20) we can write tautologically

$$c_B(\mathbf{x}, t + \Delta t) = \int d\mathbf{x}' \langle \delta[\mathbf{x}' - \mathbf{x}(t)] P_s(t) \exp(-k c_A[\mathbf{x}(t), t]\Delta t) \delta[\mathbf{x} - \mathbf{x}' - \Delta \mathbf{x}(t)] \rangle, \tag{4.24}$$

where we defined

$$\Delta \mathbf{x}(t) = \mathbf{v}[\mathbf{x}(t)]\Delta t + \sqrt{2D} \int_t^{t+\Delta t} dt' \boldsymbol{\xi}(t'). \tag{4.25}$$

The first Dirac delta on the right side of (4.24) implies that $\mathbf{x}(t) = \mathbf{x}'$ so that we can write

$$c_B(\mathbf{x}, t + \Delta t) = \int d\mathbf{x}' c_B(\mathbf{x}', t) \exp[-k c_A(\mathbf{x}', t)\Delta t] p(\mathbf{x} - \mathbf{x}'; \mathbf{x}', \Delta t), \tag{4.26}$$

where $p(\mathbf{x} - \mathbf{x}'; \mathbf{x}', \Delta t) = \langle \delta[\mathbf{x} - \mathbf{x}' - \Delta \mathbf{x}(t)|_{\mathbf{x}(t)=\mathbf{x}'}] \rangle$ denotes the probability for a particle to make a transition from $\mathbf{x}'$ to $\mathbf{x}$ within the time Δt. Performing a Kramers-Moyal expansion (Risken, 1996) of (4.26) gives

$$c_B(\mathbf{x}, t + \Delta t) = \left[1 - \nabla \cdot \mathbf{v}(\mathbf{x})\Delta t + D\Delta t \nabla^2 + \dots \right] c_B(\mathbf{x}, t) \exp\left[-k c_A(\mathbf{x}, t)\Delta t \right], \tag{4.27}$$

where the dots denote contributions of order Δt^2. We expand both sides of the equation consistently up to order Δt to obtain

$$c_B(\mathbf{x},t) + \frac{\partial c_B(\mathbf{x},t)}{\partial t}\Delta t + \cdots = \\ \left[1 - \nabla\cdot\mathbf{v}(\mathbf{x})\Delta t + D\Delta t\nabla^2\right] c_B(\mathbf{x},t) - c_B(\mathbf{x},t)kc_A(\mathbf{x},t)\Delta t + \ldots. \tag{4.28}$$

The limit $\Delta t \to 0$, gives the advection-diffusion reaction equation (ADRE)

$$\frac{\partial c_B(\mathbf{x},t)}{\partial t} + \nabla\cdot\mathbf{v}(\mathbf{x})c_B(\mathbf{x},t) - D\nabla^2 c_B = -kc_B(\mathbf{x},t)c_A(\mathbf{x},t). \tag{4.29a}$$

The derivations for $c_A(\mathbf{x},t)$ and $c_C(\mathbf{x},t)$ are analogous and yield

$$\frac{\partial c_A(\mathbf{x},t)}{\partial t} + \nabla\cdot\mathbf{v}(\mathbf{x})c_A(\mathbf{x},t) - D\nabla^2 c_A = -kc_B(\mathbf{x},t)c_A(\mathbf{x},t) \tag{4.29b}$$

$$\frac{\partial c_C(\mathbf{x},t)}{\partial t} + \nabla\cdot\mathbf{v}(\mathbf{x})c_C(\mathbf{x},t) - D\nabla^2 c_C = kc_A(\mathbf{x},t)c_B(\mathbf{x},t). \tag{4.29c}$$

Thus, the reactive random walk particle tracking scheme based on the Langevin equation (5.13) combined with the survival and reaction probabilities (4.17) and (4.18) for a well-mixed local support volume are exactly equivalent to the system (4.29) of advection-diffusion reaction equations. Note that the equivalence between the Lagrangian and Eulerian frameworks does not require the definition of a collocation probability of A and B particles as given for example in Benson and Meerschaert (2008), but merely relies on the concept of a well-mixed support volume ΔV.

4.2.3 Numerical implementation

The Langevin equation (5.13) governing the motion of particles belonging to the A, B and C species is discretized using an Euler scheme as

$$\mathbf{x}(t+\Delta t) = \mathbf{x}(t) + \mathbf{v}[\mathbf{x}(t)]\Delta t + \sqrt{2D\Delta t}\boldsymbol{\eta}(t) \tag{4.30}$$

where the $\boldsymbol{\eta}(t)$ are independent identically distributed Gaussian random variables characterized by 0 mean and unit variance. The time increment Δt is conditioned on the scale of variability τ_v of the Lagrangian velocity $\mathbf{v}[\mathbf{x}(t)]$ in that the discretization (5.14) requires that

$$\int_t^{t+\Delta t} dt'\mathbf{v}[\mathbf{x}(t')] \approx \mathbf{v}[\mathbf{x}(t)]\Delta t. \tag{4.31}$$

This means, $\mathbf{v}[\mathbf{x}(t)]$ is only weakly variable during the time Δt.

At each time step, the position of each particle is recorded and the distances between a given B and A particles are calculated. Note that the algorithm consider either the point of view of a B of an A particle. We describe the point of

view of a B particle, the one of an A particle is analogous. The number $N_A[\mathbf{x}(t)]$ of A particles within a volume ΔV centered at the position $\mathbf{x}(t)$ of the B particle determines the reaction probability (4.18). The occurrence of a reaction event is obtained from a Bernoulli trial. If the reaction occurs, the B particles and the closest A particle are removed and a particle C is placed at the middle point of the A and B particle locations. Note that these details on removal of A and B and placing the C particles have no impact on the simulated reaction behavior or the equivalence of the particle scheme with the ADRE derived in the previous section. The motion of the produced C particles follows (5.14). Recall that the notion of a well-mixed support volume ΔV is a central item for the equivalence between the Langrangian and Eulerian reaction models. For 1 dimension, the well-mixed support volume here is given by $\Delta V = 2r$, in 2 dimensions, it is given by a disk, such that $\Delta V = \pi r^2$ and in three dimensions by a sphere such that $\Delta V = 4\pi r^3/3$. The selection of the reaction radius is discussed in the following section.

4.2.4 Well-mixed support volume and reaction radius

As pointed out in the introduction, a question that has given rise to some debate concerns the determination of the volume ΔV or equivalently the determination of the reaction radius r. Edery et al. (2009) discuss the use of a normal distribution for the reaction radius, or relating the radius to the reaction rate coefficients. Benson and Meerschaert (2008) use a collocation probability with a characteristic reaction radius $r \sim \sqrt{2D\Delta t}$ based on the reasoning that the typical area probed by a particle due to random motion during a time Δt is $2D\Delta t$. For the definition and use of a collocation probability see also Hansen et al. (2014) and Paster et al. (2014).

The derivation presented in Section 4.2.2 invokes the well-mixed condition, which here means that all particles within a fixed radius, or support volume have the same probability to react in a time interval Δt. Thus, instead of a collocation probability, we use a fixed reaction radius r. Within the time Δt each particle must be able to reach any other particle in the support volume. The characteristic diffusive particle displacement during time Δt is $\sigma(\Delta t) = \sqrt{2dD\Delta t}$, where d is the spatial dimension. For $r \lesssim \sigma(\Delta t)$ the support volume may be considered well-mixed. We use here $r = \sigma(\Delta t)$. Note that this condition on the reaction radius may be relaxed at longer simulation times because the mixing scale $s(t)$ (Villermaux, 2012; Le Borgne et al., 2013; **?**) grows diffusively as $s(t) \propto \sqrt{2Dt}$ heterogeneous non-chaotic flow scenarios. The concentration content on the mixing scale may be assumed uniform. Thus, if one is interested in observation times $t \gg \Delta t$, the reaction radius may be chosen $0 < r < \sqrt{2Dt}$.

In order to resolve kinetic reactions, the time increment Δt needs to be smaller than the characteristic reaction time scale $\tau_r = 1/c_0 k$ with c_0 a characteristic concentration. Thus, as Δt is by definition of the reaction radius r the characteristic mass transfer time on the support scale, the microscopic Damköhler number is $Da_m = \Delta t c_0 k < 1$, which means that reactions at the support scale are not

limited by mass transfer.

Fast or instantaneous chemical reactions can be modeled in two ways. First, particles may react with certainty upon encounter. This means the probability $p_r(\Delta t)$ for an individual reaction is set to 1. In this case there is no condition on Δt regarding the reaction. Second, finite kinetics can be considered. If the time increment Δt is chosen larger than the reaction time τ_r, the microscopic Damköhler number is $Da_m \geq 1$ and the reaction is mass transfer limited already on the support scale. The kinetic part of the reaction is not resolved by the time discretization and the reaction is instantaneous on the relevant observation times. Note however, that Δt may be also conditioned by the temporal variability of the Lagrangian velocity, see (4.31).

The work by Porta et al. (2012a) defines a fixed support volume by discretizing space into a cubic lattice. The reaction probability in each cell is given by the species concentrations in a cube, the particle residence times, and the reaction rate coefficient. The characteristic mass transfer time across a cell of size a is a^2/D. Thus, the microscopic Damköhler number in this approach is $Da_m = c_0 k a^2/D$. In order to resolve kinetic reactions, $Da_m \leq 1$ sets a criterion for the grid size.

4.3 Validation

We validate the reactive random walk particle tracking algorithm presented in the previous section in 4 scenarios. First, we consider slow chemical reactions in a closed domain for well-mixed and segregated initial species distributions. Second, we consider fast chemical reactions for a plug flow reactor and a laminar flow reactor setup with initially segregated reactant species. For the well-mixed scenario, the numerical data are compared to the exact analytical solution for the concentration of the A species. In the remaining scenarios, we focus on the total product mass

$$m_C(t) = \int d\mathbf{x} c_c(\mathbf{x}, t), \tag{4.32}$$

and validate against analytical solutions.

4.3.1 Slow reactions

We consider a 1-dimensional domain with reflecting boundary conditions. The diffusion coefficient is set to $D = 10^{-3}$ cm^2/s, the reaction rate coefficient is $k = 8$ cm/s. The time step is $\Delta t = 10^{-2}$. According to the previous section, this setup is equivalent to the diffusion reaction problem

$$\frac{\partial c_i(x,t)}{\partial t} - D\frac{\partial^2 c_i(x,t)}{\partial x^2} = -k c_A(x,t) c_B(x,t), \qquad i = A, B \tag{4.33a}$$

$$\frac{\partial c_C(x,t)}{\partial t} - D\frac{\partial^2 c_C(x,t)}{\partial x^2} = k c_A(x,t) c_B(x,t). \tag{4.33b}$$

4.3.1.1 Well-mixed scenario

We consider an initially well-mixed reactor. This means particles are uniformly distributed across the 1-dimensional domain of length $L = 1$ cm, which implies that the initial concentrations are $c_A(x, t = 0) = c_B(x, t = 0) = c_0 = 1/2$ cm^{-1} and $c_C(x, t = 0) = 0$. The total particle number is $N_0 = 10^4$. Due to the uniform initial distributions there are no macroscopic mass transfer limitations and thus $c_i(x, t) = c_i(t)$ and the system (4.33) reduces to (4.12) with the analytical solution (4.13). Figure 4.1 compares the data from the random walk particle tracking simulations and the analytical solution (4.13). They are in agreement.

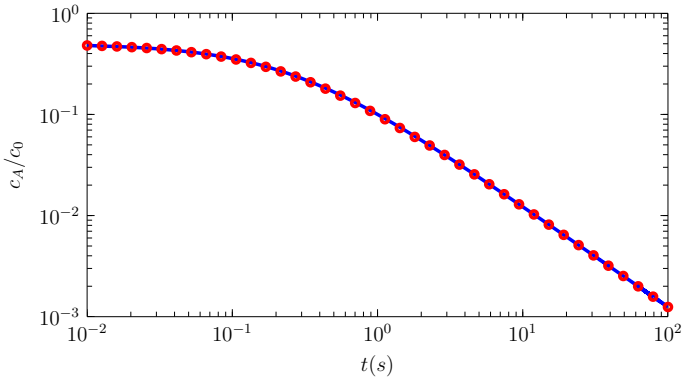

Figure 4.1: Evolution of the A species from (symbols) reactive random walk simulations and (solid lines) the analytical solution (4.13).

4.3.1.2 Segregated scenario

Here we consider initial segregation of the reactant species such that all the A particle are uniformly distribution in the left, the B particles in the right half of the domain. Thus, the initial concentrations are $c_A(x, t = 0) = c_B(x, t = 0) = c_0 = 1$ cm^{-1} and $c_C(x, t = 0) = 0$. The total particle number is $N_0 = 10^5$. The numerical results are validated against the early time solution for the total product mass. At early times, this means $t \ll \tau_r = 1/kc_0$, the concentrations of the A and B species can be approximated by (Bandopadhyay et al., 2017),

$$c_A = \frac{c_0}{2}\left[1 - \text{erf}\left(\frac{x - 1/2}{\sqrt{4Dt}}\right)\right], \qquad c_A = \frac{c_0}{2}\left[1 + \text{erf}\left(\frac{x - 1/2}{\sqrt{4Dt}}\right)\right], \tag{4.34}$$

which are the solutions for an infinite medium in the absence of reactions. These approximations are valid at early times, which are smaller than τ_r and at which the diffusion front is far away from the boundaries. Thus, the evolution of the

total product mass can be approximated by

$$\frac{dm_C(t)}{dt} = k\frac{c_0^2}{4}\int_{-\infty}^{\infty} dx \left[1 - \mathrm{erf}\left(\frac{x - 1/2}{\sqrt{4Dt}}\right)^2\right]. \tag{4.35}$$

The integrals can be solved analytically, which gives

$$\frac{dm_C(t)}{dt} = k\frac{c_0^2\sqrt{Dt}}{\sqrt{2\pi}}. \tag{4.36}$$

Thus, we obtain for the initial evolution of the product species

$$m_C(t) = \frac{kc_0^2\sqrt{2D}t^{3/2}}{3\sqrt{\pi}} \tag{4.37}$$

The numerical data is in agreement with this analytical solution as shown in Figure 4.2.

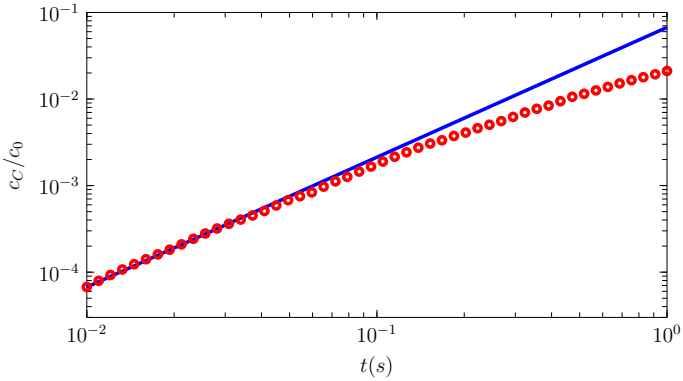

Figure 4.2: Evolution of the product mass $m_C(t)$ from (symbols) reactive random walk simulations and (solid lines) the analytical early time solution (4.37).

4.3.2 Fast reactions

We consider two scenarios of fast chemical reactions. In both scenarios, the reactants are initially segregated. The first scenario is 1-dimensional and characterized by a constant flow velocity, the second scenario is 2-dimensional and characterized by a parabolic Poiseuille flow profile.

4.3.2.1 Plug flow reactor

The plug flow scenario is inspired by the Darcy scale setup of the laboratory experiment reported in (Gramling et al., 2002). The domain size is $L = 60$ cm.

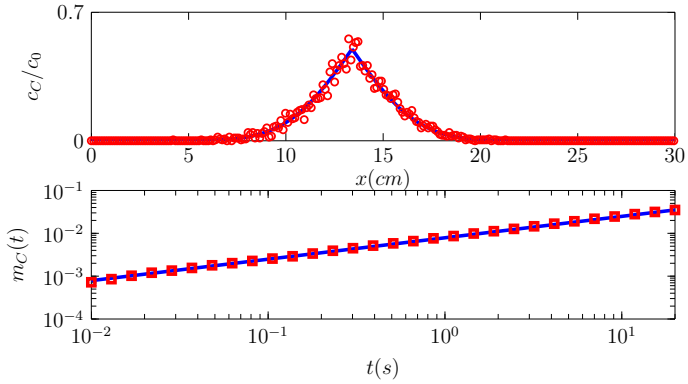

Figure 4.3: (Top) Comparison of $c_C(x,t)$ $t = 20$ s obtained from (symbols) numerical simulations and (solid line) the analytical solution (5.7). (Bottom) Total product mass $m_C(t)$ obtained from (symbols) numerical simulations and (solid line) the analytical solution (5.8).

The total particle number is $N_0 = 2 \cdot 10^5$. Initially 10^5 A particle are uniformly distributed in the left and 10^5 B particles in the right half of the domain, which yields the initial concentrations $c_A(x, t = 0) = c_B(x, t = 0) = 1/60$ cm^{-1} and $c_C(x, t = 0) = 0$. The diffusion coefficient is set to $D = 1.75 \cdot 10^{-1}$ cm^2/s. The time step is $\Delta t = 10^{-2}$ s. The reaction probability is set to $p_r = 1$. The numerical results are validated against the exact analytical solutions for the concentration of the product C, which is given by (Gramling et al., 2002)

$$c_C(x,t) = \frac{c_0}{2} \mathrm{erfc}\left(\frac{|x - vt|}{2\sqrt{Dt}}\right). \tag{4.38}$$

The total product mass $m_C(t)$ is obtained from (4.32) as

$$m_C(t) = 2c_0\sqrt{\frac{Dt}{\pi}}. \tag{4.39}$$

Figure 4.3 compares the product concentration and total product mass obtained from the reactive random walk simulations to the analytical solutions (5.7) and (5.8). The validity of the numerical approach is confirmed.

4.3.2.2 Laminar flow reactor

We consider a 2-dimensional channel of length $L_x = 20$ cm and width $L_y = 1cm$. Flow through the channel is laminar and characterized by the parabolic velocity profile

$$\mathbf{v}(\mathbf{y}) = v_0\left(1 - \frac{y^2}{L_y^2}\right)\mathbf{e_x}, \tag{4.40}$$

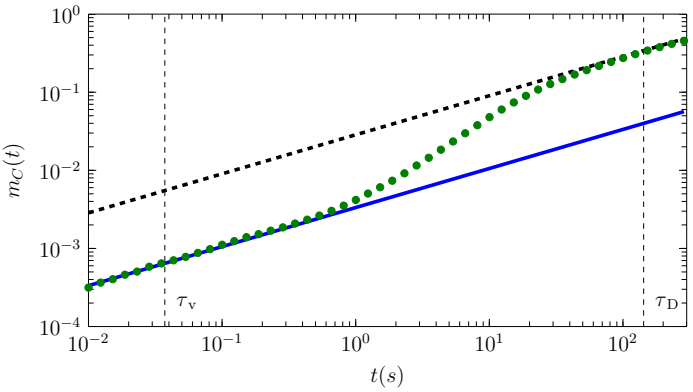

Figure 4.4: Total mass of product C obtained from (symbols) numerical simulations and the analytical (solid line) short and (dashed line) long time approximations.

where $\mathbf{e_x}$ is the unit vector in x-direction and v_0 is the maximum velocity. The mean flow velocity is $\bar{v} = 2v_0/3$. We set here $v_0 = 0.65$ cm/s. The diffusion coefficient is set to $D = 3.5 \cdot 10^{-3}$ cm^2/s. This scenario can be characterized by the Péclet number $Pe = \sqrt{\tau_D/\tau_v} = \bar{v}L_y/2D$, which compares the relative importance of advective and diffusive transport mechanisms. The diffusive time scale is $\tau_D = L_y^2/2D$, the advective time $\tau_V = 2D/\bar{v}^2$. The Péclet number here is $Pe = 61$, this means, the scenario is advection dominated. The total particle number is $N_0 = 2 \cdot 10^5$. Initially 10^5 A particles are distributed in the left and 10^5 B particles in the right half of the domain. The vertical domain boundaries are open, the horizontal boundaries are reflecting. The time step is set to $\Delta t = 10^{-2}$ s, the reaction radius here is set to $r = 2.45\,\sigma(\Delta t)$, the reaction probability is $p_r = 1$. The numerical results are validated against analytical solutions for $m_C(t)$ at early times $t < \tau_v$ and late times $t > \tau_D$. For $t < \tau_v$ transport is diffusion-dominated, this means the flow variability is subleading. The product mass is given by (5.8). For $t > \tau_D$, the species are fully mixed over the channel cross-section and transport can be characterized by the mean velocity $\bar{v}$ and the Taylor dispersion coefficient $\mathcal{D} = D + 2v_m^2 a^2/105D$. Thus, the evolution of $m_C(t)$ is given again by (5.8) with D substitute by the Taylor dispersion coefficient $\mathcal{D}$. Figure 4.4 shows the agreement between the simulation data for $m_C(t)$ and the analytical solutions for the early and late time behaviors. The intermediate behavior, which is dominated by the flow heterogeneity, is not captured by these analytical solutions. An upscaled model for the full behavior can be found in Perez et al. (2019a).

4.4 Conclusions

We demonstrate the equivalence between reactive random walk particle tracking and the advection-diffusion-reaction equation. This equivalence is established based on the concept of a well-mixed support volume, which acts as a well-mixed reactor during the time increment Δt. The reactive random walk method is simple and free of numerical dispersion and artificial oscillations compared to grid-based Eulerian approaches. All particles within the reaction radius, which represents the support volume, are statistically equal and have an equal probability to react. As a result of the locally well-mixed assumption, reactions occur at constant rate and the reaction probability p_r is determined by the reaction rate coefficient k and the time increment Δt. Thus, within a constant reaction radius, particle reactions are determined combinatorially based on the reaction probability for individual reaction events. The reaction radius is chosen of the order of the typical diffusive particle displacement $\sigma(\Delta t) = \sqrt{2D\Delta t}$ during a time step Δt. As the mixing scale in heterogeneous mixtures under non-chaotic flow conditions increases as $\sim \sqrt{Dt}$, the reaction radius may be chosen larger than $\sigma(\Delta t)$ for times $t \gg \Delta t$.

We have validated the reactive random walk method for two slow and two fast reaction scenarios dominated by diffusion and (heterogeneous) advection-diffusion. In all cases the simulation data agree with available analytical solutions. The presented method may be extended to include more complex physical and non-linear chemical processes because complex reactions, such as biodegradation or enzymatic reactions, are composed of a cascade of elementary unimolecular and bimolecular reactions similar to the one studied in this Technical Note.

Acknowledgments

We acknowledge the support of the European Research Council (ERC) through the project MHetScale (617511) and the Spanish Ministry of Economy, Industry and Competitiveness, and EU-FEDER (CGL2016-80022-R) through the project MECMAT. The numerical data can be reproduced following the numerical algorithms and parameter sets given in the paper. Alternatively the data can be obtained upon request from the corresponding author.

CHAPTER 5

Upscaling of Mixing-Limited Bimolecular Chemical Reactions in Poiseuille Flow

Abstract

We consider the fast irreversible bimolecular chemical reaction $A+B \rightarrow C$ in the Poiseuille flow through a channel, in which A displaces B. This system allows to systematically study the impact of the interaction of interface deformation and diffusion on mixing and reactive transport. At early times, the reaction is diffusion controlled. With increasing time advection begins to dominate and we find enhanced reaction efficiency due to the deformation of the interface between the two reactants. For times larger than the characteristic diffusion time across the channel, mixing and reaction are quantified by the Taylor dispersion coefficient. Predictions based on Taylor dispersion may significantly overestimate the reaction efficiency at preasymptotic times, when the system is characterized by incomplete mixing. This type of behaviors of incomplete mixing and reaction have been observed in heterogeneous systems across different scales. Channel flow allows to study them in detail for a well controlled system. We propose a dispersive lamella approach based on the concept of effective dispersion which accurately predicts the full evolution of the product mass. Specifically, this approach captures the impact of interface deformation and diffusive coalescence, which marks the transition to the Taylor regime. It gives insight into the mechanism of incomplete mixing and its consequences for reactive transport in more general porous media flows.

This Chapter is based on the paper "Perez et al. (2019). - Upscaling of mixing-limited bimolecular chemical reactions in Poiseuille flow. Water Resources Research, 54".

5.1 Introduction

The dynamics of reactive fronts and mixing interfaces is important for a wide range of natural processes from the biosphere to natural and anthropogenic contamination of aquifers. Natural aquifers exhibit heterogeneities that change the flow and transport dynamics. Heterogeneity modifies the topology of reactive fronts and mixing interfaces, which leads to chemical reaction dynamics that are very different from the ones observed in the laboratory under well-mixed equilibrium conditions (Raje and Kapoor, 2000; Gramling et al., 2002; de Anna et al., 2014b) and the ones predicted by the transport laws for homogeneous media (Steefel et al., 2005; Li et al., 2006; Dentz et al., 2011a).

Chemical species must physically come into contact one with another for chemical reactions to occur. Mixing, the process by which different substances originally segregated tend to occupy the same volume, is what makes this contact possible. Mixing controls biogeochemical transformations that are fast compared to mass transfer, such as dissolution, precipitation, or degradation (Li et al., 2006; Simoni et al., 2007; Mariani et al., 2010). Mass transfer limitations induced by medium heterogeneity causes reduced reaction and mixing efficiency compared to equivalent homogeneous medium descriptions based on hydrodynamic dispersion or macrodispersion (Gramling et al., 2002; Li et al., 2006; Luo et al., 2008; Tartakovsky et al., 2009). On the other hand, mixing due to medium heterogeneity increases reaction compared to mixing by diffusion only (Rolle et al., 2009; de Anna et al., 2014a; Jiménez-Martínez et al., 2015).

Traditionally, Darcy scale reactive transport has been described by the advection-dispersion-reaction equation (ADRE) (Steefel et al., 2005; Dentz et al., 2011a), which expresses species mass conservation due to advective-dispersive mass transfer and chemical reaction as

$$\phi \frac{\partial c_i(\mathbf{x},t)}{\partial t} = -\nabla \cdot [\mathbf{q} c_i(\mathbf{x},t) - \mathbf{D} \nabla c_i(\mathbf{x},t)] - r_i(\mathbf{x},t,\{c_j(\mathbf{x},t)\}), \tag{5.1}$$

where ϕ is porosity, c_i is the concentration of reactant i, $\mathbf{q}$ is Darcy velocity, $\mathbf{D}$ is the dispersion tensor, and r_i is the local reaction rate of species i, which in general may depend explicitly on position, time, and concentrations of all reacting species $\{c_j\}$. Reaction rates are typically estimated from laboratory experiments under well-mixed conditions in batch or flow through reactors (Steefel et al., 2005; Luo et al., 2008; Dentz et al., 2011a). Their use in (5.1) is subject to the existence of a well-mixed support volume and to mass transfer on the support scale being much faster than the chemical reaction. The first condition implies that the microscopic Peclét number, which compares the diffusion and advection time scales on the support scale, needs to be smaller than 1. The second condition implies that the microscopic Damköhler number, which compares characteristic mass transfer to reaction times, needs to be smaller than 1 (Battiato and Tartakovsky, 2011). A variety of laboratory (Kapoor et al., 1998; Raje and Kapoor, 2000; Gramling et al., 2002; de Anna et al., 2014b) and field studies (Davis et al., 2000; Hess et al., 2002) have shown that the ADRE overestimates the reaction efficiency. This may be traced back to the fact that the above conditions are often not fulfilled, this

means locally the system is not well-mixed and the mass transfer time scales are larger than the reaction time scales.

Laboratory and numerical experiments have shown that enhanced chemical reactivity can be linked to deformation of mixing interfaces (Borgne et al., 2014; de Anna et al., 2014b,a). Lamellar approaches have been long used for the quantification of mixing and reaction in spatially variable flow fields Ranz (1979); Villermaux and Duplat (2003); Duplat and Villermaux (2008); Duplat et al. (2010); Le Borgne et al. (2013); Borgne et al. (2014). They are based on the concept that a heterogeneous concentration distribution can be represented by an ensemble of non-interacting lamellae, on which diffusion is enhanced through compression of the lamella due to flow deformation. Duplat and Villermaux (2008), Villermaux (2012) and Le Borgne et al. (2013) have extended this approach for random flows to account for interactions between lamellae based on random coalescence. These approaches provide models for the mixing and reaction behaviors in the deformation and coalescence regimes.

In this paper, we study the impact of flow variability on the reaction efficiency of an instantaneous irreversible bimolecular chemical reaction $A+B \rightarrow C$. This relatively simple reaction can be seen as the building stone of more complex chemical reactions such as metabolic activity of a biofilm (Steefel et al., 2005) or remediation of water contamination by anthropogenic elements such as sulphides (Batens and Van Keer, 2003) and ammonia (Garg et al., 2000). It is an elementary reaction that allows to study in detail the impact of the fundamental mechanisms of flow deformation and diffusion on mixing and chemical reaction. We consider the laminar flow through a channel, which is characterized by the parabolic Poiseuille profile. This flow scenario serves as a model system for flow through open fractures, laminar reactors, single pores, and capillaries. This system has been studied experimentally by Kapoor et al. (1998), who emphasized the impact of concentration fluctuations around the vertical mean on the prediction of the overall reactivity. These authors considered the breakthrough of product concentration in order to characterized the system reactivity. While the flow field here is deterministic, it exhibits transport and mixing features typical for heterogeneous flow fields, such as the evolution of effective and apparent dispersion coefficients towards a macrodispersion, the Taylor dispersion coefficient, and front spreading due to spatially variable advection. In fact, as we will see in the following, the reaction behavior shows features, which are well known consequences of incomplete mixing of the (macroscopic) support scale. Thus, even though the system is idealized it allows studying the fundamental mechanisms of incomplete mixing and chemical reaction in heterogeneous systems. Thus, the developed approaches and conclusions also apply to more general, heterogeneous flow situations.

In order to study the detailed dispersion and reaction behavior, we use a numerical reactive random walk particle tracking (RWPT) (Benson and Meerschaert, 2008; Edery et al., 2009, 2010; Zhang et al., 2013; Alhashmi et al., 2015) to determine the evolution of the species concentrations and the global reactivity in terms of the total product mass. The mixing behavior is characterized in

terms of effective dispersion, which measures the average width of a point injection in the channel cross-section, or in other words, the Green function of the transport problem (Dentz and Carrera, 2007). Based on this concept we propose a dispersive lamella approach to quantify the impact of mixing on chemical reaction.

The paper is organized as follows. In Section 5.2 we describe the reactive transport problems. Section 5.3 discusses the results of reactive RWPT simulations in the Poiseuille flow. Section 5.4 determines the product evolution based on stretched lamellae and proposes the dispersive lamella approach to capture the full evolution of reactivity including stretching-enhanced mixing and coalescence.

5.2 Methodology

We consider the irreversible bimolecular chemical reaction

$$A + B \xrightarrow{k} C, \tag{5.2}$$

where k denotes the reaction rate coefficient. This elementary reaction can be considered as a constituent of more complex reactions, which can be built as combinations of bimolecular and uni-molecular reactions (Gillespie, 2000).

5.2.1 Reactive transport

In this paper, we focus on the impact of mass transfer due to spatially variable advection and diffusion on chemical reaction, which is described by the following advection-diffusion reaction equation (ADRE)

$$\frac{\partial c_i(\mathbf{x},t)}{\partial t} + \nabla \cdot \mathbf{v}(\mathbf{x}) c_i(\mathbf{x},t) - D\nabla^2 c_i = -k c_A(\mathbf{x},t) c_B(\mathbf{x},t) \tag{5.3a}$$

$$\frac{\partial c_C(\mathbf{x},t)}{\partial t} + \nabla \cdot \mathbf{v}(\mathbf{x}) c_C(\mathbf{x},t) - D\nabla^2 c_C = k c_A(\mathbf{x},t) c_B(\mathbf{x},t) \tag{5.3b}$$

for $i = A, B$, where $\mathbf{u}(\mathbf{x})$ is the flow velocity. As outlined in the Introduction, this formulation requires that the support scale underlying this continuum description to be well-mixed and that the microscopic Damköhler number be smaller than 1, this means that the support volume is considered a well-mixed reactor. The global reaction behavior is characterized by the evolution of the total mass of the reaction product

$$m_C(t) = \int d\mathbf{x} c_C(\mathbf{x},t). \tag{5.4}$$

By integration of (5.3b) over the flow and transport domain, we obtain

$$\frac{dm_C(t)}{dt} = R(t), \qquad R(t) = \int d\mathbf{x} k c_A(\mathbf{x},t) c_B(\mathbf{x},t), \tag{5.5}$$

where $R(t)$ is the reaction rate. We consider initially segregated A and B, which are distributed according to

$$c_A(\mathbf{x}, t = 0) = c_0 \mathbb{I}(-L \leq x < 0), \qquad c_B(\mathbf{x}, t = 0) = c_0 \mathbb{I}(0 \leq x < L), \tag{5.6}$$

where L is the initial extension of the domain occupied by A and B species, $\mathbb{I}(\cdot)$ is an indicator function, which is equal to 1 if the argument is true and 0 else. The C species is initially non-existent.

5.2.1.1 Constant flow

As a reference case, we consider first the constant flow velocity $\mathbf{u}(\mathbf{x}) = v\mathbf{e}_x$, with $\mathbf{e}_x$ the unit vector in x-direction. Furthermore, the chemical reaction is assumed to be fast, this means that $c_0 k$, with c_0 a characteristic concentration, is larger that the characteristic transport rate $1/\tau_v$, where $\tau_v = 2D/v^2$ is the time after which advective displacements are larger than diffusive. This criterion can be expressed by the Damköhler number which compares the reaction to the transport rate, $Da = c_0 k \tau_v$, and corresponds to $Da \gg 1$ in the following. In a domain infinitely extended in 1–direction, with the initial conditions (5.6) for $L \to \infty$ the product concentration is given by (Gramling et al., 2002)

$$c_C(x, t) = \frac{c_0}{2} \operatorname{erfc}\left(\frac{|x - vt|}{2\sqrt{Dt}}\right), \tag{5.7}$$

see also Appendix A.3.1. Note that Gramling et al. (2002) considered an inflow boundary condition, for which this solution is only approximate, while for the initial value problem posed above it is exact. The product mass is given by

$$m_C(t) = 2c_0\sqrt{\frac{2}{\pi}}\sigma(t), \qquad \sigma(t) = \sqrt{2Dt}, \tag{5.8}$$

where $\sigma(t)$ is the interface width. The scaling of the product mass as $\sqrt{t}$ can be understood as follows. Since the reaction is instantaneous, the reaction rate $R(t)$ is equal to the diffusive mass flux at the interface between the two species, which is $j_D \approx Dc_0/\sqrt{2Dt}$, where c_0 is the concentration difference across the interface and $\sqrt{2Dt}$ its width. Thus, one obtains from (5.5), $m_c(t) \approx c_0\sqrt{2Dt}$. This solution serves as the reference for the behaviors observed for spatially variable flow. Appendix A.3.1 develops analytical solutions for the initial conditions (5.6).

5.2.1.2 Poiseuille flow

In this paper, we focus on mixing and reaction in the laminar flow through a two-dimensional channel, which is a model for mixing and reaction in flow through a single pore, open fractures, and laminar flow reactors, for example. The half-width of the channel is denoted by a, the channel walls are impervious and represent no-slip boundaries for the flow. Thus, the flow velocity is aligned with the channel axis and depends only on the coordinate perpendicular to the

channel orientation, $\mathbf{u}(\mathbf{x}) = u(y)\mathbf{e}_x$. The speed $u(y)$ is given by the parabolic Poiseuille profile

$$u(y) = v_0 \left(1 - \frac{y^2}{a^2}\right), \tag{5.9}$$

where v_0 is the maximum flow velocity. The mean flow velocity across the channel is given by $v_m = 2v_0/3$. The A and B species are initially segregated according to (5.6) and the C species is non existent. At the horizontal domain boundaries at $y = \pm a$ the solute flux is zero. Under these conditions, there is no closed form analytical solution. Thus, the reactive transport problem (5.3) is solved numerically using a reactive random walk particle tracking (RWPT) method (Perez et al., 2019b), whose analysis and implementation are presented in the next section. Kapoor et al. (1998) studied a similar system, namely reactive transport in parabolic pipe flow, using laboratory experiments and numerical simulations, which gives qualitatively similar results to the ones reported in the following.

Transport can be characterized by the diffusion time across the channel diameter $\tau_D = (2a)^2/2D$ and the characteristic advection time $\tau_v = 2D/v_m^2$, which measures the time at which longitudinal advective and diffusive displacements are equal. For times $t < \tau_v$ diffusion is the dominant transport process, for $t > \tau_v$ advection starts dominating. These time scales define the Péclet number

$$Pe = \sqrt{\frac{\tau_D}{\tau_v}} = \frac{v_m a}{2D}. \tag{5.10}$$

If $Pe \ll 1$, diffusion is the dominant transport mechanism and the particles mix completely over the channel cross section before advection starts to impact on the longitudinal particle displacement. For $Pe \gg 1$, the solute mixes across the channel after an advective profile along the flow field (5.9) has been established. The Damköhler number here compares the characteristic advection time τ_v to the characteristic reaction time $1/c_0 k$,

$$Da = c_0 k \tau_v. \tag{5.11}$$

The $DaPe$ number for this system is given by

$$DaPe = c_0 k \tau_D. \tag{5.12}$$

It compares the mixing time across the channel cross-section to the characteristic reaction time. For $DaPe \gg 1$, the system is characterized by incomplete mixing.

5.2.2 Numerical simulations

In the following, we briefly describe the numerical reactive random walk particle tracking method used to solve the reactive transport problem, and the numerical setup.

5.2.2.1 Random walk particle tracking

The numerical simulations are based on random walk particle tracking combined with a probabilistic rules for the reaction. The equation that governs the advective-diffusive motion of particles belonging to the A, B and C species is the Langevin equation (Risken, 1996)

$$\frac{d\mathbf{x}(t)}{dt} = \mathbf{v}[\mathbf{x}(t)] + \sqrt{2D}\boldsymbol{\xi}(t), \tag{5.13}$$

where $\mathbf{x}(t)$ is the trajectory of a particle and $\boldsymbol{\xi}(t)$ is a vectorial Gaussian white noise characterized by zero mean $\langle\boldsymbol{\xi}(t)\rangle = \mathbf{0}$ and covariance $\langle\xi_i(t)\xi_j(t')\rangle = \delta_{ij}\delta(t-t')$, where δ_{ij} is the Kronecker delta. The flow velocity is $\mathbf{u}(\mathbf{x}) = u(y)\mathbf{e}_x$ with $u(y)$ given by (5.9). No flux boundary conditions at the horizontal channel boundaries at $y = \pm a$ are implemented through reflection of particles.

The Langevin equation (5.13) is discretized using an Euler scheme as

$$\mathbf{x}(t+\Delta t) = \mathbf{x}(t) + \mathbf{v}[\mathbf{x}(t)]\Delta t + \sqrt{2D\Delta t}\boldsymbol{\eta}(t) \tag{5.14}$$

where the $\eta(t)$ are independent identically distributed Gaussian random variables characterized by 0 mean and unit variance. At each time step, the position of each particle is recorded and the distance between a given A and B particle is calculated. We describe the point of view of a B particle, the one of an A particle is analogous. The survival probability $P_s[\mathbf{x}(t)]$ of a B particle in the time interval $[t, t+\Delta t]$ depends on the number $N_A[\mathbf{x}(t)]$ of A particles within a well-mixed volume ΔV centered at the position $\mathbf{x}(t)$ of a B particle (Perez et al., 2019b) as

$$P_s[\mathbf{x}(t)] = \exp\left[-p_r(\Delta t)N_A[\mathbf{x}(t)]\right], \tag{5.15}$$

where $p_r(\Delta t) = km_p\Delta t/(N_0\Delta V)$ is the probability for a single reaction event, m_p is the mass carried by each particle, N_0 is the total number of particles. Without loss of generality, we set here $m_p = 1$. The local reaction volume $\Delta V = \pi r^2$, where the reaction radius is chosen as $r = \sqrt{24D\Delta t}$ (Benson and Meerschaert, 2008). The impact of the choice of the reaction radius on the overall reaction behavior is studied in Perez et al. (2019b). The occurrence of a reaction event is determined through a Bernoulli trial based on the survival probability (5.15). If the reaction occurs, the B particle and the closest A particle are removed and a particle C is placed at the middle point of the A and B particle locations. Note that these details on removal of A and B and placing the C particles have no impact on the simulated reaction behavior or the equivalence of the particle scheme with the ADRE derived in the previous section. The motion of the produced C particles follows (5.14). The total number of C particles, or total mass, is calculated as

$$m_C(t) = N_c(t). \tag{5.16}$$

where $N_c(t)$ is the number of C particles at time t. The equivalence between this reactive RWPT method and the Eulerian reactive transport formulation (5.3) and

its validation can be found in Perez et al. (2019b). Appendix A.1 discusses the impact of finite particle numbers on the product mass. Based on this assessment, the simulations use a total number of $N_0 > 10^6$ particles.

In order to illustrate the concentration fields formed by the particles in the RWPT model, we use an adaptive Gaussian kernel density estimator (Botev et al., 2010),

$$c_i(\mathbf{x}, t) = \sum_{p=1}^{N_c(t)} K_h \left(\mathbf{x} - \mathbf{x}_{p,i}(t)\right), \tag{5.17}$$

where $i = A, B, C$, $\mathbf{x}_{p,i}(t)$ is location of the pth particle of species i, and $K_h(\mathbf{x})$ is a Gaussian probability density function of mean $\mathbf{0}$ and variance h^2. The bandwidth h is determined according to the procedure detailed in Botev et al. (2010). Note that other authors have used kernel density estimators for accurate predictions on local solute mixing and reactive transport in case of limited particle numbers (Fernàndez-Garcia and Sanchez-Vila, 2011; Rahbaralam et al., 2015; Sole-Mari and Fernàndez-Garcia, 2018). The reactive random walk simulation according to the algorithm described above does not require kernel density estimators. In fact, we make sure that the particle number is sufficiently high to avoid finite size effects, as discussed in Appendix A.1. Here, the reconstruction of the concentration fields with kernel density estimator is only used to illustrate the concentration distributions of the reacting species.

5.2.2.2 Numerical setup

We consider here three advection-dominated transport scenarios with $Pe = 14, 48$ and 96 whose specific parameters are detailed in Table 5.1. The Damköhler number is for all scenarios $Da > 5$ such that reactions at times larger than τ_v can be considered instantaneous. The $DaPe$ number is $DaPe > 70$. Thus, reactive transport is strongly affected by incomplete mixing and the system cannot be considered well-mixed for a wide range of times. The reactive transport problem is solved with the random walk particle tracking simulator described in the previous section. As initial condition, we consider uniform areal distributions of A and B particles from $x = -3 \cdot 10^{-1}$ m to $x = 0$ m and $x = 0$ m to $x = 3 \cdot 10^{-1}$ m, respectively. The characteristic reaction time is $1/c_0 k = 10^{-2}$ s, the time step is $\Delta t = 10^{-2}$ s. The reaction radius is equal to $r = \sqrt{24 D \Delta t}$. Note that the chosen diffusion coefficients are high with respect to the values of solutes in water but comparable to the ones reported for NAPL contaminants (Lee and Chrysikopoulos, 1995). The number of particles required to suppress finite size effects, this means, artificial incomplete mixing, depends on the Péclet number, see also Appendix A.1.

5.2.3 The lamella concept and effective dispersion

In this section, we briefly summarize the concept of the stretched lamella (Ranz, 1979) to quantify the concentration content of a solute under the action of ad-

Table 5.1: Parameters applied on the reactive RWPT model.

	$Pe = 14$	$Pe = 48$	$Pe = 96$
D (m^2/s)	$2 \cdot 10^{-6}$	$4.5 \cdot 10^{-7}$	$2.25 \cdot 10^{-7}$
v_0 (m/s)	$8.5 \cdot 10^{-3}$	$6.5 \cdot 10^{-3}$	$6.5 \cdot 10^{-3}$
N_0	$6 \cdot 10^5$	10^6	$3 \cdot 10^6$

vection and diffusion. Then we present an alternative approach, termed here the dispersive lamella based on the concept of effective dispersion (Kitanidis, 1988; Dagan, 1990; Dentz and Carrera, 2007). To this end, we consider an instantaneous line injection perpendicular to the direction of flow in the channel, this means $c(\mathbf{x}, t = 0) = \delta(x)/2a$. The concentration $c(\mathbf{x}, t)$ can be represented in terms of the Green function $g(\mathbf{x}, t|y')$ as

$$c(\mathbf{x}, t) = \frac{1}{2a} \int_{-a}^{a} dy' g(\mathbf{x}, t|y'), \tag{5.18}$$

where $g(\mathbf{x}, t|y')$ satisfies

$$\frac{\partial g(\mathbf{x}, t|y')}{\partial t} + u(y) \frac{\partial g(\mathbf{x}, t|y')}{\partial x} - D\nabla^2 g(\mathbf{x}, t|y') = 0, \tag{5.19}$$

for the initial condition $g(\mathbf{x}, t|y') = \delta(x)\delta(y - y')$ and no-flux boundary conditions at the horizontal boundaries. The lamellar approaches discussed in the following can be seen as approximations for the Green function $g(\mathbf{x}, t|y')$, for which in general no closed form analytical solution can be found.

5.2.3.1 The stretched lamella

In order to quantify the impact of fluid deformation and the associated mixing behavior on chemical reactions, Ranz (1979) developed the lamellae method. This method has been the basis for the quantification of mixing and reaction in heterogeneous flow fields (Ranz, 1979; Duplat and Villermaux, 2008; Meunier and Villermaux, 2010; Villermaux, 2012; Le Borgne et al., 2013; Borgne et al., 2014; de Anna et al., 2014b; Bandopadhyay et al., 2017). The lamella approach decomposes the material line into a set of non-interacting infinitesimal linear line segments (lamellae), which are transported purely advectively, are deformed by the action of the flow field, and mix with the ambient fluid due to diffusion as illustrated in Figure 5.1. The concentration content along the parabolic front is determined by diffusion and the local shear deformation. The concentration in the center, where the shear deformation is minimum, is much lower than at the sides where shear is increasing. The stretched lamella approach, described in the following, approximates the Green function $g(\mathbf{x}, t|y')$.

First, the advection-diffusion problem is transformed into the coordinate system of a purely advectively transported strip, which deforms and rotates a according to the flow action, see Figure 5.1. A strip located at the vertical position

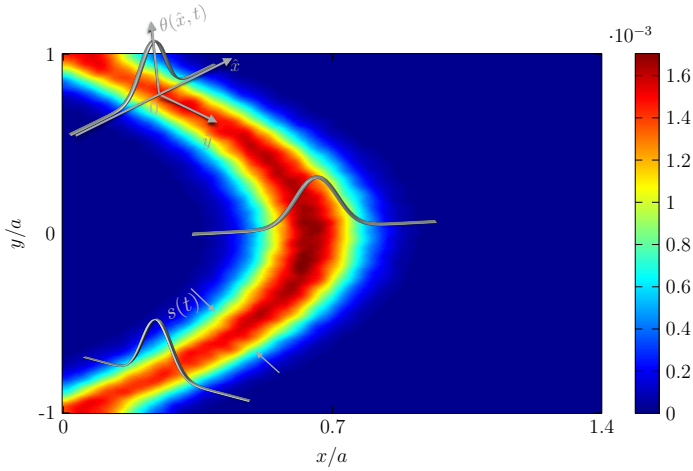

Figure 5.1: Illustration of the stretched lamella approach (after Villermaux, 2012). The lamella elongates due to flow deformation and mixes due to diffusion. The concentration profile across a lamella is Gaussian shaped. The concentration map is obtained by random walk particle tracking for a line injection, $Pe = 96$ at $t = 20\tau_v$.

y' moves with the constant velocity $u(y')$ and deforms and rotates due to shear action $\alpha(y') = du(y')/dy'$. The coordinate transform is

$$\hat{\mathbf{x}} = \mathbf{A}^\top(t|y')\left[\mathbf{x} - \mathbf{x}_a(t|y')\right], \qquad \mathbf{x}_a(t|y') = \begin{bmatrix} u(y')t \\ y' \end{bmatrix}, \tag{5.20}$$

where $\mathbf{A}(t|y')$ is the orthogonal matrix

$$\mathbf{A}(t|y') = \frac{1}{\lambda(t)^2}\begin{bmatrix} \alpha(y')t & -1 \\ 1 & \alpha(y')t \end{bmatrix} \tag{5.21}$$

which rotates into the coordinate system, whose x'-axis is perpendicular to the strip. Note that the strip orientation and length are given by

$$\delta\mathbf{z}(t|y') = \delta y \begin{pmatrix} \alpha(y')t \\ 1 \end{pmatrix}, \qquad \lambda(t|y') = \frac{|\delta\mathbf{z}(t|y')|}{\delta y'} = \sqrt{1 + \alpha(y')^2 t^2}, \tag{5.22}$$

where $\delta y'$ is the infinitesimal initial strip length. The Green function $g(\mathbf{x}, t|y')$ is expressed in terms of the Green function $\hat{g}(\hat{\mathbf{x}}, t|y')$ in the moving coordinate system as

$$g(\mathbf{x}, t|y') = \hat{g}\left(\mathbf{A}^\top(t|y')\left[\mathbf{x} - \mathbf{x}_a(t|y')\right], t|y'\right). \tag{5.23}$$

By inserting the latter into Eq. (5.19), we obtain after some algebra

$$\frac{\hat{g}(\hat{\mathbf{x}},t|y')}{\partial t}+\boldsymbol{\epsilon}(t|y')\hat{\mathbf{x}}\cdot\nabla\hat{g}(\hat{\mathbf{x}},t|y')-D\nabla^2\hat{g}(\hat{\mathbf{x}},t|y')=0, \tag{5.24}$$

where $\boldsymbol{\epsilon}(t|y')$ is the deformation rate tensor in the moving coordinate system,

$$\boldsymbol{\epsilon}(t|y')=\frac{1}{\lambda(t)^2}\begin{bmatrix}\alpha(y')^2t & \alpha(y')^3t^2-\alpha(y')\\ 0 & -\alpha(y')^2t\end{bmatrix}. \tag{5.25}$$

Typically mass transfer across the strip is disregarded and the Green function only depends on the coordinate x' perpendicular to the strip,

$$\hat{g}(\hat{\mathbf{x}},t|y')=\lambda(t|y')\theta(\hat{x},t|y')\delta(y-y'), \tag{5.26}$$

where $\theta(\hat{x},t|y')$ satisfies

$$\frac{\partial\theta(\hat{x},t|y')}{\partial t}-\gamma(t|y')\hat{x}\frac{\partial\theta(\hat{x},t|y')}{\partial\hat{x}}-D\frac{\partial^2\theta(\hat{x},t|y')}{\partial\hat{x}^2}=0. \tag{5.27}$$

The elongation rate $\gamma(t|y')$ is defined by

$$\gamma(t|y')=\frac{1}{\lambda(t|y')}\frac{d\lambda(t|y')}{dt}=\frac{\alpha(y')^2t}{1+\alpha(y')^2t^2}. \tag{5.28}$$

Note that in this approach, the lamellae do not sample the transverse velocity contrast and do not interact. They are independent. They displace due to advection only and mix due to stretching enhanced diffusion. Dispersion of the interface in this approach is ballistic because each lamella moves at its own constant velocity $u(y')$.

Here we approximate the shear rate $\alpha(y)$ by its vertical average

$$\alpha(y)\approx\overline{\alpha}=\frac{1}{2a}\int_{-a}^{a}dy\alpha(y)=\frac{v_0}{a}. \tag{5.29}$$

In this approximation, $\gamma(t|y')=\gamma(t)$, $\lambda(t|y')=\lambda(t)$ and $\theta(\hat{x},t|y')=\theta(\hat{x},t)$ are independent from y'. Equation (5.27) is the basis for the lamellar reaction model used in Section 5.4. The chemical reaction is solved for a single lamella and the overall reactivity is obtained by integration over all stretched lamellae.

We emphasize that the stretched lamella approach is based on non-interacting lamellae, this means, the merging of lamellae due to transverse diffusion and the sampling of the vertical flow contrast are not taken into account in this model. Each lamella remains on its initial streamline. Thus, when one considers the overall dispersion of the line, it increases ballistically because each line segment moves at its initial velocity $u(y')$. This approximation fails at times that are of the order of the diffusion time over the channel cross-section, $\tau_D=(2a)^2/2D$.

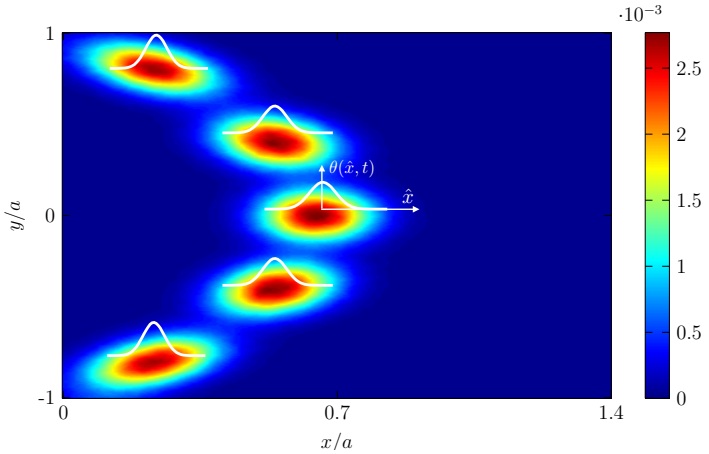

Figure 5.2: Illustration of the dispersive lamella approach. Concentration $g(\mathbf{x}, t|y')$ evolving from point injections at $y' = -0.8, -0.5, 0, 0.5, 0.8\, a$ at $t = 20\tau_v$ for $Pe = 96$. The concentration profile across a lamella is a Gaussian whose width is described by $\sigma_e(t)$.

5.2.3.2 The dispersive lamella

Here we present an alternative approach based on the concept of effective dispersion to account for the action of transverse diffusion. In the stretched lamella approach, the concept of the lamella describes a material element that deforms and diffuses in the flow field. In the dispersive lamella approach proposed here, the lamella describes a material element that disperses as a result of the diffusive sampling of the vertical velocity contrast. This concept is illustrated in Figure 5.2, which shows the evolution of the Green function $g(\mathbf{x}, t|y')$ from point sources at different positions in the channel cross section. As pointed out above, the plumes close to the channel boundaries are more deformed and thus disperse more than those located in the center. This deformation is accounted for in the stretched lamella approach. With increasing time, however, a lamella samples the velocity contrast across the channel cross section due to transverse diffusion, and eventually covers the whole cross section as shown in Figure 5.3. This mechanism, which leads to the phenomenon of Taylor dispersion, is not accounted for in the stretched lamella approach.

Here, instead of transformation into the coordinate system of a purely advectively transported strip, we transform into the coordinate system that moves with the center of mass $m(t|y')$ of the Green function $g(\mathbf{x}, t|y')$. The position

vector in the transformed system is thus

$$\hat{\mathbf{x}} = \begin{bmatrix} x - m(t|y') \\ y \end{bmatrix}, \qquad m(t|y') = \int d\mathbf{x} x g(\mathbf{x}, t|y'). \tag{5.30}$$

The Green function then reads in terms of the Green function $\hat{g}(\hat{\mathbf{x}}, t|y')$ as

$$g(\mathbf{x}, t|y') = \hat{g}[x - m(t|y'), y, t|y']. \tag{5.31}$$

Inserting the latter into Eq. (5.19), we obtain

$$\frac{\partial \hat{g}(\hat{\mathbf{x}}, t|y')}{\partial t} + v'(y, t|y') \frac{\partial^2 \hat{g}(\hat{\mathbf{x}}, t|y')}{\partial \hat{x}^2} - D\hat{\nabla}^2 \hat{g}(\hat{\mathbf{x}}, t|y') = 0, \tag{5.32}$$

where $v'(t|y')$ is the velocity fluctuation around the center of mass velocity,

$$v'(y, t|y') = u(y) - v(t|y'), \qquad v(t|y') = \frac{m(t|y')}{dt}. \tag{5.33}$$

Transformation into the coordinate system that evolves with the center of mass velocity $v(t|y')$, guarantees that the effect of transverse diffusion on the interface shape is accounted for correctly. Recall, that the stretched lamella approach gives a ballistic interface evolution at all times. In order to account for the impact of diffusive sampling of the vertical velocity contrast on the interface evolution, we approximate $\hat{g}(\hat{\mathbf{x}}, t|y')$ by the following projection

$$\hat{g}(\hat{\mathbf{x}}, t|y') \approx G(y, t|y') \theta(\hat{x}, t|y'), \tag{5.34}$$

where $\theta(\hat{x}, t|y')$ is the vertically integrated concentration defined by

$$\theta(\hat{x}, t|y') = \int_{-a}^{a} dy \hat{g}(\hat{\mathbf{x}}, t|y'), \tag{5.35}$$

and

$$G(y, t|y') = \int_{-\infty}^{\infty} d\hat{x} \hat{g}(\hat{\mathbf{x}}, t|y'), \tag{5.36}$$

is the Green function for transverse diffusion. The vertically integrated $\theta(\hat{x}, t|y')$ satisfies the transport equation

$$\frac{\partial \theta(\hat{x}, t|y')}{\partial t} - D^e(t|y') \frac{\partial^2 \theta(\hat{x}, t|y')}{\partial \hat{x}^2} = 0, \tag{5.37}$$

see Appendix A.2. The effective dispersion coefficient $D^e(t|y')$ describes the rate of change of the variance of $g(\mathbf{x}, t|y')$ in flow direction,

$$D^e(t|y') = \frac{1}{2} \frac{d\sigma^2(t|y')}{dt}, \qquad \sigma^2(t|y') = \int d\mathbf{x} \left[x - m(t|y')\right] g(\mathbf{x}, t|y'). \tag{5.38}$$

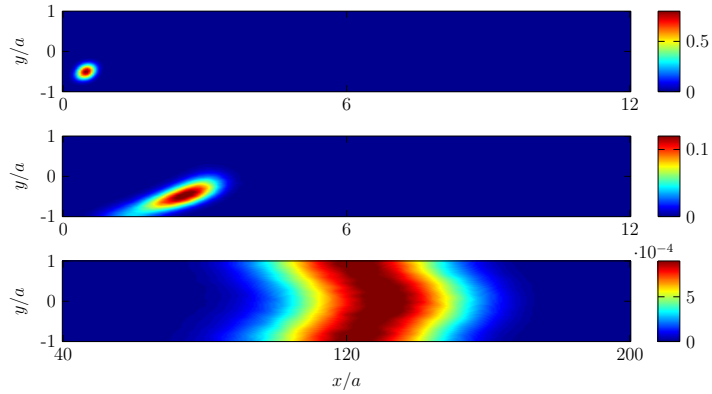

Figure 5.3: Evolution of the concentration distribution $g(\mathbf{x}, t|y')$ evolving from a point injection at $y' = -0.5\,a$ at (top to bottom) $t = 3.5, 70\,\tau_v$ and τ_D for $Pe = 62$.

Equation (5.37) characterizes the concentration content of a dispersive lamella, which deforms due to the action of the flow field and disperses due to vertical sampling of the flow variability by transverse diffusion as illustrated in Figures 5.2 and 5.3. Thus, it accounts for the diffusive sampling across the cross section which is disregarded by the stretched lamella approach.

Exact analytical expressions for $m(t|y')$ and $\sigma^2(t|y')$ can be found in Dentz and Carrera (2007). Note that $m(t|y') = v(y')t$ at $t \ll \tau_D$ and $m(t|y') = v_m t$ at $t \gg \tau_D$. Similarly, $\sigma^2(t|y') = 2Dt$ for $t \ll \tau_D$ and $\sigma^2(t|y') = 2Dt + 2\mathcal{D}t$ for $t \gg \tau_D$, where $\mathcal{D} = 2v_m^2 a^2/105D$ is the Taylor dispersion coefficient (Taylor, 1953). The effective dispersion coefficient $D^e(t|y')$ has been studied in detail in Dentz and Carrera (2007). In the following, we approximate $D^e(t|y')$ by its average over the channel cross section,

$$D^e(t) = \frac{1}{2a}\int_{-a}^{a} dy' D^e(t|y'). \tag{5.39}$$

Thus, $\theta(\hat{x}, t|y') = \theta(\hat{x}, t)$ is independent from y'. The effective dispersion coefficient represents the average dispersion of the initial line source. The corresponding effective variance is

$$\sigma_e^2(t) = \frac{1}{2a}\int_{-a}^{a} dy' \sigma^2(t|y'). \tag{5.40}$$

The effective dispersion coefficient $D^e(t)$ can be written as (Dentz and Carrera, 2007)

$$D^e(t) = 2D^a(t) - D^a(2t), \tag{5.41}$$

where $D^a(t)$ is the apparent dispersion coefficient. It is obtained from the apparent variance $\sigma_a^2(t)$

$$\sigma_a^2(t) = \frac{1}{2a} \int_{-a}^{a} dy' \int d\mathbf{x}(x - v_m t)^2 g(\mathbf{x}, t|y'), \tag{5.42}$$

which measures the spread of the solute distribution $c(\mathbf{x}, t)$ about its center of mass position $v_m t$. The apparent dispersion coefficient $D^a(t)$ is defined in analogy to (5.38) as

$$D^a(t) = \frac{1}{2} \frac{d\sigma_a^2(t)}{dt}. \tag{5.43}$$

As a consequence of (5.41), the effective variance $\sigma_e^2(t)$ can be written as

$$\sigma_e^2(t) = 2\sigma_a^2(t) - \frac{\sigma_a^2(2t)}{2}. \tag{5.44}$$

We obtain an explicit analytical expression for $D^e(t)$ by noting that Haber and Mauri (1988) developed the following analytical expression for $\sigma_a^2(t)$ for two-dimensional laminar flow

$$\sigma_a^2(t) = 2Dt + 2\mathcal{D}t \left(1 - \frac{1 - e^{-\phi \frac{\pi^2 Dt}{4a^2}}}{\phi \frac{\pi^2 Dt}{4a^2}} \right), \tag{5.45}$$

where $\phi = (n+1)^2$ with n the number of symmetry planes of the flow. For the channel flow under consideration here $\phi = 4$. Using the approximation (5.45) in (5.41) and (5.44) gives explicit expressions for the effective dispersion coefficient and variance. Figure 5.4 shows the evolution of the effective and apparent variances $\sigma_e^2(t)$ and $\sigma_a^2(t)$ determined from numerical random walk simulations and the analytical expressions based on (5.45). At early times for $t < \tau_v$ both variances behave in the same way as $2Dt$. For increasing times, $\tau_v < t < \tau_D$, $\sigma_a^2(t)$ grows faster than $\sigma_e^2(t)$ due to advective deformation (spreading) of the solute front. When $t > \tau_D$ both variances converge towards the same behavior of $2(D + \mathcal{D})st$. The analytical solutions compare well with the numerical data.

Equation (5.37) with $D^e(t|y') = D^e(t)$ is the basis for the dispersive lamella approach employed in Section 5.4 for the prediction of reactive transport. The reactive transport problem is solved for a single dispersive lamella. The overall reactivity is then obtained by integration over all dispersive lamellae that evolve from the initial solute distribution.

5.3 Mixing and reaction in the flow through a channel

In this section, we study mixing and reaction in channel flow for the scenarios described in Section 5.2.2.2. Figures 5.5 and 5.6 shows the concentration maps

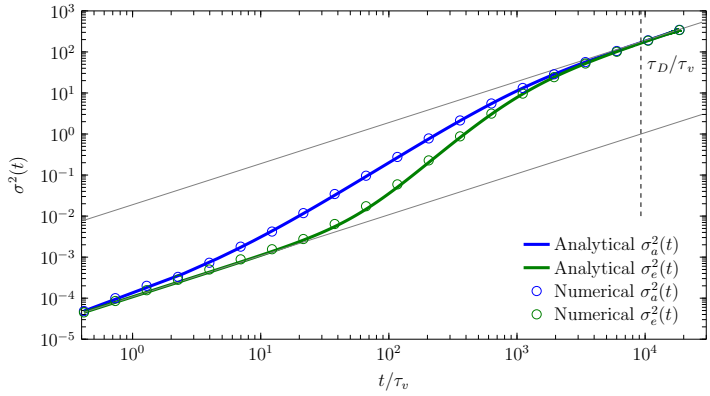

Figure 5.4: Evolutions of $\sigma_a^2(t)$ and $\sigma_e^2(t)$ from RWPT (symbols) and the analytical approximations (5.44) and (5.45) (solid lines) for the setup characterized by $Pe = 96$. The grey solid lines denote the limits behaviors (lower) $2Dt$ and upper $2(D + \mathcal{D})t$.

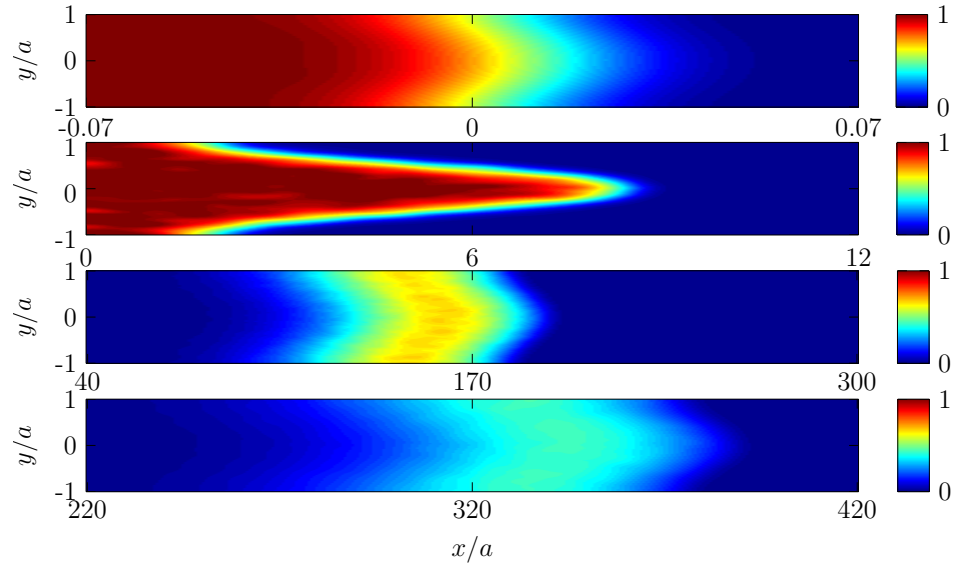

Figure 5.5: Concentration maps of A at times (top to bottom) $t = 0.4, 290\,\tau_v, \tau_D$ and $2\tau_D$ for $Pe = 96$.

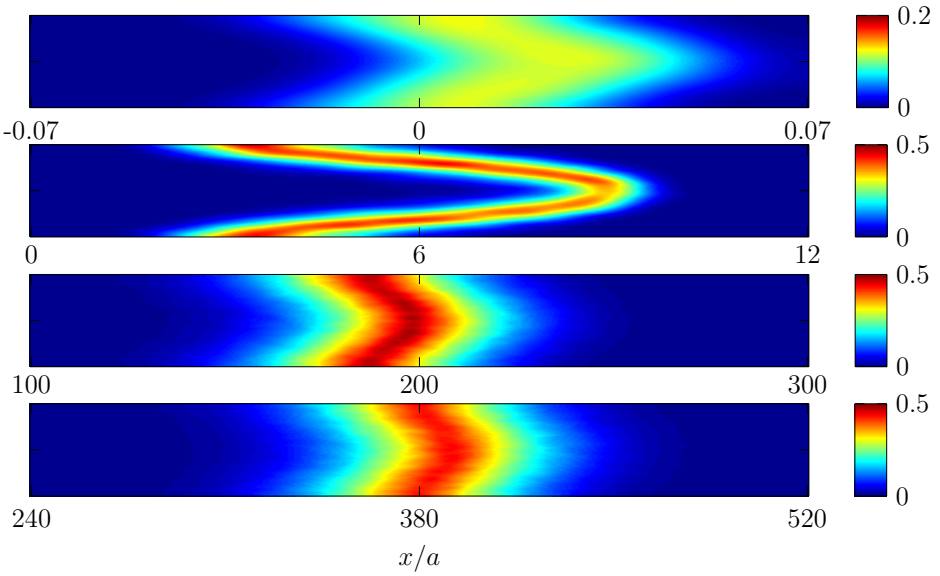

Figure 5.6: Concentration maps of C at times (top to bottom) $t = 0.4, 290\,\tau_v, \tau_D$ and $2\tau_D$ for $Pe = 96$.

of reactant A and product C for $Pe = 96$. The evolution of the product mass is shown in Figure 5.7 for the three Pe under consideration. The evolution of the reaction front is governed by the competition between diffusive expansion and the deformation caused by the velocity field. At early times, $t \leq \tau_v$, molecular diffusion controls the chemical reaction through mass transfer across the interface (Raje and Kapoor, 2000; de Anna et al., 2014a,b). The distribution of the product concentration is uniform in the vertical direction and it behaves according to (5.7) along x. The product mass in this regime increases diffusively according to (5.8) as illustrated in Figure 5.7.

For increasing times $\tau_v \leq t \ll \tau_D$, the interface deforms following the parabolic velocity profiles and its shape is described by $x_f(y,t) = u(y)t$. The interface length increases and as a result the global reactivity increases. Flow variability enhances the reaction efficiency compared to uniform flow as pointed out by Kapoor et al. (1998). The impact of deformation of the mixing front is analogous to observations made at the Darcy scale in heterogeneous flows (Barros et al., 2012; Borgne et al., 2014).

For times $\tau_v \ll t \leq \tau_D$, the interface length decreases due to diffusive mixing across the channel, which may be seen as the diffusive coalescence of the lamellar segments that make up the interface (see also the discussion in de Anna et al., 2014b). The growth rate of the product mass decreases. For times $t \gg \tau_D$, the interface straightens and the system can be considered well-mixed in the cross-section of the channel. The interface width can be described by the Taylor

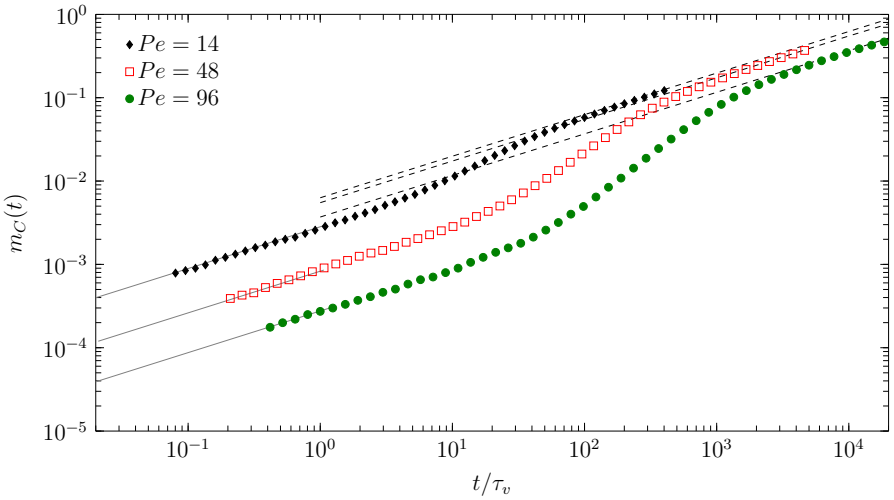

Figure 5.7: The evolution of $m_C(t)$ obtained from reactive RWPT for different Pe is shown by symbols. The early time estimation of the product mass evolution (5.8) is shown by solid lines, the late time evolution given by (5.8) parameterized by the Taylor dispersion coefficient $\mathcal{D}$ is denoted by dashed lines.

dispersion coefficient (Taylor, 1953), which here is given by $\mathcal{D} = 2v_m^2 a^2/105D$. Taylor dispersion quantifies the impact of the interplay of interface deformation and diffusive coalescence on asymptotic mixing. Despite the finiteness of the initial distributions of A and B, mass production is well described by (5.8) for $D = \mathcal{D}$ as illustrated in Figure 5.7. This is further discussed in the next section. Note that extrapolation of the asymptotic behavior to pre-asymptotic times $t < \tau_D$, may significantly overestimate the reactivity. The reason is that at times $\tau_v < t < \tau_D$ the system is characterized by incomplete mixing. In the following, we investigate the quantification of the evolution of the reaction efficiency with emphasis on stretching and coalescence behavior during the intermediate time regime $\tau_v < t < \tau_D$ and the transition to the asymptotic Taylor regime.

5.4 Incomplete mixing

As pointed out in the previous section, the asymptotic reactive transport description in terms of the Taylor dispersion coefficient does not quantify properly the chemical reaction at pre-asymptotic times, for which the species concentrations are not fully mixed transversely. In the following, we first apply the stretched lamella approach to account for the impact of the deformation of the interface between the A and B species on the overall reactivity. Then, we develop an approach, termed the dispersive lamella, to capture the full reaction behavior, which relies on the concept of effective dispersion. This approach relies on the

quantification of the effective interface width and its evolution and accounts for both stretching enhanced mixing and diffusive coalescence.

5.4.1 The stretched lamella

We first model the system reactivity using the stretched lamella approach, which describes the evolution of concentration by Eq. (5.27), where we set $\alpha = \overline{\alpha}$ such that $\gamma(t|y') = \gamma(t)$. Thus, reaction and diffusion across a single lamella are described by (see also, Bandopadhyay et al., 2017)

$$\frac{\partial \theta_i(\hat{x},t)}{\partial t} - \gamma(t)\hat{x}\frac{\partial \theta_i}{\partial \hat{x}} + D\frac{\partial^2 \theta_i(\hat{x},t)}{\partial \hat{x}^2} = -k\theta_A(\hat{x},t)\theta_B(\hat{x},t) \tag{5.46a}$$

$$\frac{\partial \theta_C(\hat{x},t)}{\partial t} - \gamma(t)\hat{x}\frac{\partial \theta_i}{\partial \hat{x}} + D\frac{\partial^2 \theta_C(\hat{x},t)}{\partial \hat{x}^2} = k\theta_A(\hat{x},t)\theta_B(\hat{x},t), \tag{5.46b}$$

where $\hat{x}$ is the direction perpendicular to the direction of stretching, D stands for the diffusion coefficient, and $i = A, B$. This problem can be solved for fast reactions, which gives for the concentration of C

$$\theta_C(\hat{x},t) = \frac{2ac_0}{2}\mathrm{erfc}\left[\frac{|\hat{x}|}{\sqrt{2s(t)}}\right], \tag{5.47}$$

for $L \to \infty$ in the initial conditions (5.6), see Appendix (A.3.2). The concentration of C in the strip coordinate system is obtained by using (5.26) as

$$c_C(\hat{x},t) = \frac{1}{2a}\int_{-a}^{a} dy'\lambda(t|y')\theta_C(\hat{x},t)\delta(y-y') = \lambda(t)\frac{c_0}{2}\mathrm{erfc}\left[\frac{|\hat{x}|}{\sqrt{2s(t)}}\right] \tag{5.48}$$

The total product mass is then given by integration over space according to (5.4), which gives for the total mass

$$m_C(t) = c_0\sqrt{\frac{2}{\pi}}\ell(t)s(t), \tag{5.49}$$

where $\ell(t) = 2a\lambda(t)$ is the interface length and $s(t)$ its width. Corrections to the species concentration and product mass due to the fact that L is finite here are discussed in Appendix (A.3.2) The interface length and width are approximately given by

$$\ell(t) = 2a\sqrt{1+\overline{\alpha}^2t^2}, \qquad s(t) = \sqrt{\frac{2D(t+\overline{\alpha}^2t^3/3)}{1+\overline{\alpha}^2t^2}}. \tag{5.50}$$

Note that $\ell(t)s(t)$ measures the area of the mixing zone. At times $t \ll \overline{\alpha}^{-1}$ expression (5.49) reduces to (5.8) for reaction-diffusion in uniform flow. For $t \gg \overline{\alpha}^{-1}$, expression (5.49) predicts that

$$m_C(t) = 2c_0a\overline{\alpha}\sqrt{\frac{4D}{3\pi}}t^{3/2}. \tag{5.51}$$

The prediction (5.49) of the product mass is illustrated in Figure 5.8 for $Pe =$ 48 and 96. We omit the data for $Pe = 14$ because it behaves qualitatively in the same way while the time scales τ_D and τ_v are less separated. The stretched lamella model predicts the early time behavior and the behavior in the intermediate regime for $t \ll \tau_D$. Note that the lamellar reaction model is based on independent lamella. As soon as the individual strips start interacting due to diffusion across the channel, the prediction (5.49) breaks down. In the following, we will present an approach that accounts for the full evolution of the product mass.

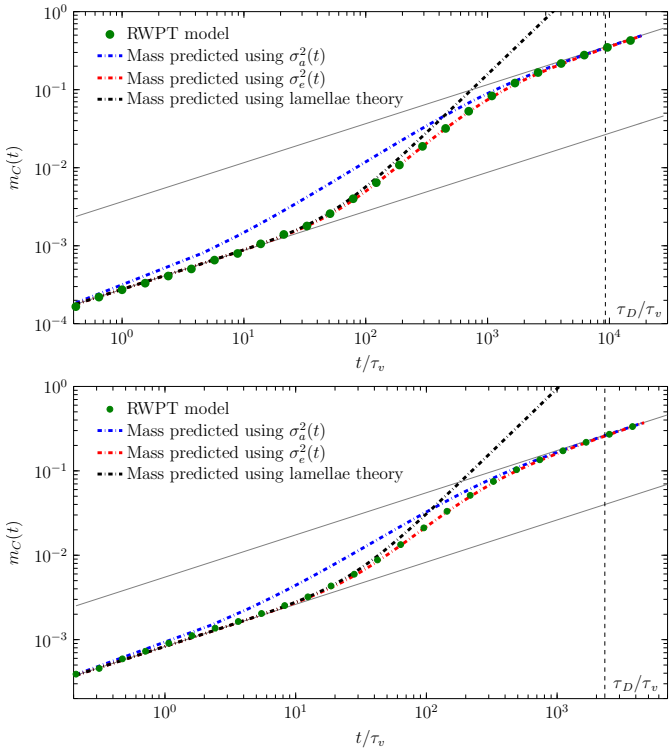

Figure 5.8: Evolution of $m_C(t)$ for (top to bottom) $Pe = 96$, $Pe = 48$ from reactive RWPT (symbols), from the dispersive lamella (5.55) parameterized by (blue dash-dotted line) the apparent variance $\sigma_a^2(t)$ and (red dash-dotted lines) the effective variance $\sigma_e^2(t)$. The black dash-dotted line denotes the evolution of $m_C(t)$ obtained from the stretched lamella (5.49).

5.4.2 The dispersive lamella

The approach outlined in the previous section considers elementary units, lamellae, which make up the initial interface. These lamellae are independent and mass transfer across these non-interacting elementary units is due to diffusion

and the local deformation action of the flow field. As discussed in Section 5.4, the dispersive lamella considers point elements that make up the initial interface, and follow their advective-diffusive motion in the flow field. In this approach, the evolution of the solute concentration is described by (5.37). Thus, the evolution of the species concentrations due to reactions at the interface is given by

$$\frac{\partial\theta_i(\hat{x},t)}{\partial t} - D^e(t)\frac{\partial^2\theta_i(\hat{x},t)}{\partial\hat{x}^2} = -k\theta_A(\hat{x},t)\theta_B(\hat{x},t), \tag{5.52a}$$

$$\frac{\partial\theta_C(\hat{x},t)}{\partial t} - D^e(t)\frac{\partial^2\theta_C(\hat{x},t)}{\partial\hat{x}^2} = k\theta_A(\hat{x},t)\theta_B(\hat{x},t). \tag{5.52b}$$

for $i = A, B$, where we set the effective dispersion coefficient $D^e(t|y') = D^e(t)$ as discussed in Section (5.4). For the initial conditions (5.6) with $L \to \infty$, the concentration of C across the lamella is given by

$$\theta_C(\hat{x},t) = \frac{2ac_0}{2}\mathrm{erfc}\left[\frac{|\hat{x}|}{\sqrt{2\sigma_e^2(t)}}\right], \tag{5.53}$$

see Appendix A.3.3. Using expression (5.34) we obtain for the concentration of C at the interface

$$c_C(\hat{x},t) = \frac{1}{2a}\int_{-a}^{a} dy' G(y,t|y')\theta(\hat{x},t) = \frac{c_0}{2}\mathrm{erfc}\left[\frac{|\hat{x}|}{\sqrt{2\sigma_e^2(t)}}\right]. \tag{5.54}$$

The total mass of C produced is obtained by integration of (5.53) according to (5.4) as

$$m_C(t) = 2c_0\sqrt{\frac{2}{\pi}}a\sigma_e(t), \tag{5.55}$$

see also (5.8). The area of the mixing zone here is given by $2a\sigma_e(t)$. Recall that $\sigma_e(t)$ is a measure for the effective interface width. Corrections due to the finiteness of L are discussed in Appendix A.3.3.

Figure 5.8 shows the evolution of the product mass obtained from the numerical random walk simulations and the analytical estimate (5.55) from the dispersive lamella approach for $Pe = 48$ and 96. As shown in Figure 5.7 the behavior for $Pe = 14$ is qualitatively similar, but the transition regime of incomplete mixing is short. Thus we omit this data here. The dispersive lamella approach gives equally good results for this case.

We have also plotted the evolution of product mass for an interface that evolves with the apparent width $\sigma_a(t)$, For $t < \tau_v$ diffusion dominates and all three approaches agree with the simulations results. For times $\tau_v < t \ll \tau_D$, the stretched and dispersive lamellae provide a good description of the product mass evolution. The interface model based on $\sigma_a(t)$ overestimates the product mass because it overestimates the interface width as discussed above. For times $\tau_v \ll t < \tau_D$, the stretched lamella model fails to predict the simulation data

because it does not account for the diffusive interaction of individual strips. The dispersive lamella on the other hand describes the reaction behavior well also in this interaction regime. In the late time regime $t \gg \tau_D$, both the dispersive lamella model and the interface model based on $\sigma_a(t)$ describe the data very well, while the stretched lamella model fails to match the data. Note that, despite the finite extensions of the initial species concentrations, the solution (5.55) provides a very good estimate even though the distribution of the A species is notably disperse as shown in Figure (5.5). As shown in Appendix A.3.3, expression (5.55) provides a good solution for finite initial extension L of the species concentration as long as $\sigma_e(t) \ll \sqrt{2}L$, which is the case for the times under consideration here. For larger times, the product mass eventually goes toward the constant $m_C(t) = 2aLc_0$, which means all the product species have been consumed. The dispersive lamella approach agrees with the simulation data at all times. In particular, it captures both stretching enhanced mixing and the diffusive coalescence in the intermediate and late time regimes.

5.5 Conclusions

We quantify the impact of flow variability on a fast irreversible bimolecular reactions in Poiseuille flow through a channel. This system shows features of incomplete mixing known for more complex porous media flows, namely the overestimation of the reaction efficiency by the use of macroscale dispersion coefficient, here, the Taylor dispersion coefficient. This overestimation is caused by incomplete mixing on the support scale, which here refers to the channel cross-section. Only when the channel cross-section is completely mixed by transverse diffusion, this means for times greater than the diffusive time scale over the channel cross section $2a$, $\tau_D = (2a)^2/2D$, quantifies the Taylor dispersion coefficient $\mathcal{D} = 2v_m^2 a^2/105D$ a macroscopic mixing effect that account for the interaction of flow variability and diffusion. At preasymptotic times for $t < \tau_D$ this is very different.

We distinguish three different pre-asymptotic behaviors, which are separated by the characteristics advection scale $\tau_v = 2D/v_m$ and the diffusion scale τ_D. The time scale τ_v measures the time at which longitudinal advective and diffusive displacements are equal. At times smaller $t < \tau_v$, the product mass increases $\sim \sqrt{Dt}$ as in a constant plug flow reactor. Mixing and reaction are due to diffusion only. For increasing times $\tau_v < t \ll \tau_D$ the reaction behavior is dominated by the deformation of the diffuse interface, or equivalently, the stretching of the independent lamellae that constitute the interface. The linear growth of the interface length together with the diffusive increase of its width leads to $m_C(t) \sim t^{3/2}$. Then at later times for $\tau_v \ll t < \tau_D$, the lamellae that form the interface start interacting, or coalescing, which marks the cross-over to the Taylor regime for which $m_C(t) \sim \sqrt{(D + \mathcal{D})t}$. Note that on one hand, we observe an increase of reactivity due to the variability of velocity compared to uniform flow and diffusion only. On the other hand, we observe the consequences of incomplete mixing because the asymptotic Taylor dispersion coefficient overestimates the reactiv-

ity. Similar phenomena have been observed for reactive transport on the Darcy scale, where the hydrodynamic dispersion coefficient turns out to overestimate the system reactivity (Gramling et al., 2002; Li et al., 2006; Luo et al., 2008; Tartakovsky et al., 2009). This emphasizes the importance of incomplete mixing and the correct quantification of it for the sound modeling of macroscale reactive transport in heterogeneous flows in general.

The stretched lamella approach (Ranz, 1979; Villermaux and Duplat, 2003; Duplat and Villermaux, 2008; Duplat et al., 2010; Le Borgne et al., 2013; Borgne et al., 2014) is able to quantify the impact of interface deformation and accounts for the impact of preasymptotic incomplete mixing on the system reactivity. The stretched lamella approach can be see as an approximation to the Green function of the advection-diffusion problem in the channel. It considers diffusion and advection in the coordinate system attached to an advectively transported material element, which, upon linearization of the advection term renders an exactly solvable model, which depends on the local deformation properties of the flow field and diffusion. As this model is based on independent lamellae, it does not account for the impact of transverse diffusion on the interface evolution, and thus cannot account for the full evolution of reactivity.

We develop a dispersive lamella approach, which describes the full temporal evolution of the reaction product accurately. Like the stretched lamella approach, the developed model is based on an approximation of the Green function for the advection-diffusion problem. Here, however, we transform into the coordinate system moving with the center of mass velocity of a partial plume representing the Green function. The impact of transverse diffusion on the interface evolution is quantified through a projection operation, which includes vertical averaging across the channel cross section. From this projection emerges an effective equation for the evolution of the Green function which is characterized by the effective dispersion coefficient, which describes the average growth rate of the width of the Green function. In fact, in the moving coordinate system, the evolution of the Green function is governed by a dispersion equation characterized by the time-dependent effective dispersion coefficient $D^e(t)$, which accounts for both stretching enhanced diffusion at early times and front coalescence at late times. Based on an analytical expression for $D^e(t)$, the dispersive lamella quantifies the full evolution of the product mass and particularly the stretching and coalescence processes in a single modeling framework.

The proposed approach can be generalized straightforwardly to three dimensions and randomly stratified porous media, for which expressions for the effective and apparent dispersion coefficients exists both for infinite and confined media (Bolster et al., 2011). Furthermore, the fact that asymptotic (macro) dispersion, here, Taylor dispersion, overestimates mixing and reaction (incomplete mixing) has been observed in porous media on the pore and Darcy scales (e.g., Gramling et al., 2002; Dentz et al., 2011a). Due to this analogy, the findings and modeling approaches in terms of effective dispersion may have an impact for effective reactive transport modeling in heterogeneous flows in a range of applications.

Acknowledgments

We acknowledge the support of the European Research Council (ERC) through the project MHetScale (617511) and the Spanish Ministry of Economy, Industry and Competitiveness-FEDER (CGL2016-80022-R). The numerical data used in the article can be obtained by following the steps and using the parameter values detailed in the paper. We thank Alberto Bellin, Diogo Bolster, he editor Xavier Sanchez-Vila, associate editor Daniel Fernandez-Garcia and two anonymous reviewers for their valuable comments and recommendations.

CHAPTER 6

Upscaling of Mixing-Limited Chemical Reactions in Porous Media

6.1 Introduction

The quantification of the impact of pore structure and flow heterogeneity on chemical reactions in porous media is crucial to several hydrogeological applications such as contaminant transport (Steefel et al., 2005), nuclear waste disposal (Van Loon and Glaus, 1997), and CO_2 sequestration (Chen et al., 2013). In porous media flows, heterogeneity leads to distortion of the mixing interface between different chemical species that affects the global reactivity of the system. The resulting kinetics can then be very different from the ones derived from Fickian theories (Dentz et al., 2011a; Steefel et al., 2005) or in well-mixed reactors at the laboratory (de Anna et al., 2014a; Willingham et al., 2008; Gramling et al., 2002; Raje and Kapoor, 2000).

Mixing is the process by which substances originally segregated into different volumes of space tend to occupy the same volume. Mixing brings reactants together, enabling them to react. Mixing-controlled reactions are usually fast irreversible reactions (Mariani et al., 2010; Pogson et al., 2006; Van Loon and Glaus, 1997), as well as slower reactions whose initial conditions are far from equilibrium (Li et al., 2006). Mixing-controlled reactions can be affected by medium heterogeneity, which enhances the system reactivity if compared to reactions driven by diffusion only (Perez et al., 2019b; Jiménez-Martínez et al., 2015; Rolle et al., 2009; Kapoor et al., 1998), or reducing global reaction behavior when compared to homogeneous media (de Anna et al., 2014a; Gramling et al., 2002; Raje and Kapoor, 2000). In such cases, reactants are not perfectly mixed because the con-

centration of the chemical species displays significant variations within a given pore. Such incomplete mixing among reactants have been observed in nearly homogeneous media (Gramling et al., 2002) and heterogeneous porous media (Boon et al., 2017).

Classical reactive transport models, based on the advection-dispersion-reaction equation (ADRE) assume reactants complete mixing at the scale of interest. The ADRE is defined as

$$\phi \frac{\partial c_i(\mathbf{x},t)}{\partial t} = -\nabla \cdot [\mathbf{q} c_i(\mathbf{x},t) - \mathbf{D} \nabla c_i(\mathbf{x},t)] + r_i), \tag{6.1}$$

where ϕ is porosity, c_i is the concentration of reactant i, $\mathbf{q}$ is Darcy velocity, $\mathbf{D}$ is the dispersion tensor, and r_i represents the space-time-dependent rate at which species i is produced (or removed) by the reaction. The ADRE formulation is based on volume averaging and chemical homogenization. The first assumption neglects incomplete mixing of reactants (Gramling et al., 2002; Raje and Kapoor, 2000) and the second one makes the reaction rate r_i, a crucial term in (6.1) estimated under well-mixed conditions in laboratory experiments, be greater than the observed reaction rate under natural conditions (Dentz et al., 2011a; Tartakovsky et al., 2009; Battiato et al., 2009). Several numerical (Tartakovsky et al., 2009; Battiato and Tartakovsky, 2011), laboratory (de Anna et al., 2014a; Willingham et al., 2008; Gramling et al., 2002; Raje and Kapoor, 2000), and field studies (Hess et al., 2002; Davis et al., 2000) have shown that the mixing assumptions inherent to ADRE models can break down and the results incur in a reaction overprediction of the reactive system.

Recent alternative reactive transport models have explored the link between effective reactivity and heterogeneous flows by studying the kinematics of mixing. Their primary interest lies on the characterization of mixing-limited reactions based on the deformation of the material fluid elements, called lamellae (Ranz, 1979). The lamellar representation provides a powerful approach to quantify the impact of fluid deformation on mixing (de Anna et al., 2014a). This methodology assumes that the effective upscaled reaction rate in chemical systems is controlled by the interface length and width which is generally assumed to grow diffusively with time (Borgne et al., 2014; de Anna et al., 2014a). While this approximation may be reasonable for some systems, it neglects the action of compression on the width of the reaction front (de Anna et al., 2014a). Furthermore, it does not take into account the dynamics of the merged lamellae that form the interface due to transverse diffusion (see Chapter 5). An alternative model proposed by Perez et al. (2019b) allows an accurate description of the evolution of the reactants mixing interface, and thus the chemical reaction, in a spatially variable flow. The methodology called dispersive lamella uses the concept of effective dispersion to account for the action of transverse diffusion. The chemical representation of mixing is based on a reactive random walk particle tracking (RWPT) model that represents the chemical species by particles. Particles react according to some probabilistic rules when they are within some interaction distance. The dispersive lamella model has been shown to match analytical solutions and capture the chemical dynamics in a single tube.

This Chapter focuses on the quantification of the global mixing behavior of an instantaneous irreversible reaction in a complex porous medium. We aim to provide an explicit relation between fluid deformation and its impact on the temporal evolution of chemical reactivity using the dispersive lamella approach. The instantaneous chemical reaction, in the form $A + B \rightarrow C$, allows one to study in detail the role of flow deformation, medium heterogeneity, and diffusion on mixing. This elementary reaction, which can constitute more complex reactions, is frequent in Earth systems and very relevant to large-scale remediation of water contamination by anthropogenic elements such as sulphides (Batens and Van Keer, 2003).

We first investigate the effect of pore structure heterogeneity on the chemical reaction by performing numerical simulations in a 2D synthetic porous medium characterized by a random packing of grains of equal size. We use a reactive RWPT model to simulate the bimolecular reactive transport, which is fully equivalent to the ADRE (see Chapter 2). In addition, the developed dispersive lamella approach in Perez et al. (2019b) is applied to the pore-scale experiment reported by Jiménez-Martínez et al. (2015).

6.2 Analysis of mixing and reaction in a synthetic medium

We aim to investigate the impact of pore structure heterogeneity on the mixing degree of the reactants. We perform a direct numerical simulation to model the fluid-fluid chemical reaction

$$A + B \rightarrow C \tag{6.2}$$

in a 2-D heterogeneous porous medium using a reactive RWPT transport model. We quantify the total amount of the product mass in the porous medium and compare it to an ADRE model prediction (Gramling et al., 2002). In addition, we use the dispersive lamella approach to estimate the full evolution of the global reactivity of the system.

6.2.1 Framework for mixing and reaction at the pore scale

The reactive RWPT model consists of four parts: geometry, flow, particle transport, and reaction. The geometry of the 2D synthetic porous medium consists of a random close packing of equally sized grains. The model dimensions are $L_x \times L_y = 0.0075\text{m} \times 0.002$ m. The grain diameter $d = 0.93 \times 10^{-4}\text{m}$, the average size of pores $L_p = 9 \times 10^{-5}\text{m}$, and porosity $\phi = 0.5$. More details of the generation of the medium can be found in Chapter 2.

We obtain the flow field in the pore space by solving the incompressible Newtonian flow governed by the Stokes equations

$$\nabla \cdot \mathbf{v} = 0, \tag{6.3}$$

$$-\nabla P + \mu \nabla \mathbf{v} = \rho \left(\frac{\partial \mathbf{v}}{\partial t} + \mathbf{v} \cdot \nabla \mathbf{v} \right), \tag{6.4}$$

where $\mathbf{v}$ is the velocity vector (m s^{-1}), P(kg m s^{-2}) is the pressure, ρ is the water density ($\rho = 1000 kg/m^3$), and μ is the dynamic viscosity ($\mu = 10^{-3}$ kg m^{-1} s^{-1}). The Stokes equation were solved using the simpleFOAM solver that belongs to the open-source code OpenFOAM (Weller et al., 1998). We apply constant pressure boundaries conditions at the inlet and the outlet faces of the porous medium, while on the other faces and grains no-slip boundary conditions are implemented. We add 100 layers at the inlet and at the outlet of the domain to minimize boundary effects. Figure 6.1 shows the computed velocity fields at the pore space, with a Reynolds number $Re \ll 1$, defined as $Re = \rho \bar{v} L_y / \mu$ ($\bar{v}$ is the mean flow velocity).

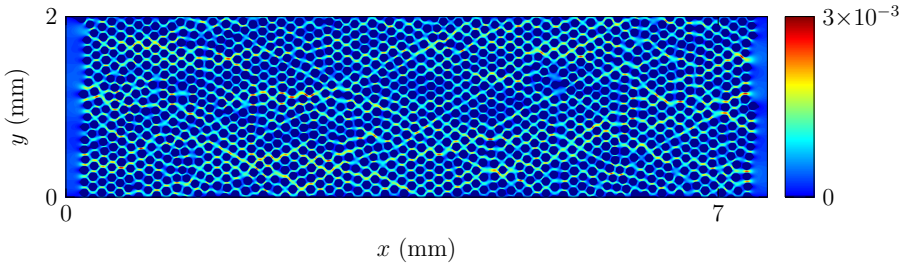

Figure 6.1: Velocity magnitude field (m s^{-1}) in the synthetic heterogeneous porous medium.

We simulate the bimolecular reaction representing the reactants introducing two types of particles A and B. We track the motion of the reactant particles for every time-step Δt (s) by advection and diffusion,

$$\mathbf{x}(t + \Delta t) = \mathbf{x}(t) + \mathbf{v}[\mathbf{x}(t)]\Delta t + \sqrt{2D\Delta t}\boldsymbol{\eta}(t), \tag{6.5}$$

where $\mathbf{x}$ is the position of the particles at time t, $\boldsymbol{\eta}(t)$ are independent distributed Gaussian random variables characterized by $\mathbf{0}$ mean and unit variance, and D ($m^2 s^{-1}$) is the molecular diffusion coefficient. For the advection step, we use a streamline-based approach to move particles through the grid cell developed in Puyguiraud et al. (2019). The method uses a velocity interpolation to honor the no-slip boundary conditions at pore voids bounded by solid walls, which contrasts to Pollock algorithm (Pollock, 1988) commonly used for field and Darcy-scale applications. Particle trajectories are simulated until they exit the synthetic medium or react.

Reaction is simulated following the reactive RWPT methodology presented in Chapter 2. Here, we describe the main features of this work. Initially, species A is placed uniformly at random throughout the pore space between the inlet plane $x = 0.25$mm and $x = 4.25$mm, and there is no B species in the medium($c_B(\mathbf{x}, 0) = 0$). We use this initial spatial distribution of species A to ensure well-mixed conditions of reactants reducing computational cost. Note that placing reactant A all over the domain increases the simulation computational

Parameter	Value
Mean velocity (m s^{-1})	4×10^{-4}
Diffusion coefficient (m^2 s^{-1})	3×10^{-10}
N_{0A}	3×10^6
Peclet number	60

Table 6.1: Transport parameters used in the reactive RWPT model.

cost because the transport and reaction equations will be applied to particles that are near to the outlet of the domain. Particles close to the domain exit do not react as their trajectory leaves the medium in very short time. Thus, reactant A placement guarantees well-mixed conditions, which here means that all reactant particles within an interaction radius, or support volume, have the same reaction probability in a time interval Δt. The reactant B is introduced at the inlet using a flux-weighted injection. At each time step, we record the position of each particle as it migrates through the domain and calculate the distance between a given A particle and a B particle. The probability of reaction P_r of the B particle in the time interval $[t, t + \Delta t]$, depends on the number $N_A[\mathbf{x}(t)]$ of A particles within an interaction well-mixed support volume ΔV centered at the position $\mathbf{x}(t)$ of the B particle as

$$P_r = 1 - \exp\left[-p(\Delta t) N_A\left[\mathbf{x}(t)\right]\right], \tag{6.6}$$

where the probability of a single reaction event $p(\Delta t) = k\Delta t/(N_{0A}\Delta V)$ depends on the chemistry of the problem characterized by the reaction rate coefficient k, and the initial total number of A particles present in the domain N_{0A}. The interaction well-mixed support volume $\Delta V = \pi r^2$ is defined with an effective reaction radius $r = \sqrt{24D\Delta t}$. The selection of r relates to the characteristic diffusive particle displacement during time Δt, which is $\sigma(\Delta t) = 2dD\Delta t$, where d is the spatial dimension. For $r \leq \sigma(\Delta t)$ the support volume may be considered well mixed if $N_0 \to \infty$. Otherwise, $r \geq \sigma(\Delta t)$ in order to capture the local degree of mixing at which reaction takes place. The limits and criteria for the choice of the reaction radius can be found in Chapter 2. The reaction occurs if P_r is bigger than a random uniformly distributed number between 0 and 1. After reaction, the A and B particles are removed and a particle C is placed at the middle point of the A and B particle locations. The migration of C particles in the domain also follows the transport rules specified in equation (6.5).

The reactive transport scenario is characterized by the dimensionless Péclet and Damköhler numbers. The Péclet number, defined as $Pe = L_p\bar{v}/(2D)$, is the ratio of the characteristic diffusion time $\tau_D = L_p^2/(2D)$ and the advective time in a pore $\tau_v = L_p/\bar{v}$. We define the Damköhler number as $Da = \tau_v/\tau_r$, where $\tau_r = 1/(kc_0)$ is the reaction time scale. The considered reactive transport case here is characterized by a $Pe = 60$ and $Da = 3 \times 10^4$. The specific parameters are detailed in Table 6.1.

6.2.2 The dispersive lamella description of mixing

In this section, we present the concept of the dispersive lamella used to quantify the impact of fluid mixing on chemical reactions. This representation of mixing assumes that solutes tend to organize into structures that are formed by the repeated action of advection as they move through heterogeneous media. These structures, called lamellae, can be seen as a decomposition of the mixing front into point elements that disperse as a result of the diffusive sampling of the vertical velocity contrast. This concept of not independent lamellae, called dispersive lamellae, differs from the stretched lamella model (Bandopadhyay et al., 2017; Borgne et al., 2014; Le Borgne et al., 2013; Villermaux, 2012; Meunier and Villermaux, 2010; Villermaux and Duplat, 2003; Ranz, 1979) because of the interacting lamellae. The dispersive lamella approach is based on the concept of effective dispersion and accounts for the action of transverse diffusion in contrast to the stretched lamella model.

We start from a pulse line injection at the inlet of the medium, which is composed of simultaneous point injections,with initial conditions distribution $c_0(\mathbf{x})$. Then, in analogy to section 5.2.3.2, the concentration distribution of each point injection is represented in terms of the Green function $g(\mathbf{x}, t \mid \mathbf{x}')$ as The solute is initial distributed along a line perpendicular to the mean flow direction,

$$c(\mathbf{x}, t = 0) = c_0(\mathbf{x}) = \frac{1}{L_y}\delta(x_1). \tag{6.7}$$

The concentration $c(\mathbf{x}, t)$ satifies the advection-diffusion equation

$$\frac{\partial c(\mathbf{x}, t)}{\partial t} + \mathbf{v}(\mathbf{x}) \cdot \nabla c(\mathbf{x}, t) - D\nabla^2 c(\mathbf{x}, t) = 0, \tag{6.8}$$

which is equivalent to the Langevin equation (6.5). As in section 5.2.3.2, the concentration distribution is represented in terms of the Green function $g(\mathbf{x}, t|\mathbf{x}')$ as

$$c(\mathbf{x}, t) = \frac{1}{L_y}\int_0^{L_y} dy' g(\mathbf{x}, t \mid y'). \tag{6.9}$$

The Green function satisfies (6.8) for the initial condition $g(\mathbf{x}, t = 0|y') = \delta(x)\delta(y - y')$. As in Section 5.2.3.2, we transform into the coordinate system that moves with the center of mass of the Green function

$$\hat{\mathbf{x}} = \mathbf{x} - \mathbf{m}(t \mid y'), \tag{6.10}$$

where

$$\mathbf{m}(t \mid y') = \int d\mathbf{x}\, \mathbf{x} g(\mathbf{x}, t \mid y'). \tag{6.11}$$

Thus, $g(\mathbf{x}, t \mid y')$ can be written in terms of $\hat{g}(\hat{\mathbf{x}}, t \mid y')$, the Green function in the moving coordinate system as

$$g(\mathbf{x}, t \mid y') = \hat{g}\left[\mathbf{x} - \mathbf{m}(t \mid \mathbf{x}'), t \mid y'\right]. \tag{6.12}$$

We now approximate $\hat{g}\left[\hat{\mathbf{x}} - \mathbf{m}(t \mid \mathbf{x}'), t \mid y'\right]$ as

$$\hat{g}(\hat{\mathbf{x}}, t \mid y') \approx \theta(\hat{x}, t \mid y') G(\hat{y}, t \mid y'), \tag{6.13}$$

where $\theta(\hat{x}, t \mid y')$ is the vertically integrated Green function

$$\theta(\hat{x}, t) = \int_0^{L_y} dy\, \hat{g}(\hat{\mathbf{x}}, t \mid y') \tag{6.14}$$

and $G(\hat{y}, t \mid y')$ the longitudinally integrated Green function

$$G(\hat{y}, t \mid y') = \int d\hat{x}\, \hat{g}(\hat{\mathbf{x}}, t \mid y'). \tag{6.15}$$

Both $\theta(\hat{x}, t \mid y')$ and $G(\hat{y}, t \mid y')$ are approximated as Gaussians,

$$\theta(\hat{x}, t \mid y') = \frac{\exp\left[\frac{-(\hat{x}-x')^2}{2\sigma_y^2}\right]}{\sqrt{2\pi\sigma_x^2}}, \tag{6.16}$$

$$G(\hat{y}, t \mid y') = \frac{\exp\left[\frac{-(\hat{y}-y')^2}{2\sigma_y^2}\right]}{\sqrt{2\pi\sigma_y^2}}. \tag{6.17}$$

where $\sigma_x^2(t)$ and $\sigma_y^2(t)$ are the effective spatial variances. The are defined by

$$\sigma_x^2(t) = \int d\mathbf{x}' \int d\mathbf{x}[x - m_x(t \mid y')]^2 g(\mathbf{x}, t \mid y') c_0(\mathbf{x}') \tag{6.18}$$

$$\sigma_y^2(t) = \int d\mathbf{x}' \int d\mathbf{x}[y - m_y(t \mid y')]^2 g(\mathbf{x}, t \mid y') c_0(\mathbf{x}'). \tag{6.19}$$

Note the $\sigma_x^2(t)$ is a measure for the effective interface width. The point injection concept is shown in Figure 6.2, which shows the evolution of the Green function $g(\mathbf{x}, t \mid y')$ from one point source at $y = 0.45$mm. Figure 6.3 shows the vertically and horizontally integrated Green functions obtained from the numerical simulations. They are of Gaussian shape and can be well approximated by (6.16) and (6.17). In addition, we define the apparent variance $\sigma_a^2(t)$

$$\sigma_a^2(t) = \int d\mathbf{x}' c_0(\mathbf{x}') \int d\mathbf{x}[x - \overline{m}_x(t)]^2 g(\mathbf{x}, t \mid y'), \tag{6.20}$$

$$\overline{m}_x(t) = \int d\mathbf{x}' c_0(\mathbf{x}') m_x(t \mid y'), \tag{6.21}$$

which is a measure for the dispersion of the interface.

Figure 6.4 shows the temporal evolution of apparent variance $\sigma_a^2(t)$ and effective variance $\sigma_e^2(t)$. The calculated $\sigma_a^2(t)$ and $\sigma_e^2(t)$ are similar at early times, $t < 1.1 \times 10^{-3}$ pore volume. In this temporal regime, we find that the behavior in both variances is similar to $2Dt$, which suggests a diffusion dominated

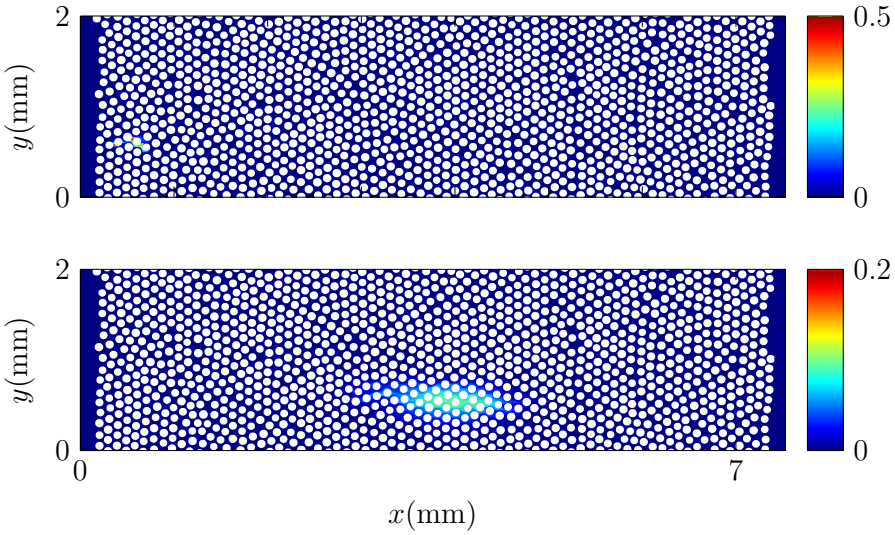

Figure 6.2: Evolution of the concentration distribution $g(\mathbf{x}, t \mid y')$ evolving from a point injection at $y = 3 \times 10^{-4}$ m at $t = 1.1 \times 10^{-3}$ pore volume (top) and $t = 0.28$ pore volume (bottom) for $Pe = 60$.

regime. This observation is reflected in the top-left inset in Figure 6.4 which shows a nearly homogeneous front from the spatial distribution of particles at $t = 1.1 \times 10^{-3}$ pore volume. The snapshot suggests that the front is not affected by the advective heterogeneity yet. For later times, $1.1 \times 10^{-3} < t < 0.45$ pore volume, the apparent variance $\sigma_a^2(t)$ grows faster than the effective variance $\sigma_e^2(t)$ because the plume experiences the velocities contrast from the advective field and is deformed. The advective deformation, or spreading, is responsible for the rapid increase of $\sigma_a^2(t)$ over $\sigma_e^2(t)$. Note that the effect of the advective deformation can be seen in the top-right inset in Figure 6.4, where we see the deformation of the plume.

6.2.3 Reaction behavior at pore scale

In the Fickian approach the reaction support volume is assumed to be well-mixed. In this framework, the evolution of the concentrations c_i can be described by the advection-dispersion-reaction equation (6.1). The global reaction behavior can be characterized by the evolution of the total mass of the reaction product

$$m_C(t) = \int c_C(\mathbf{x}, t) d\mathbf{x}. \tag{6.22}$$

For an instantaneous bimolecular reaction in a nearly homogeneous porous medium Gramling et al. (2002) characterized the evolution for the total mass of

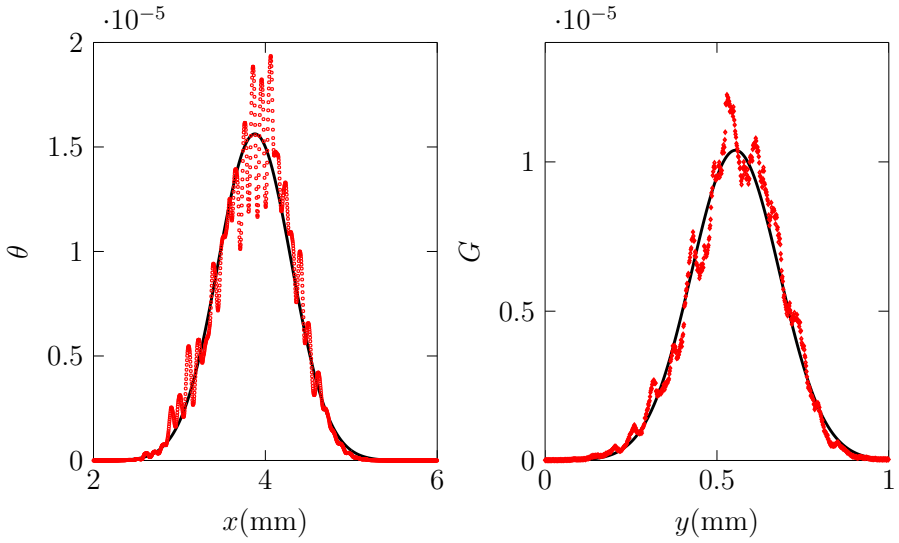

Figure 6.3: Concentration distribution integrated in x and y and predicted Gaussian concentration using σ_x and $m_x(t \mid x')$ (black solid line) in left plot. Concentration distribution integrated in x (red diamonds) and predicted Gaussian concentration using σ_y and $m_y(t \mid y')$ (black solid line) in right plot. Both plots corresponds to a point injection at $y = 4.5 \times 10^{-4}$ m at $t = 0.28$ pore volume for $Pe = 60$.

C from (6.1) as,

$$m_C(t) = c_0 L_y \phi \sqrt{\frac{4 D_h t}{\pi}}, \tag{6.23}$$

where c_0 is a characteristic concentration, and D_h is the hydrodynamic dispersion coefficient that describes the spreading of solutes as defined by

$$D_h = \lim_{t \to \infty} \frac{\sigma_a^2}{2t}. \tag{6.24}$$

The $\sqrt{t}$ scaling of the evolution of the product C mass in (6.23) can be described in terms of the reaction rate, which is equal to the diffusive mass flux at the interface between the two reactants. The mass obtained from (6.23) serves as a reference for observed behaviors in spatially variable flows. Figure 6.5 compares the total mass of product, calculated from the numerical simulations and the analytical prediction (6.23). The analytical solution overpredicts the product mass with respect to the numerical simulation by $\sim$ 27%. This finding agrees with the observations made by Gramling et al. (2002), in which the authors measured the outflow concentrations of the product formed during a mixing-limited reaction.

As suggested by our results in Figure 6.5 and the experimental observations in Gramling et al. (2002), the reactive transport description based on the hydro-

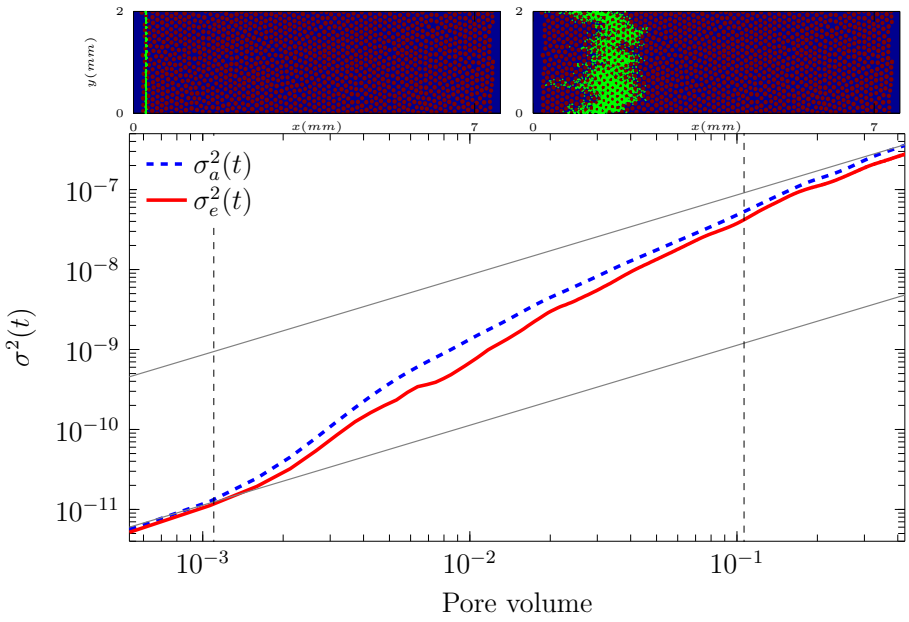

Figure 6.4: Evolutions $\sigma_e^2(t)$ and $\sigma_a^2(t)$ from the RWPT numerical simulation for the studied case characterized by $Pe = 60$. The grey solid lines indicate the behaviors $2Dt$ (lower) and $2D_h t$ (upper). The insets corresponds to the spatial distribution of the pulse injection at $t = 0.0011$ (top-left) and $t = 0.11$ pore volume (top-right). The vertical black dashed lines indicate the time that corresponds to the insets.

dynamic dispersion coefficient does not quantify properly the chemical reaction. For the initial conditions, the concentration of C across the lamella is given by

$$\theta_C(\hat{x}, t) = \frac{L_y c_0}{2}\left[\frac{\mid \hat{x} \mid}{\sqrt{2\sigma_e^2(t)}}\right], \tag{6.25}$$

and the concentration of C at the interface is

$$c_C(\hat{x}, t) = \frac{1}{L_y}\int_0^{L_y} dy' G(\hat{y}, t \mid \mathbf{x}')\theta_C(\hat{x}, t) = \frac{c_0}{2}\text{erfc}\left[\frac{\mid \hat{x} \mid}{\sqrt{2\sigma_e^2(t)}}\right]. \tag{6.26}$$

The total mass of C produced is obtained by integrating (6.26)

$$m_C(t) = \phi\int_0^{L_y} dy \int dx \frac{c_0}{2}\text{erfc}\left[\frac{\mid x \mid}{\sqrt{2\sigma_e^2}}\right], \tag{6.27}$$

which gives

$$m_C(t) = c_0 L_y \phi \sigma_e(t)\sqrt{\frac{2}{\pi}}. \tag{6.28}$$

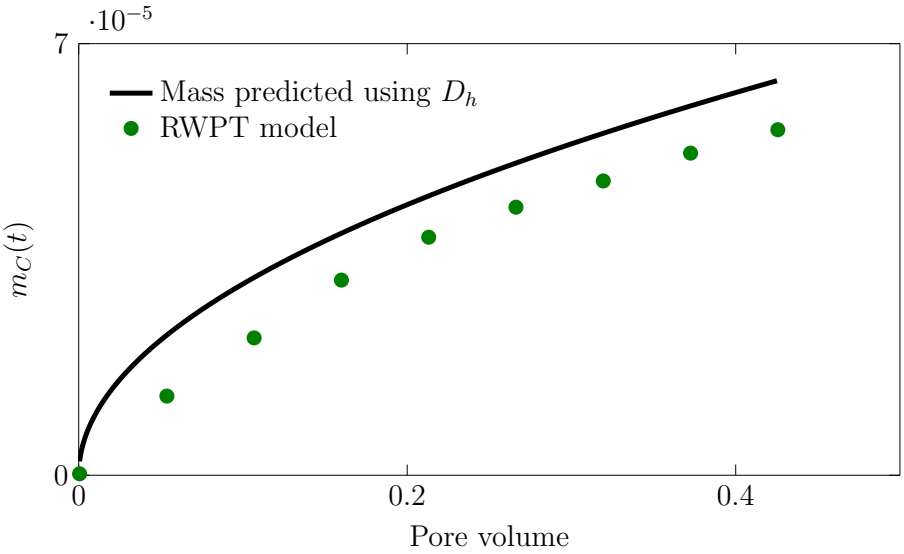

Figure 6.5: Product mass evolutions $m_C(t)$ for $Pe = 60$ from the reactive RWPT simulation in the porous medium (symbols), and from the hydrodynamic dispersion coefficient (black solid line). The analytical solution overpredicts the product total mass in the medium due to complete mixing assumption between reactants. Note that this figure shows the same a behavior as the results from Gramling et al. (2002) in Figure 3.6 in Chapter 3.

This expression accounts for the impact of the interface deformation on the overall reactivity as $L_y\phi\sigma_e(t)$ gives the area of the mixing zone. Figure 6.6 shows the evolution of the C product mass obtained from the reactive RWPT model and the estimate (6.28) from the dispersive lamella approach. For comparison we plot also the evolution of product mass for an interface that evolves with the apparent width $\sigma_a^2(t)$. For early times, $t < 1.1 \times 10^{-3}$ pore volume, diffusion is the main mechanism driving the reaction, as a result mass predictions using $\sigma_a^2(t)$ and $\sigma_e^2(t)$ are similar and agrees with the solution estimated from (6.23) coupled with a constant diffusion coefficient (D). For later times, $t < 1.1 \times 10^{-3} < t < 0.45$ pore volume, advection dominates. We find enhanced-mixing behavior as the product formation increases fast. This occurs due to greater degree of mixing of reactants locally. In this regime, the dispersive lamella approach coupled with $\sigma_e^2(t)$ provides a good description of the C product mass evolution. The increased reaction behavior observed occurs preferentially as the reactant particles sample more of the flow heterogeneity, which increases the width of the interface allowing more mixing. We find that the mass prediction based on $\sigma_a^2(t)$ fails to characterize the evolution of the product mass because it overestimates the reactants interface as discussed above.

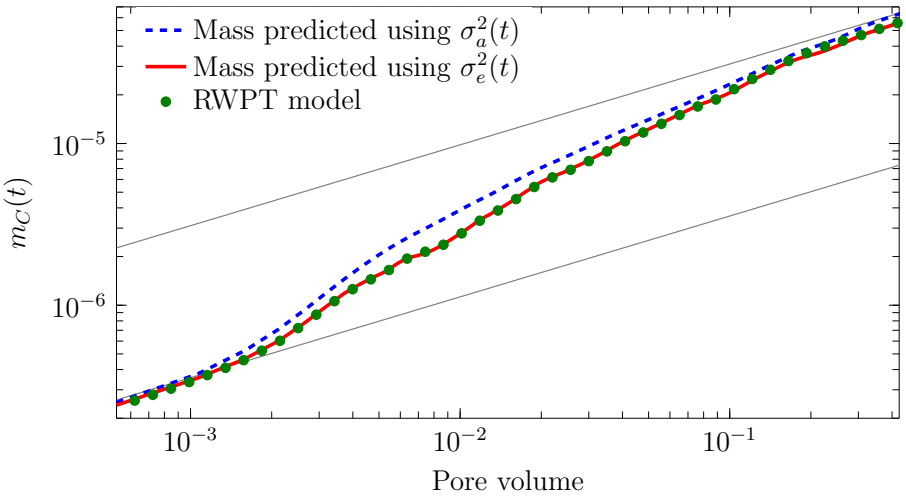

Figure 6.6: Evolutions $m_C(t)$ for $Pe = 60$ from the reactive RWPT simulation (symbols), from the dispersive lamella parameterized by the apparent variance $\sigma_a^2(t)$ (blue dashed-line) and the effective variance $\sigma_e^2(t)$ (red line).

6.3 Analysis of mixing and reaction in Jiménez-Martínez et al. (2015) experimental study

We now aim to validate the dispersive lamella model prediction for the total mass in the reaction (6.2) using the experimental data from Jiménez-Martínez et al. (2015)

6.3.1 Experimental material and reaction methodology

The considered flow cell of Jiménez-Martínez et al. (2015) is a 2D medium composed of circular grains randomly distributed. The geometry is characterized by two length scales, the average pore throat $a = 1.07\,\text{mm}$, and the average pore size $\lambda = 1.75\,\text{mm}$. The porosity and absolute permeability are $\phi = 0.77$ and $\kappa = 7.5 \times 10^3\,\text{mm}^2$. Note that for the image analysis of experimental concentration distributions we used a medium mask that reduced ϕ to 0.5. This helps us to reduce experimental noise in the concentration fields. The size of the medium is 131 mm of length and 82 mm of width, with thickness of 0.5 mm. The inlet consists of a two-layer triangular shape designed to prevent prior mxing of fluids before entering the medium. The fluid used is a 60-40 % by weight water-glycerol solution dyed with Fluorescein, with dynamic viscosity $\nu = 3.72 \times 10^{-2}\text{kg m}^{-1}\,\text{s}^{-1}$ and density $\rho = 1.099 \times 10^3\text{kg} \cdot \text{m}^3$. The measurement of concentrations is performed by light technique (de Anna et al., 2014a). The model is illuminated from below with a panel light source that produces a spatially homogeneous intensity. An optical filter excites the fluorescent tracer and a camera placed on

Parameter	Value
Flow rate ($mm^3\ s^{-1}$)	0.55
Mean velocity ($m\ s^{-1}$)	1.7×10^{-5}
Diffusion coefficient ($m^2\ s^{-1}$)	1.049×10^{-10}
Peclet number	54

Table 6.2: Flow and transport parameters used in Jiménez-Martínez et al. (2015)

top of the model captures light intensity with a resolution of 3545×2279 pixels per image. Later, the light intensity is translated to concentrations by normalizing the intensity within the pixels with the maximum intensity. The measured intensity depends linearly on the concentration on most of the available concentration range, which makes the measurements of small concentrations much more accurate.

The experimental protocol consists of a continuous injection of the solution dyed with fluorescein. The injection is characterized by an imposed controlled flow rate Q between the inlet and outlet boundaries of the cell using a syringe pump. The porous medium is initially saturated with a background solution of low concentration used to distinguish from the water-glycerol solution. The flow and transport parameters are given in table 6.2 We consider that the mixing of the injected liquid and the resident liquid in the experiment, miscible with each other, triggers an instantaneous irreversible chemical reaction in the form (6.2) in order to quantify the impact of mixing on chemical reactivity. These type of reactions are characterized by a reaction time scale τ_r small with respect to the advective time scale τ_v, that is of a Damköhler number $Da = \tau_v/\tau_r \gg 1$.

We use the methodology presented in Gramling et al. (2002), which is a generalized method to quantify fluid mixing in fast reactions in porous media. The general assumption is that the reaction product dynamics can be calculated directly from the conservative species. We describe the instantaneous irreversible chemical reaction (6.2) from the conservative concentration fields of reactant A (c_{A+C}). Note that c_{A+C} is the total molar concentration of reactant A. We now find the expression for the combined concentration of reactant B and product C (c_{B+C}), which is displaced by the inflowing reactant A,

$$c_{B+C}(\mathbf{x}, t) = 1 - c_{A+C}(\mathbf{x}, t). \tag{6.29}$$

This result assumes that the dispersion coefficient is the same for the A, B and C species, and follows directly from the linearity of an advective-dispersive equation.

For the instantaneous bimolecular reaction (6.2) considered here, the amount of product C is determined by the concentration of the limiting reactants A and B. Thus, the concentration c_C can be calculated directly from the two known concentrations, c_{A+C} and c_{B+C} as,

$$c_C(\mathbf{x}, t) = \min\{c_{A+C}(\mathbf{x}, t), c_{B+C}(\mathbf{x}, t)\} \tag{6.30}$$

This solution predicts that c_C will be at the mixing interface of reactants A and B, and its concentration peak remains equal to 0.5 as the reactants and product move

through the porous medium. This can be understood by considering that both reactants are completely consumed at the advective front because the reaction is instantaneous. The concentration of the product C is equal to half of the initial concentration of the reactants (Gramling et al., 2002). The reaction will stop once the reactants are completely consumed. The total mass of product m_C in the reaction can be found by integrating all product C produced in the column as (6.22).

6.3.2 Mixing dynamics of the reaction front

We now present the results of mixing of the reaction front. Snapshots of the concentration field of reactant A and product C are shown in Figures 6.7 and 6.8 at two different times $t = 0.12$ (top) and 0.77 (bottom) pore volume. The developed finger structures of A at early times (top Figure 6.7) penetrate the channels between grains and lead to a significant increase of the mixing zone between the two reactants (Jiménez-Martínez et al., 2015; de Anna et al., 2014b). The mixing interface between reactants is stretched by the flow heterogeneity and a dispersive lamella topology emerges. As mentioned earlier, this type of reactive mixing occurs under advection by heterogeneous flows (Perez et al., 2019b). This finding agrees with the observations of rapid grow of $\sigma_e^2(t)$ and $\sigma_a^2(t)$ (see Figure 6.11) at early times made where velocities contrast produces deformation of the concentration distribution c_{A+C}. As a consequence of this, the concentration distribution of product C (top Figure 6.8) is distorted. Note that one can observe pore-scale fluctuations in concentrations of C, as we find concentration islands far from the concentration distribution centerline. This can be understood as since the reaction front between reactants is not uniform causes forward and backward tailing regions that are seen in measured breakthrough curves in Jiménez-Martínez et al. (2015). At later times, the interface length decreases due to diffusive mixing across channels and we find less spatial variability in the distribution of c_{A+C} (Figure 6.7 bottom). This occurs because fingers disappear as they merge transversally through diffusion. This mechanism called coalescence of the dispersive lamellae stops the growth of the interface length. This observation has also been observed in other reactive transport experiments (de Anna et al., 2014a,b; Willingham et al., 2008).

As mentioned previously, the concentration fields within the pores are not fully mixed. The temporal evolution of $m_C(t)$ Figure 6.9 shows that product mass prediction in terms of the hydrodynamic dispersion coefficient calculated from (6.23) does not capture properly the chemical reaction and overestimates $m_C(t)$. This occurs because the reactive transport description made with D_h assumes that the species concentrations are fully mixed transversely. However, we observe pore-scale fluctuations in concentrations of C that suggest incomplete mixing of reactants.

The product mass prediction from (6.23) in terms of a constant diffusion coefficient D results in a understimation of $m_C(t)$. Molecular diffusion controls the chemical reaction through mass transfer across the interface only at times smaller

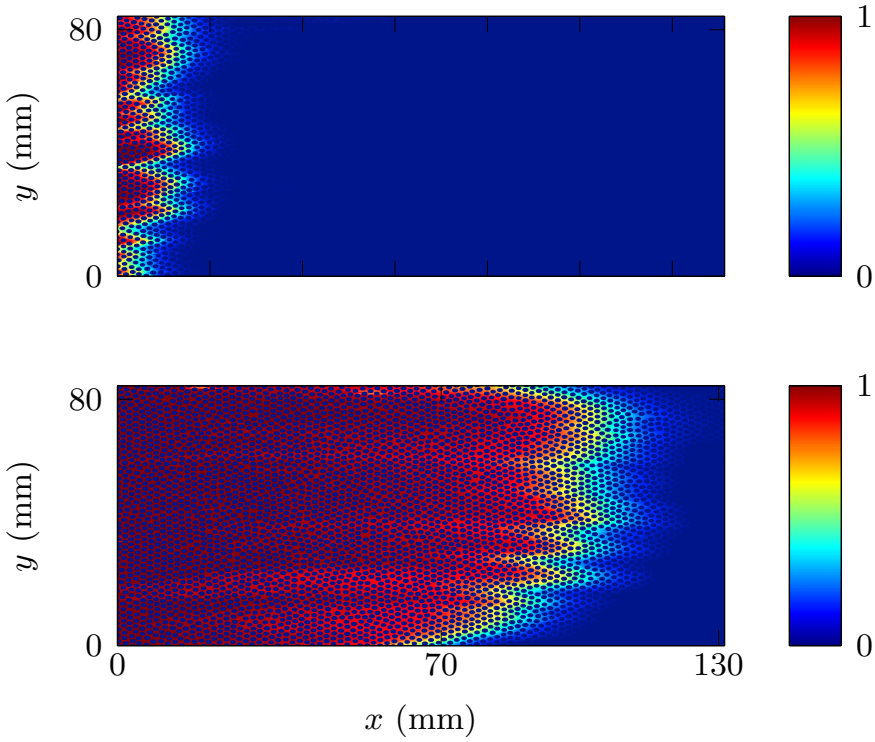

Figure 6.7: Concentration maps of c_{A+C} at times (top to bottom) $t = 0.12$ and 0.77 pore volume. The concentration distribution of reactant A (top) confirms the formation of fingers. The coalescence of the dispersive lamellae (bottom) is represented by the merging of the concentration front of reactant A.

than times where the solute covers the same distance by diffusion and by advective transport with the mean flow velocity. This temporal regime is not captured during the experimental observations of the reactions, and as consequence we see that the prediction made by using D fails.

6.3.3 The dispersive lamella representation of mixing in experiment

In the following, we apply the dispersive lamella to predict properly the total mass of C accounting for the impact of the deformation of the mixing interface between reactants. Note that for the calculation of the apparante and effective variance, $\sigma_a^2(t)$ and $\sigma_e^2(t)$, in the experiment we cannot follow point injections as in the RWPT model. We overcome this limitation by finding the apparent and

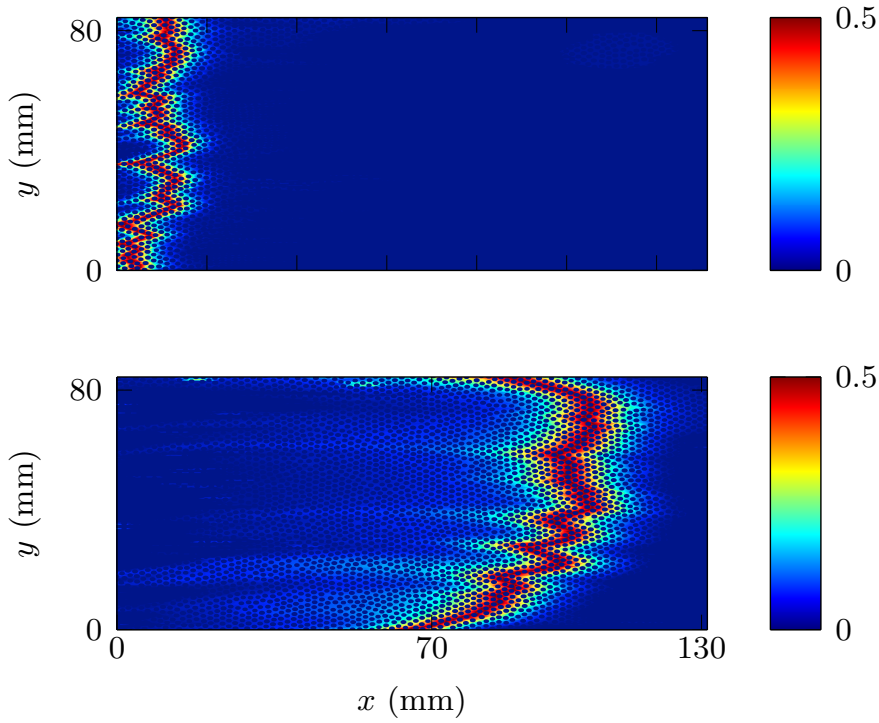

Figure 6.8: Concentration maps of c_C at times (top to bottom) $t = 0.12$ and 0.77 pore volume. Deformation of concentration distribution of C (top) caused by the flow field that distorts the mixing interface between reactants. The different zones of the reaction front undergo an aggregation process by diffusive coalescence that changes the mixing front topology (bottom).

effective width of $\hat{C}(t)$ defined by

$$\hat{C}(\mathbf{x}, t) = c_C(\mathbf{x}, t)\left[1 - c_C(\mathbf{x}, t)\right]. \tag{6.31}$$

The quantity $\hat{C}(t)$ is related to the segregation intensity (Danckwerts, 1952) and represents an accurate measure of the effectiveness of the mixing (Kapoor et al., 1997) (Figure 6.10). We find the moments of $\hat{C}(t)$ as

$$\Theta_j = \int_\Omega x^j \hat{C}(x, y, t) dx dy \tag{6.32}$$

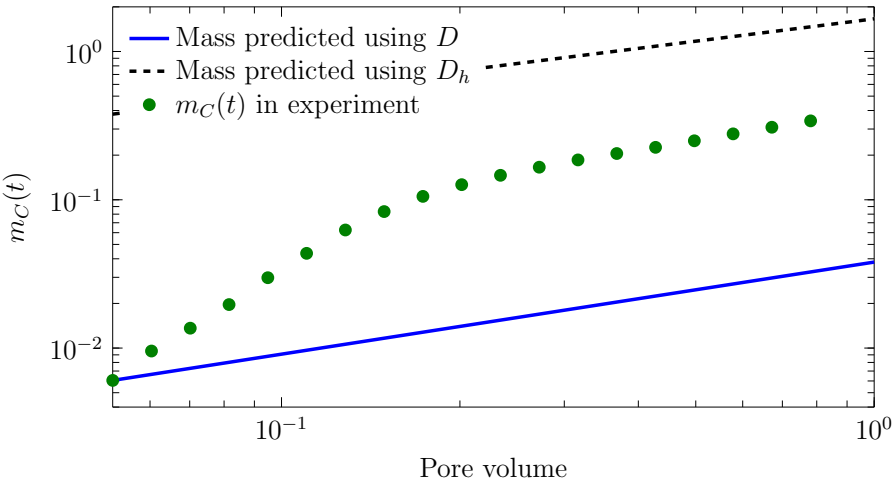

Figure 6.9: Evolution of $m_C(t)$ produced in the experiment (green dots) and the model prediction (6.23) coupled with D (blue solid line) and with D_h (black dashed line). Analytical predictions with D and D_h are not able to reproduce $m_C(t)$ in the experiment.

where Ω the size of the domain. The mean ($\bar{x}$) and apparent variance ($\sigma_a^2(t)$) can then be derived using the following expressions

$$\bar{x} = \frac{\Theta_1}{\Theta_0} \tag{6.33}$$

$$\sigma_a^2(t) = \frac{\Theta_2}{\Theta_0} - \bar{x}^2. \tag{6.34}$$

In order to find $\sigma_e^2(t)$ we discretize the width of the medium into bins. For this, we use the pixel discretization of the images (2279 pixels or bins) and quantify $\sigma_e^2(t)$ as

$$\sigma_i^2(t) = \sigma\left[\hat{C}(x, y_i < y < y_i + \Delta y, t)\right] \tag{6.35}$$

$$\sigma_e^2(t) = \langle \sigma_i^2(t) \rangle, \tag{6.36}$$

where the angular brackets denote the average over all y_i of the domain width.

In addition, we use Savitzky-Golay smoothing filters (Savitzky and Golay, 1964) to reduce concentration noise in the concentration distributions. The Savitzky-Golay filter is preferred over standard filtering techniques because is a simple algorithm that performs optimal results removing noise inherent in the experimental reactive transport data (Fendorf et al., 1999).

As discussed in section 6.2.2, the dispersive lamella considers material elements that constitute the mixing interface and follow the advective and diffusive motion in the flow field. Thus, the evolution of the species concentration under

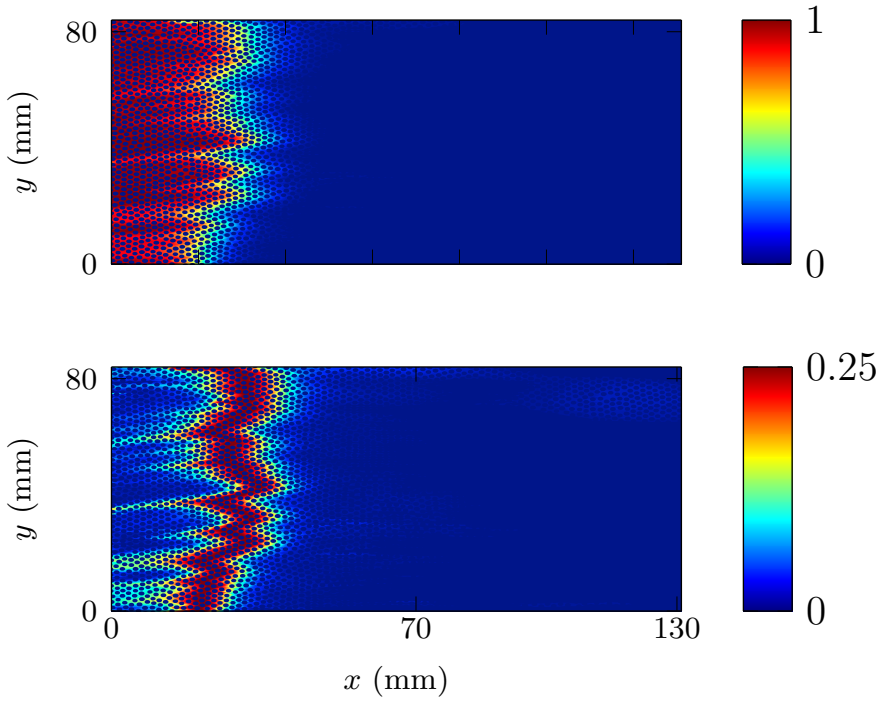

Figure 6.10: Concentration map of c_{A+C} (top) and map of $\hat{C}$ that allow us to measure the width of the interface (bottom) at $t = 0.36$ pore volume.

reaction at the mixing interface evolves with an effective dispersion coefficient that varies in time. We derived the total amount of product C following equation (6.28). The prediction of mass of C calculated using $\sigma_a^2(t)$ considers the total spread of the mixing front between reactants, while $m_C(t)$ predicted using $\sigma_e^2(t)$ takes into account the effective width of the mixing front.

Figure 6.11 shows the evolution of the effective and apparent variance $\sigma_e^2(t)$ and $\sigma_a^2(t)$ of the mixing zone distribution in the experiment. We find that $\sigma_a^2(t)$ is larger than $\sigma_e^2(t)$. This occurs because $\sigma_a^2(t)$ quantifies the spread of the mixing interface while $\sigma_e^2(t)$ measures the effective width of the interface. We distinguish two times regimes based on the growth of both variances. At early times, $t < 0.13$ pore volume, $\sigma_e^2(t)$ grows faster than $\sigma_a^2(t)$ because of the advective deformation of the reactant A front. For increasing times, intermediate regime ($0.13 < t < 0.9$ pore volume), we find that spreading is responsible for the increase in $\sigma_a^2(t)$ as this variance captures well this mechanism. The temporal evolution of the mass of product C (Figure 6.12) shows that at early times the reaction system is limited by the mixing of A and B. Note that this limiting effect is controlled by the advection heterogeneity that allows for the rapid formation of C. In this regime, we find that the prediction of the dispersive lamella agrees with

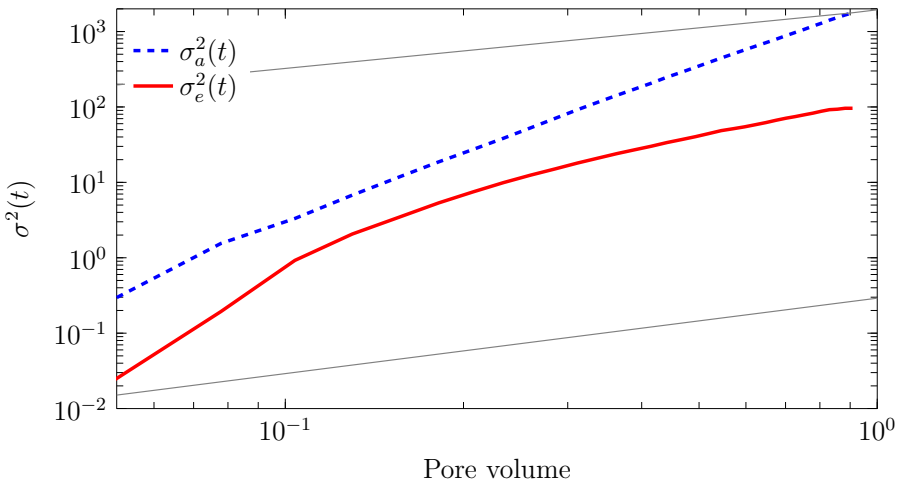

Figure 6.11: Evolutions of $\sigma_a^2(t)$ and $\sigma_e^2(t)$ calculated in experiment. The grey solid lines corresponds to $2Dt$ (lower) and $2D_h t$ (upper) behaviors.

$m_C(t)$ calculated from the experiment because $\sigma_e^2(t)$ acknowledges for stretching-enhanced mixing, and captures the faster production of C mass. On the other hand, the prediction for $m_C(t)$ using $\sigma_a^2(t)$ overpredicts the total product mass because it overestimates the interface width between reactants. For increasing times, $0.13 < t < 0.9$ pore volume, the dispersive lamella using $\sigma_e^2(t)$ predicts accurately $m_C(t)$ produced in the reaction as the effective variance accounts for the diffusive interaction of the lamellae. In this regime, the reaction behavior is clearly described by the coalescence of the lamella that affects the production rate of C. Particularly, it is well-known that in the coalescence regime, the scaling of the product mass is related to the evolution in time of the D_h prediction (de Anna et al., 2014b; Jiménez-Martínez et al., 2015). The predicted $m_C(t)$ using $\sigma_a^2(t)$ fails by overpredicting the product mass as the apparent variance does not capture well the interaction regime between lamellae and overestimates the interface width as discussed earlier.

6.4 Summary and conclusions

We estimate the impact of pore structure and flow heterogeneity on mixing interfaces and its role on the global reaction behavior of a mixing-limited chemical reaction. This is done by applying the dispersive lamella model (Perez et al., 2019a) to a reactive RWPT model in a synthetic medium, and to a pore-scale experimental visualization. The method, based on the effective dispersion coefficient, accurately captures the reaction dynamics in the two cases studied. This representation shows that the evolution of a fluid-fluid chemical reaction in which the reactants are under spatially variable advection, the total amount of product

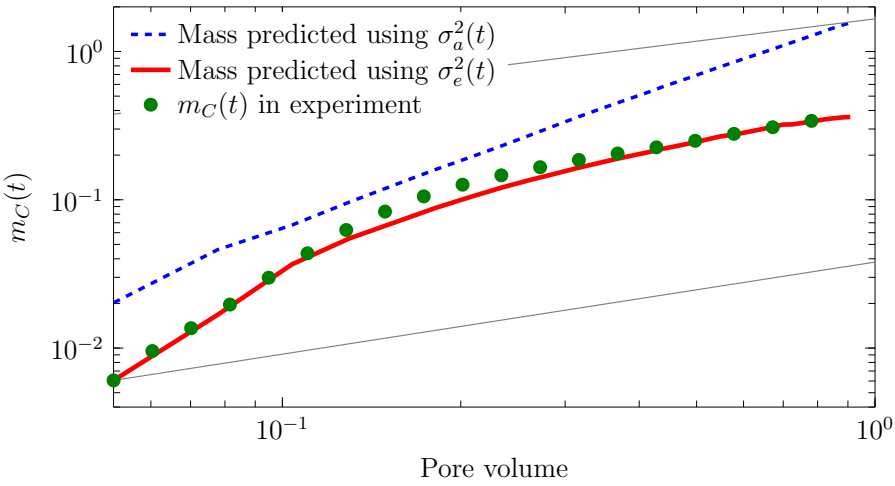

Figure 6.12: Evolution of $m_C(t)$ from the experimental visualization (green dots), and predictions from the dispersive lamella (6.28) parameterized by $\sigma_a^2(t)$ (blue solid line) and $\sigma_e^2(t)$ (red solid line). The grey solid lines corresponds to the analytical prediction (6.23) coupled with D (lower) and D_h upper.

formed can be predicted in terms of the effective dispersion coefficient. The dispersive lamella prediction agrees with the product mass measured in the studied cases, the effective approach quantifies the contribution to the global reaction behavior of the amount of mixing between reactants due to diffusion and due to spreading, and the degree of heterogeneity in the flow field.

Simulation results show that at early times diffusion is the main mechanism driving the reaction. While at later times an increased mixing of chemical species occur, this is induced by particles sampling spatial velocity fluctuations that lead to fluid deformation. We observe an overestimation of the system reactivity by the hydrodinamic dispersion coefficient. Similar phenomena have been observed for reactive transport on the Darcy scale (Gramling et al., 2002; Tartakovsky et al., 2009; Battiato and Tartakovsky, 2011).

In the experimental visualization, the amount of reaction is controlled by the combination of pore-scale mixing due to spreading and the degree of heterogeneity in the flow field. Our results suggest that the reactive displacement of the two chemicals are mixed within the heterogeneous porous medium but cannot be considered well mixed at the pore scale. The mass production rate at early times is controlled by the geometry of the mixing front between the two reactants. The late time increase $\sim \sqrt{t}$ of the product mass suggest that reaction is dominated by lamellae coalescence.

These findings have direct repercussions on effective reactive transport modeling of heterogeneous flows in a range of applications, such as reactive contaminant transport in hydrological systems, since our reactive and effective framework

may serve for understanding and quantifying more complex chemical reactions in porous media flows.

CHAPTER 7

Summary and conclusions

This Chapter concludes the thesis by summarizing the main results. We provide a general summary, in which we recall the key messages and emphasize the main contributions detailed in the thesis. Finally, we give an outlook on further research challenges that we consider of significant interest.

7.1 Summary and general conclusions

We have performed reactive transport simulations to investigate the mechanisms that lead to chemical reaction dynamics that are very different from the ones observed in the laboratory under well-mixed equilibrium conditions and the ones predicted by the transport laws for homogeneous environments.

A novel method has been developed for the simulation of fluid-fluid chemical reactions in porous media using a reaction probability based on a well-mixed reactor. The concept of the well-mixed support volume allow us to establish the equivalence between our reactive random walk particle tracking (RWPT) and the advection-dispersion-reaction equation (ADRE). The approach has been validated against analytical solutions for constant and variable flow scenarios under slow and fast reaction kinetics. The developed methodology is simple and free of numerical dispersion and artificial oscillations compared to grid-based Eulerian approaches.

Throughout this thesis, we have focused on the repercussions of the mixing degree between reactants, which is known to play a key role on the reaction behavior. It has been shown that pore structure heterogeneity, reactive fronts and deformed interfaces affects the degree of mixing of the chemical species. We have shown that the ADRE overpredicts the amount of mixing in the different scenarios studied. For example, we quantified the impact of flow variability on a fast irreversible reaction in a Poiseuille flow through a pore channel. The investigated system shows reactant's incomplete mixing that are present in more complex porous media flows. The overestimation of the global reaction efficiency

by the use of macroscale dispersion coefficient, Taylor dispersion coefficient in this case, which quantifies the macroscopic mixing effect that accounts for the interaction of flow variability and diffusion only when the channel cross section is completely mixed by diffusion.

We characterized features of incomplete mixing in a sinthetic porous medium. The results from the reactive transport simulations showed that the amount of reaction is affected by the mixing degree of the reactants. Predictions using the hydrodynamic dispersion coefficient and assumes complete mixing between reactants overpredicted the global reaction behavior in the medium. Similar phenomena have been observed for reactive transport on the Darcy scale, where the hydrodynamic dispersion coefficient turned out to overestimate the global reactivity of the system (Gramling et al., 2002). This emphasizes the importance of incomplete mixing and its correct quantification for modeling macroscale reactive transport in heterogeneous porous media in general. In addition, the study of a reactive displacement in a laboratory experiment exhibited imperfect mixing dynamics of the two reactants. Analysis of the reaction revealed that, the system reactivity mainly depends on the amount of mixing between reactants due to diffusion, on the amount of mixing between reactants due to spreading, and on the degree of heterogeneity of the flow field. The relative contributions of these three factors on the reaction behavior makes ADRE predictions fail in the total estimation of the reaction product.

We have proposed a methodology, the dispersive lamella approach that is able to describe the full temporal evolution of the reaction product accurately. The developed model is based on an Gaussian approximation of the Green function for the advection-diffusion problem. The evolution of the Green function is governed by a dispersion equation characterized by a time-dependant effective dispersion coefficient, which accounts for both stretching-enhanced diffusion at early times and front coalescence at late times. In the dispersive lamella approach, the impact of transverse diffusion on the evolution of the front is quantified through vertical averaging across the porous medium. In general, for the reactive longitudinal displacement considered in this thesis, the impact of transverse mixing is negligible compared to the longitudinal mixing and hence in the reaction.

The proposed methodology quantified the impact of flow heterogeneities on the amount of fluid mixing in a pore channel. Specifically, the approach accounts for the consequences of interface deformation, and revealed that at early times, the reaction is controlled by diffusion. At later times, advection dominate and we find enhanced reaction efficiency because the deformed interface between the reactants. For times larger than the characteristic diffusion time, mixing and reaction are quantified by the Taylor dispersion coefficient. Simulations in a more complex porus medium revealed that estimations from the dispersive lamella approach matched the evolution of the total mass of product in the reaction. The dispersive lamella predictions captured the kinetics of the reaction, which are controlled by the geometry of the interface front between the two chemicals. Again, the results showed a reaction diffusion-controlled regime at early times, and advective domination for increasing times that leads to enhanced-mixing

behavior. The method catches very well the different temporal regimes that characterize the reaction.

The developed dispersive lamella approach was applied to the pore-scale laboratory experiment reported by Jiménez-Martínez et al. (2015). The results provide an explicit relation between the impact of fluid deformation on mixing and the evolution of the chemical reactivity of the system. Here, the dispersive lamella estimations accounts for the identified finger structures at early times due to the penetration of the solute in the medium. This finger structures caused a significant increase of the mixing dynamics between the two reactants.The reaction is controlled by the deformed interface. For increasing times, fingers disappear as they merge through diffusion. The prediction based on the dispersive lamella accounts for this coalescence regime and produces accurate results. The proposed methodology is able to efficiently predict reactions in d-dimensional systems with homogeneous and spatially variable advection as it takes into account the role of flow deformation, medium heterogeneity and diffusion.

Outlook

In order to provide a better understanding of reactive transport in heterogeneous porous media, and the impact of the underlying physical mechanisms, we suggest future extensions of the work presented in this thesis:

1. Complex reactions non-linear chemical processes: biodegradation or enzymatic reactions, are composed of a cascade of elementary unimolecular and bimolecular reactions similar to the one studied in this thesis.

2. Multiphase reactive transport: Combine the fluid-fluid reactions with fluid-solid reactions, such as mineral dissolution or precipitation.

3. Rock samples: The work can be expanded to study reactive transport dynamics in complex rock samples, such as carbonates. It may also be necessary to include the impact of sub-resolution heterogeneity, such as microporosity, into upscaled models.

APPENDIX A

Upscaling of Mixing-Limited Bimolecular Chemical Reactions in Poiseuille Flow

A.1 Finite size effects in modeling the reaction

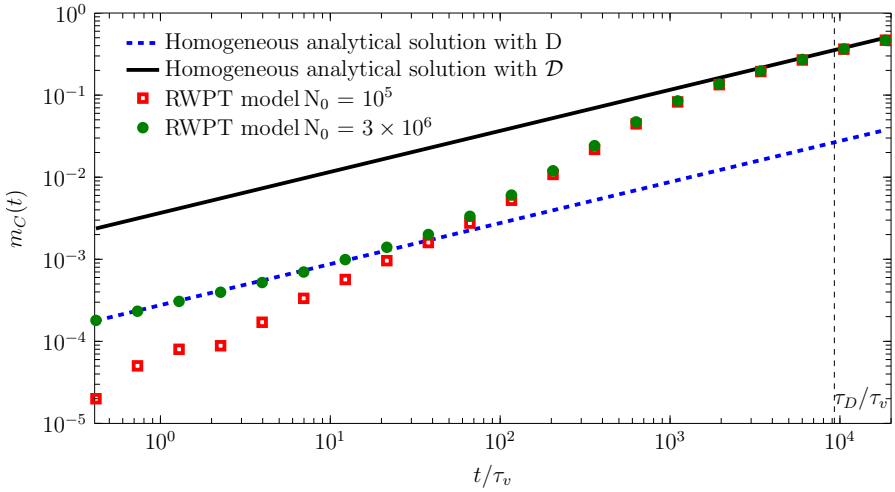

Figure A.1: Evolution of $m_C(t)$ for different particle numbers. Expression (5.8) with (dashed line) D and (solid line) $\mathcal{D}$ predict the early and later time behavior of $m_C(t)$, respectively.

We illustrate the impact of the total particle number in the chemical reaction comparing the simulations for $Pe = 96$ for $3 \cdot 10^6$ particles and 10^5 particles. Figure A.1 compares numerical data to the exact analytical solution (5.8) parameterized by D and $\mathcal{D}$, which is valid at early times $t \ll \tau_v$ and late times $t \gg \tau_D$. We find that at times $t \leq \tau_v$, when D controls the reaction, lower N_0 creates artificial concentration fluctuations due to fluctuations of particle numbers between subvolumes, which simulates an artificial incomplete mixing. Thus, reactivity may be underestimated as a result of this effect. Clearly, the insufficient number of particles to model the reaction produces a loss in accuracy. This artificial effect must not be confused with the occurrence of true incomplete mixing. The data from the simulation with $N_0 = 3 \cdot 10^6$ particles accurately matches the analytical solution at early times. At intermediate times, $\tau_v \leq t \ll \tau_D$, where true, physical incomplete mixing dominates, the simulations at both N_0 behave similarly because the artificial incomplete mixing is overshadowed by the true physical effect. Similarly, at asymptotic times, both particle numbers give good estimates because Taylor dispersion is the result of the diffusive sampling of the cross-sectional velocity over time, which is less affected by a low particle number. In order to exclude artificial incomplete mixing and finite size effects, the reactive random walk particle tracking results are performed with $N_0 > 10^6$ particles. Note that the particle number necessary to avoid the effect of artificial incomplete mixing at early times depends on the Péclet number. For low Péclet numbers, particles explore a larger radius per random walk step $\propto \sqrt{2D\Delta t}$ and therefore mix faster locally than at high Péclet numbers. The physically well-mixed support volume is larger than for high Pe. Thus, for a lower total particle number, one has at low Pe the same number of particles inside a well-mixed support volume as for a higher particle number at high Pe fro which the well-mixed support volume is much smaller.

A.2 The dispersive lamella

Here we briefly derive Equation (5.37), which forms the basis for the dispersive lamella approach. We separate $\hat{g}(\hat{\mathbf{x}}, t|y')$ into the projection $G(y, t|y')\theta(\hat{x}, t|y')$ and fluctuations $\theta'(\mathbf{x}, t|y')$ about it such that

$$\hat{g}(\hat{\mathbf{x}}, t|y') = G(y, t|y')\theta(\hat{x}, t|y') + \theta'(\hat{\mathbf{x}}, t|y'). \tag{A.1}$$

Inserting this decomposition into (5.32) gives

$$\begin{aligned}
&\frac{\partial G(y,t|y')\theta(\hat{x},t|y')}{\partial t} + \frac{\partial \theta'(\hat{\mathbf{x}},t|y')}{\partial t} + \left[u'(y) - v'(t|y')\right] G(y,t|y') \frac{\partial \theta(\hat{x},t|y')}{\partial \hat{x}} \\
&= -\left[u'(y) - v'(t|y')\right] \frac{\partial \theta'(\hat{\mathbf{x}},t|y')}{\partial \hat{x}} + D\left(\frac{\partial^2}{\partial \hat{x}^2} + \frac{\partial^2}{\partial y^2}\right) \left[G(y,t|y')\theta(\hat{x},t|y') + \theta'(\hat{\mathbf{x}},t|y')\right],
\end{aligned} \tag{A.2}$$

where we used that $v'(\hat{y}, t|y') = u(y) - v(t|y')$, which can be written as $v'(\hat{y}, t|y') = u(y) - v_m - [v(t|y') - v_m] \equiv u'(y) - v'(t|y')$. The fluctuation of the center of mass

velocity $v'(t|y')$ is given by (Dentz and Carrera, 2007)

$$v'(t|y') = \int_{-a}^{a} dy u'(y) G(y,t|y'). \tag{A.3}$$

Furthermore, we note that the Green function $G(y,t|y')$ satisfies

$$\frac{\partial G(y,t|y')}{\partial t} - D\frac{\partial^2 G(y,t|y')}{\partial y^2} = 0 \tag{A.4}$$

for the initial condition $G(y,t=0|y') = \delta(y-y')$. This implies that

$$\frac{\partial G(y,t|y')\theta(\hat{x},t|y')}{\partial t} - D\frac{\partial^2}{\partial y^2} G(y,t|y')\theta(\hat{x},t|y') = \tag{A.5}$$

$$G(y,t|y')\frac{\partial \theta(\hat{x},t|y')}{\partial t} + \theta(\hat{x},t|y')\left[\frac{\partial G(y,t|y')}{\partial t} - D\frac{\partial^2}{\partial y^2} G(y,t|y')\right] \tag{A.6}$$

$$= G(y,t|y')\frac{\partial \theta(\hat{x},t|y')}{\partial t} \tag{A.7}$$

Thus, we can write Eq. (A.2) as

$$\begin{aligned} &G(y,t|y')\frac{\partial \theta(\hat{x},t|y')}{\partial t} + \frac{\partial \theta'(\hat{\mathbf{x}},t|y')}{\partial t} + \left[u'(y) - v'(t|y')\right] G(y,t|y')\frac{\partial \theta(\hat{x},t|y')}{\partial \hat{x}} \\ &= -\left[u'(y) - v'(t|y')\right]\frac{\partial \theta'(\hat{\mathbf{x}},t|y')}{\partial \hat{x}} + D\frac{\partial^2}{\partial y^2}\theta'(\hat{\mathbf{x}},t|y') + D\frac{\partial^2}{\partial \hat{x}^2}\left[G(y,t|y')\theta(\hat{x},t|y') + \theta'(\hat{\mathbf{x}},t|y')\right], \end{aligned} \tag{A.8}$$

Vertical integration gives

$$\frac{\partial \theta(\hat{x},t|y')}{\partial t} = -\int_{-a}^{a} dy \left[u'(y) - v'(t|y')\right]\frac{\partial \theta'(\hat{\mathbf{x}},t|y')}{\partial \hat{x}} + D\frac{\partial^2}{\partial \hat{x}^2}\theta(\hat{x},t|y') \tag{A.9}$$

By subtracting the latter from Eq. (A.9), we obtain for the fluctuation $\theta'(\hat{\mathbf{x}},t|y')$

$$\frac{\partial \theta'(\hat{\mathbf{x}},t|y')}{\partial t} - D\frac{\partial^2 \theta'(\hat{\mathbf{x}},t|y')}{\partial y^2} = -\left[u'(y) - v'(t|y')\right] G(y,t|y')\frac{\partial \theta(\hat{x},t|y')}{\partial \hat{x}} \tag{A.10}$$

where we disregard terms of second order in the fluctuating quantities and diffusion in flow direction because transverse diffusion is the key sampling mechanism. By using the Green function $G(y,t|y')$ of vertical diffusion we can write $\theta'(\hat{\mathbf{x}},t|y')$ as

$$\theta'(\hat{\mathbf{x}},t|y') = -\int_{0}^{t} dt' \int_{-a}^{a} dy'' \left[u'(y'') - v'(t'|y')\right] G(y,t-t'|y'') G(y'',t'|y')\frac{\partial \theta(\hat{x},t'|y')}{\partial \hat{x}}. \tag{A.11}$$

Inserting this expression into the right side of (A.2) gives

$$\frac{\partial\theta(\hat{x},t|y')}{\partial t} = \int_0^t dt'\mathcal{K}(t,t'|y')\frac{\partial^2\theta(\hat{x},t'|y')}{\partial\hat{x}^2} + D\frac{\partial^2}{\partial\hat{x}^2}\theta(\hat{x},t|y'). \tag{A.12}$$

where we defined the dispersion kernel by

$$\mathcal{K}(t,t'|y') = \int_{-a}^{a} dy \int_{-a}^{a} dy'' \left[u'(y) - v'(t|y')\right]\left[u'(y'') - v'(t'|y')\right] G(y,t-t'|y'')G(y'',t'|y'). \tag{A.13}$$

The latter can be written as

$$\mathcal{K}(t,t'|y') = \int_{-a}^{a} dy''u'(y'')G(y'',t'|y')v'(t-t'|y'') - v'(t|y')v'(t'|y'), \tag{A.14}$$

where we used (A.3) and the Markov property of the Green function, which means that

$$\int_{-a}^{a} dy''G(y,t-t'|y'')G(y'',t'|y') = G(y,t|y') \tag{A.15}$$

The time integral of $\mathcal{K}(t,t'|y')$ is equal to the effective dispersion coefficient $D^e(t|y')$ defined in Dentz and Carrera (2007)

$$\begin{aligned} D^e(t|y') &= \int_0^t dt'\mathcal{K}(t,t'|y') \\ &= \int_0^t dt' \int_{-a}^{a} dy''u'(y'')G(y'',t'|y')v'(t-t'|y'') - v'(t|y') \int_0^t dt'v'(t'|y'). \end{aligned} \tag{A.16}$$

The memory term on the right side of (A.12) can be localized in time for $t-t' \ll t$,

$$\frac{\partial\theta(\hat{x},t|y')}{\partial t} = \left[\int_0^t dt'\mathcal{K}(t,t'|y')\right]\frac{\partial^2\theta(\hat{x},t|y')}{\partial\hat{x}^2} + D\frac{\partial^2}{\partial\hat{x}^2}\theta(\hat{x},t|y'), \tag{A.17}$$

which gives Eq. (5.37) for the dispersive lamella.

A.3 Analytical solution for a finite initial condition

We derive here analytical solutions for the initial conditions (5.6). In the following, we give analytical solutions for the species concentrations and the product mass for a homogeneous medium, the stretched lamella and the dispersive

lamella approaches. First we note that the concentrations $c_{AC} = c_A + c_B$ and $c_{BC} = c_B + c_C$ satisfy conservative advection-diffusion equations for the same initial conditions as c_A and c_B because c_C is initially 0. As we consider an instantaneous reaction, the A and B species cannot coexist and thus, the product concentration is given by

$$c_C(x,t) = \min\left[c_{AC}(x,t), c_{BC}(x,t)\right], \tag{A.18}$$

because $c_{AC} = c_C$ if $c_A < c_B$ and vice versa.

A.3.1 Homogeneous medium

Thus, for a homogeneous medium with $v(x) = v =$ constant, the solutions for c_{AC} and c_{BC} are

$$c_{AC}(x,t) = \frac{c_0}{2}\left[\mathrm{erfc}\left(\frac{x-vt}{\sqrt{4Dt}}\right) - \mathrm{erfc}\left(\frac{x+L-vt}{\sqrt{4Dt}}\right)\right] \tag{A.19}$$

$$c_{BC}(x,t) = \frac{c_0}{2}\left[\mathrm{erfc}\left(\frac{x-L-vt}{\sqrt{4Dt}}\right) - \mathrm{erfc}\left(\frac{x-vt}{\sqrt{4Dt}}\right)\right] \tag{A.20}$$

The product concentration is given by c_{AC} for $x \geq vt$ and by c_{BC} for $x < vt$. In the limit $L \to \infty$, the concentration of C is given by (5.7). Thus, we obtain for the product mass $m_C(t)$

$$m_C(t) = \int_{-\infty}^{vt} dx c_{BC}(x,t) + \int_{vt}^{\infty} dx c_{AC}(x,t), \tag{A.21}$$

which we can write because of symmetry as

$$m_c(t) = 2\int_{vt}^{\infty} dx c_{AC}(x,t). \tag{A.22}$$

Inserting (A.20) gives

$$m_c(t) = c_0 \int_0^L dx \mathrm{erfc}\left(\frac{x}{\sqrt{4Dt}}\right) = c_0\sqrt{4Dt}\int_0^{L/\sqrt{4Dt}} dx \mathrm{erfc}\,(x) \tag{A.23}$$

Performing the remaining integral, we obtain

$$m_C(t) = c_0\sqrt{\frac{4Dt}{\pi}}\left[1 - \exp(-4\tau_L/t) + \sqrt{4\pi\tau_L/t}\,\mathrm{erfc}(\sqrt{4\tau_L/t}\right], \tag{A.24}$$

where we defined the diffusion time $\tau_L = L^2/D$ over the initial extension of the species. For $t \ll \tau_L$, the evolution of the product mass is essentially equal to the one for $L \to \infty$ and given by $m_C(t) = 2c_0\sqrt{Dt/\pi}$. For $t \gg \tau_L$ it behaves as

$$m_C(t) = c_0 L\left(1 - \frac{1}{\sqrt{4\pi t/\tau_L}}\right) + \ldots. \tag{A.25}$$

A.3.2 Stretched lamella

The stretched lamella approach requires solution of the equation

$$\frac{\partial\theta(\hat{x},t)}{\partial t} - \gamma(t)\hat{x}\frac{\partial\theta(\hat{x})}{\partial\hat{x}} - D\frac{\partial\theta(\hat{x},t)}{\partial\hat{x}^2} = 0, \tag{A.26}$$

where θ stands for the concentrations $\theta_{AC} = \theta_A + \theta_C$ and $\theta_{BC} = \theta_B + \theta_C$, respectively. In order to solve (A.26), we consider the variable transform according to Ranz (1979),

$$z = \hat{x}\exp\left[\Gamma(t)\right], \qquad \Gamma(t) = \int_0^t dt\gamma(t') \tag{A.27}$$

and

$$\eta(t) = \int_0^t dt' \exp[2\Gamma(t)], \tag{A.28}$$

Note that

$$\exp[\Gamma(t)] = \lambda(t), \tag{A.29}$$

where $\lambda(t)$ is given by (5.22). We set $\theta(\hat{x},t) = \theta_0[\hat{x}\lambda(t),\eta(t)]$, where $\theta_0(z,\eta)$ satisfies

$$\frac{\partial\theta_0(z,\eta)}{\partial\eta} - D\frac{\partial^2\theta_0(z,\eta)}{\partial z^2} = 0. \tag{A.30}$$

The latter is a diffusion equation whose solution for the initial condition $\theta(z,\eta = 0) = \mathbb{I}(-L_1 \leq z < L_2)$ is

$$\theta_0(z,\eta) = \frac{1}{2}\left[\text{erfc}\left(\frac{z+L_1}{\sqrt{4D\eta}}\right) - \text{erfc}\left(\frac{z-L_2}{\sqrt{4D\eta}}\right)\right] \tag{A.31}$$

Thus, we obtain for $\theta(\hat{x},t)$

$$\theta(\hat{x},t) = \frac{1}{2}\left[\text{erfc}\left(\frac{\hat{x}_1 + L_1\lambda(t)^{-1}}{\sqrt{2s(t)^2}}\right) - \text{erfc}\left(\frac{z - L_2\lambda(t)^{-1}}{\sqrt{2s(t)^2}}\right)\right], \tag{A.32}$$

where we defined

$$s(t)^2 = 2D\lambda(t)^{-2}\int_0^t dt'\lambda(t')^2. \tag{A.33}$$

Using expression (5.28) with $\alpha(y') = \overline{\alpha}$ gives expression (5.50) for $s(t)$. We obtain $\theta_{AC}(\hat{z},t)$ and $\theta_{BC}(\hat{z},t)$ by setting in (A.39) $L_1 = -L$ and $L_2 = 0$, and $L_1 = 0$

and $L_2 = L$, respectively. The solution (5.47) is obtained in the limit $L \to \infty$. Along the same lines as in the previous section, we obtain for the product mass across a single stretched lamella

$$\delta m_C(t) = c_0 \sqrt{\frac{2}{\pi}} \lambda(t) s(t) \left(1 - \exp[-A(t)^2] + \sqrt{\pi} A(t) \mathrm{erfc}\,[A(t)]\right), \tag{A.34}$$

where we defined $A(t) = L \exp[-\Gamma(t)]/\sqrt{2s(t)^2}$.

A.3.3 Dispersive lamella

The solution method is fully analogous to the previous section. The dispersive lamella approach requires solution of the equation

$$\frac{\partial \theta(\hat{x}, t)}{\partial t} - D^e(t) \frac{\partial \theta(\hat{x}, t)}{\partial \hat{x}^2} = 0, \tag{A.35}$$

where θ stands for the concentrations $\theta_{AC} = \theta_A + \theta_C$ and $\theta_{BC} = \theta_B + \theta_C$, respectively. In order to solve (A.26), we consider the variable transform

$$\eta(t) = \int_0^t dt' D^e(t'), \tag{A.36}$$

and set $\theta(\hat{x}, t) = \theta_0[\hat{x}, \eta(t)]$, where $\theta_0(z, \eta)$ satisfies

$$\frac{\partial \theta_0(z, \eta)}{\partial \eta} - \frac{\partial^2 \theta_0(\hat{x}, \eta)}{\partial \hat{x}^2} = 0. \tag{A.37}$$

The latter is a diffusion equation whose solution for a the initial condition $\theta(\hat{x}, \eta = 0) = \mathbb{I}(-L_1 \leq \hat{x} < L_2)$ is

$$\theta_0(\hat{x}, \eta) = \frac{1}{2} \left[\mathrm{erfc} \left(\frac{\hat{x} + L_1}{\sqrt{4\eta}} \right) - \mathrm{erfc} \left(\frac{z - L_2}{\sqrt{4\eta}} \right) \right] \tag{A.38}$$

Thus, we obtain for $\theta(\hat{x}, t)$

$$\theta(\hat{x}, t) = \frac{1}{2} \left[\mathrm{erfc} \left(\frac{\hat{x}_1 + L_1}{\sqrt{2\sigma_e^2(t)}} \right) - \mathrm{erfc} \left(\frac{\hat{x}_1 - L_2}{\sqrt{2\sigma_e^2(t)}} \right) \right], \tag{A.39}$$

where $\sigma_e^2(t)$ is given by (5.40). Along the same lines as above, we obtain for the product mass of a single dispersive lamella

$$\delta m_C(t) = c_0 \sqrt{\frac{2}{\pi}} \sigma_e(t) \left(1 - \exp[-A_e(t)^2] + \sqrt{\pi} A_e(t) \mathrm{erfc}\,[A_e(t)]\right), \tag{A.40}$$

where we defined $A_e(t) = L/\sqrt{2\sigma_e(t)^2}$. The solutions (5.53) and (5.55) are obtained in the limit $L \to \infty$. Note the the product mass $m_C(t)$ can be approximated by the product mass for $L \to \infty$ as long as $A_e(t) \ll 1$, this means $\sigma_e(t) \ll \sqrt{2}L$.

APPENDIX B

Publications and conference presentations

Publications in scientific journals

- **Perez, L. J.**, Hidalgo, J. J., and Dentz, M. (2019). Reactive random walk particle tracking and its equivalence with the advection-diffusion-reaction equation. *Water Resources Research*, 55.
- **Perez, L. J.**, Hidalgo, J. J., and Dentz, M. (2019). Upscaling of mixing-limited bimolecular chemical reactions in Poiseuille flow. *Water Resources Research*, 54.

Presentations in conferences

2019

- **Perez, L.J.**, Puyguiraud, A., Hidalgo, J. J., Jimenez-Martinez, J., and Dentz, M. - Incomplete mixing effects on chemical reactions in heterogeneous media: Numerical simulations and laboratory experiments. Interpore - Valencia (Spain).

2018

- **Perez, L.J.**, Puyguiraud, A., Hidalgo, J. J., Jimenez-Martinez, J., and Dentz, M. - Mixing-limited bimolecular chemical reactions at pore-scale. AGU Fall Meeting - Washington DC (USA).
- **Perez, L.J.**, Hidalgo, J. J., and Dentz, M. - Mixing-limited chemical reactions in porous media. GHS Seminar - Barcelona (Spain).

- **Perez, L.J.**, Hidalgo, J. J., and Dentz, M. - Chemical reactions under flow heterogeneities. CMWR - Saint Malo (France).
- **Perez, L.J.**, Hidalgo, J. J., and Dentz, M. - Upscaling of mixing-limited chemical reactions in a laminar flow through a pore channel. EGU General Assembly 2018 - Vienna (Austria).

2017

- **Perez, L.J.**, Hidalgo, J. J., and Dentz, M. - Upscaling of mixing-limited chemical reactions in a Poiseuille flow through a pore channel. GHS Seminar - Barcelona (Spain).
- **Perez, L.J.**, Hidalgo, J. J., and Dentz, M. - Effects of incomplete mixing on chemical reactions under flow heterogeneities. Interpore 2017 - Rotterdam (The Netherlands).

2016

- **Perez, L.J.**, Hidalgo, J. J., and Dentz, M. - Mixing-limited chemical reactions under flow heterogeneities and incomplete mixing. EGU General Assembly 2016 - Vienna (Austria).

2015

- **Perez, L.J.**, Hidalgo, J. J., and Dentz, M. - Chemical reactions under flow heterogeneities and incomplete mixing at pore scale. Goldschmidt Conference 2015 - Prague (Czech Republic).
- **Perez, L.J.**, Hidalgo, J. J., and Dentz, M. - Mixing-limited chemical reactions at pore scale. 3rd Cargèse Summer School on flow and transport in porous and fractured media - Cargèse (France).

Bibliography

Alhashmi, Z., Blunt, M., and Bijeljic, B. (2015). Predictions of dynamic changes in reaction rates as a consequence of incomplete mixing using pore scale reactive transport modeling on images of porous media. *Journal of Contaminant Hydrology*, 179:171–181.

Alhashmi, Z., Blunt, M., and Bijeljic, B. (2016). The impact of pore structure heterogeneity, transport, and reaction conditions on fluid–fluid reaction rate studied on images of pore space. *Transport in Porous Media*, 115(2):215–237.

Andrews, S. S. and Bray, D. (2004). Stochastic simulation of chemical reactions with spatial resolution and single molecule detail. *Physical Biology*, 1(3):137.

Bandopadhyay, A., Le Borgne, T., Méheust, Y., and Dentz, M. (2017). Enhanced reaction kinetics and reactive mixing scale dynamics in mixing fronts under shear flow for arbitrary damköhler numbers. *Advances in Water Resources*, 100:78–95.

Barros, F. P., Dentz, M., Koch, J., and Nowak, W. (2012). Flow topology and scalar mixing in spatially heterogeneous flow fields. *Geophysical Research Letters*, 39(8).

Batens, N. and Van Keer, R. (2003). On a numerical relaxation method for a chemical reaction-diffusion problem with an instantaneous and irreversible reaction. *Chemical Engineering Science*, 58(21):4815–4822.

Battiato, I. and Tartakovsky, D. (2011). Applicability regimes for macroscopic models of reactive transport in porous media. *Journal of Contaminant Hydrology*, 120:18–26.

Battiato, I., Tartakovsky, D. M., Tartakovsky, A. M., and Scheibe, T. (2009). On breakdown of macroscopic models of mixing-controlled heterogeneous reactions in porous media. *Advances in Water Resources*, 32(11):1664–1673.

Benson, D. A. and Meerschaert, M. M. (2008). Simulation of chemical reaction via particle tracking: Diffusion-limited versus thermodynamic rate-limited regimes. *Water Resources Research*, 44(12). W12201.

Bentley, J. L. (1975). Multidimensional binary search trees used for associative searching. *Communications of the ACM*, 18(9):509–517.

Berkowitz, B., Dror, I., Hansen, S. K., and Scher, H. (2016). Measurements and models of reactive transport in geological media. *Reviews of Geophysics*, 54(4):930–986.

Bolster, D., de Anna, P., Benson, D. A., and Tartakovsky, A. M. (2012). Incomplete mixing and reactions with fractional dispersion. *Advances in Water Resources*, 37:86–93.

Bolster, D., Valdés-Parada, F. J., LeBorgne, T., Dentz, M., and Carrera, J. (2011). Mixing in confined stratified aquifers. *Journal of Contaminant Hydrology*, 120-121:198–212.

Boon, M., Bijeljic, B., and Krevor, S. (2017). Observations of the impact of rock heterogeneity on solute spreading and mixing. *Water Resources Research*, 53(6):4624–4642.

Borden, R. C., Daniel, R. A., LeBrun, L. E., and Davis, C. W. (1997). Intrinsic biodegradation of mtbe and btex in a gasoline-contaminated aquifer. *Water Resources Research*, 33(5):1105–1115.

Borgne, T. L., Ginn, T. R., and Dentz, M. (2014). Impact of fluid deformation on mixing-induced chemical reactions in heterogeneous flows. *Geophysical Research Letters*, 41(22):7898–7906.

Botev, Z. I., Grotowski, J. F., Kroese, D. P., et al. (2010). Kernel density estimation via diffusion. *The Annals of Statistics*, 38(5):2916–2957.

Carlotti, F., Chapman, R., Dower, S. K., and Qwarnstrom, E. E. (1999). Activation of nuclear factor κb in single living cells dependence of nuclear translocation and anti-apoptotic function on egfprela concentration. *Journal of Biological Chemistry*, 274(53):37941–37949.

Chen, C., Zeng, L., and Shi, L. (2013). Continuum-scale convective mixing in geological co2 sequestration in anisotropic and heterogeneous saline aquifers. *Advances in Water Resources*, 53:175–187.

Chiogna, G. and Bellin, A. (2013). Analytical solution for reactive solute transport considering incomplete mixing within a reference elementary volume. *Water Resources Research*, 49(5):2589–2600.

Dagan, G. (1990). Transport in heterogeneous porous formations: Spatial moments, ergodicity, and effective dispersion. *Water Resources Research*, 26(6):1281–1290.

Danckwerts, P. (1952). The definition and measurement of some characteristics of mixtures. *Applied Scientific Research, Section A*, 3(4):279–296.

Davis, J., Kent, D., Coston, J., Hess, K., and Joye, J. (2000). Multispecies reactive tracer test in an aquifer with spatially variable chemical conditions. *Water Resources Research*, 36(1):119–134.

de Anna, P., Dentz, M., Tartakovsky, A., and Borgne, T. L. (2014a). The filamentary structure of mixing fronts and its control on reaction kinetics in porous media flows. *Geophysical Research Letters*.

de Anna, P., Jimenez-Martinez, J., Tabuteau, H., Turuban, R., Borgne, T. L., Derrien, M., and Méheust, Y. (2014b). Mixing and reaction kinetics in porous media: An experimental pore scale quantification. *Environmental Science & Technology*, 48(1):508–516.

de Anna, P., Le Borgne, T., Dentz, M., Bolster, D., and Davy, P. (2011). Anomalous kinetics in diffusion limited reactions linked to non-gaussian concentration probability distribution function. *The Journal of Chemical Physics*, 135(17):174104.

Dentz, M., Borgne, T. L., Englert, A., and Bijeljic, B. (2011a). Mixing, spreading and reaction in heterogeneous media: A brief review. *Journal of Contaminant Hydrology*, 120-121:1–17.

Dentz, M. and Carrera, J. (2007). Mixing and spreading in stratified flow. *Physics of Fluids*, 19(1):017107.

Dentz, M., Gouze, P., and Carrera, J. (2011b). Effective non-local reaction kinetics for transport in physically and chemically heterogeneous media. *Journal of Contaminant Hydrology*, 120-121:222–236.

Ding, D., Benson, D. A., Paster, A., and Bolster, D. (2013). Modeling bimolecular reactions and transport in porous media via particle tracking. *Advances in Water Resources*, 53:56–65.

Duplat, J., Innocenti, C., and Villermaux, E. (2010). A nonsequential turbulent mixing process. *Physics of Fluids*, 22(3):035104.

Duplat, J. and Villermaux, E. (2008). Mixing by random stirring in confined mixtures. *Journal of Fluid Mechanics*, 617:51.

Edery, Y., Dror, I., Scher, H., and Berkowitz, B. (2015). Anomalous reactive transport in porous media: Experiments and modeling. *Physical Review E*, 91(5):052130.

Edery, Y., Scher, H., and Berkowitz, B. (2009). Modeling bimolecular reactions and transport in porous media. *Geophysical Research Letters*, 36(2):n/a–n/a.

Edery, Y., Scher, H., and Berkowitz, B. (2010). Particle tracking model of bimolecular reactive transport in porous media. *Water Resources Research*, 46(7):n/a–n/a.

Fendorf, S., Jardine, P. M., Patterson, R. R., Taylor, D. L., and Brooks, S. C. (1999). Pyrolusite surface transformations measured in real-time during the reactive transport of co (ii) edta2-. *Geochimica et Cosmochimica Acta*, 63(19-20):3049–3057.

Fernàndez-Garcia, D. and Sanchez-Vila, X. (2011). Optimal reconstruction of concentrations, gradients and reaction rates from particle distributions. *Journal of Contaminant Hydrology*, 120-121:99–114.

Garg, R., Nair, S., and Bhaskarwar, A. N. (2000). Mass transfer with instantaneous chemical reaction in finite gas–liquid systems. *Chemical Engineering Journal*, 76(2):89–98.

Gérard, T. and De Wit, A. (2009). Miscible viscous fingering induced by a simple a+ b c chemical reaction. *Physical Review E*, 79(1):016308.

Gillespie, D. T. (2000). The chemical langevin equation. *The Journal of Chemical Physics*, 113(1):297–306.

Gjetvaj, F., Russian, A., Gouze, P., and Dentz, M. (2015). Dual control of flow field heterogeneity and immobile porosity on non-f ickian transport in b erea sandstone. *Water Resources Research*, 51(10):8273–8293.

Gramling, C. M., Harvey, C. F., and Meigs, L. C. (2002). Reactive transport in porous media: a comparison of model prediction with laboratory visualization. *Environmental Science & Technology*, 36(11):2508–2514.

Haber, S. and Mauri, R. (1988). Lagrangian approach to time-dependent laminar dispersion in rectangular conduits. part 1. two-dimensional flows. *Journal of Fluid Mechanics*, 190:201–215.

Hansen, S. K., Scher, H., and Berkowitz, B. (2014). First-principles derivation of reactive transport modeling parameters for particle tracking and pde approaches. *Advances in Water Resources*, 69:146–158.

Hess, K. M., Davis, J. A., Kent, D. B., and Coston, J. A. (2002). Multispecies reactive tracer test in an aquifer with spatially variable chemical conditions, cape cod, massachusetts: Dispersive transport of bromide and nickel. *Water Resources Research*, 38(8).

Hornof, V. and Baig, F. (1995). Influence of interfacial reaction and mobility ratio on the displacement of oil in a hele-shaw cell. *Experiments in Fluids*, 18(6):448–453.

Jiménez-Martínez, J., de Anna, P., Tabuteau, H., Turuban, R., Borgne, T. L., and Méheust, Y. (2015). Pore-scale mechanisms for the enhancement of mixing in unsaturated porous media and implications for chemical reactions. *Geophysical Research Letters*, 42(13):5316–5324.

Kang, K. and Redner, S. (1985). Fluctuation-dominated kinetics in diffusion-controlled reactions. *Physical Review A*, 32(1):435.

Kapoor, V., Gelhar, L. W., and Miralles-Wilhelm, F. (1997). Bimolecular second-order reactions in spatially varying flows: Segregation induced scale-dependent transformation rates. *Water Resources Research*, 33(4):527–536.

Kapoor, V., Jafvert, C. T., and Lyn, D. A. (1998). Experimental study of a bimolecular reaction in Poiseuille flow. *Water Resources Research*, 34(8):1997–2004.

Kitanidis, P. K. (1988). Prediction by the method of moments of transport in a heterogeneous formation. *Journal of Hydrology*, 102(1-4):453–473.

Koyaguchi, T. and Woods, A. W. (1996). On the formation of eruption columns following explosive mixing of magma and surface-water. *Journal of Geophysical Research: Solid Earth*, 101(B3):5561–5574.

Le Borgne, T., Dentz, M., and Villermaux, E. (2013). Stretching, coalescence, and mixing in porous media. *Physical Review Letters*, 110(20):204501.

Lee, K. and Chrysikopoulos, C. (1995). Numerical modeling of three-dimensional contaminant migration from dissolution of multicomponent napl pools in saturated porous media. *Environmental Geology*, 26(3):157–165.

Li, L., Peters, C. A., and Celia, M. A. (2006). Upscaling geochemical reaction rates using pore-scale network modeling. *Advances in Water Resources*, 29(9):1351–1370.

Luo, J., Dentz, M., Carrera, J., and Kitanidis, P. (2008). Effective reaction parameters for mixing controlled reactions in heterogeneous media. *Water Resources Research*, 44(2).

Mariani, M., Labas, M., Brandi, R., Cassano, A., and Zalazar, C. (2010). Degradation of a mixture of pollutants in water using the UV/H2O2 process. *Water Science and Technology*, 61(12):3026–3032.

Meunier, P. and Villermaux, E. (2010). The diffusive strip method for scalar mixing in two dimensions. *Journal of Fluid Mechanics*, 662:134–172.

Monson, E. and Kopelman, R. (2004). Nonclassical kinetics of an elementary A + B $\rightarrow$ C reaction-diffusion system showing effects of a speckled initial reactant distribution and eventual self-segregation: Experiments. *Physical Review E*, 69(2):021103.

Mostaghimi, P., Bijeljic, B., Blunt, M., et al. (2012). Simulation of flow and dispersion on pore-space images. *SPE Journal*, 17(04):1–131.

Najafi, H. S. and Hajinezhad, H. (2008). Solving one-dimensional advection-dispersion with reaction using some finite-difference methods. *Applied Mathematical Sciences*, 2(53):2611–2618.

Oates, P. M. and Harvey, C. F. (2006). A colorimetric reaction to quantify fluid mixing. *Experiments in Fluids*, 41(5):673–683.

Oosterlaken-Dijksterhuis, M. A., van Eijk, M., van Golde, L. M., and Haagsman, H. P. (1992). Lipid mixing is mediated by the hydrophobic surfactant protein sp-b but not by sp-c. *Biochimica et Biophysica Acta (BBA)-Biomembranes*, 1110(1):45–50.

Ovchinnikov, A. and Zeldovich, Y. B. (1978). Role of density fluctuations in bimolecular reaction kinetics. *Chemical Physics*, 28(1-2):215–218.

Paster, A., Aquino, T., and Bolster, D. (2015). Incomplete mixing and reactions in laminar shear flow. *Physical Review E*, 92(1):012922.

Paster, A., Bolster, D., and Benson, D. A. (2014). Connecting the dots: Semi-analytical and random walk numerical solutions of the diffusion–reaction equation with stochastic initial conditions. *Journal of Computational Physics*, 263:91–112.

Perez, L. J., Hidalgo, J. J., and Dentz, M. (2019a). Reactive random walk particle tracking and its equivalence with the advection-diffusion-reaction equation. *Water Resources Research*, 55(1):847–855.

Perez, L. J., Hidalgo, J. J., and Dentz, M. (2019b). Upscaling of mixing-limited bimolecular chemical reactions in poiseuille flow. *Water Resources Research*, 55(1):249–269.

Petrungaro, G., Morelli, L. G., and Uriu, K. (2018). Information flow in the presence of cell mixing and signaling delays during embryonic development. In *Seminars in cell & developmental biology*. Elsevier.

Pogson, M., Smallwood, R., Qwarnstrom, E., and Holcombe, M. (2006). Formal agent-based modelling of intracellular chemical interactions. *Biosystems*, 85(1):37–45.

Pollock, D. W. (1988). Semianalytical computation of path lines for finite-difference models. *Ground Water*, 26(6):743–750.

Porta, G., Thovert, J.-F., Riva, M., Guadagnini, A., and Adler, P. (2012a). Microscale simulation and numerical upscaling of a reactive flow in a plane channel. *Physical Review E*, 86(3):036102.

Porta, G. M., Riva, M., and Guadagnini, A. (2012b). Upscaling solute transport in porous media in the presence of an irreversible bimolecular reaction. *Advances in Water Resources*, 35:151–162.

Puyguiraud, A., Gouze, P., and Dentz, M. (2019). Stochastic dynamics of lagrangian pore-scale velocities in three-dimensional porous media. *Water Resources Research*, 55(2):1196–1217.

Rahbaralam, M., Fernàndez-Garcia, D., and Sanchez-Vila, X. (2015). Do we really need a large number of particles to simulate bimolecular reactive transport with random walk methods? a kernel density estimation approach. *Journal of Computational Physics*, 303:95–104.

Raje, D. S. and Kapoor, V. (2000). Experimental study of bimolecular reaction kinetics in porous media. *Environmental Science & Technology*, 34(7):1234–1239.

Ranz, W. E. (1979). Applications of a stretch model to mixing, diffusion, and reaction in laminar and turbulent flows. *AIChE Journal*, 25(1):41–47.

Renard, F., Gratier, J.-P., Ortoleva, P., Brosse, E., and Bazin, B. (1998). Self-organization during reactive fluid flow in a porous medium. *Geophysical Research Letters*, 25(3):385–388.

Risken, H. (1996). *The Fokker-Planck Equation*. Springer Heidelberg New York.

Roberts, P. V., Goltz, M. N., and Mackay, D. M. (1986). A natural gradient experiment on solute transport in a sand aquifer: 3. retardation estimates and mass balances for organic solutes. *Water Resources Research*, 22(13):2047–2058.

Rolle, M., Eberhardt, C., Chiogna, G., Cirpka, O. A., and Grathwohl, P. (2009). Enhancement of dilution and transverse reactive mixing in porous media: Experiments and model-based interpretation. *Journal of Contaminant Hydrology*, 110(3):130–142.

Salamon, P., Fernàndez-Garcia, D., and Gómez-Hernández, J. J. (2006). A review and numerical assessment of the random walk particle tracking method. *Journal of Contaminant Hydrology*, 87(3-4):277–305.

Sanchez-Vila, X., Fernàndez-Garcia, D., and Guadagnini, A. (2010). Interpretation of column experiments of transport of solutes undergoing an irreversible bimolecular reaction using a continuum approximation. *Water Resources Research*, 46(12).

Savitzky, A. and Golay, M. J. (1964). Smoothing and differentiation of data by simplified least squares procedures. *Analytical Chemistry*, 36(8):1627–1639.

Schmidt, M. J., Pankavich, S., and Benson, D. A. (2017). A kernel-based lagrangian method for imperfectly-mixed chemical reactions. *Journal Computational Physics*, 336:288–307.

Serrano, A. G. and Pérez-Gil, J. (2006). Protein–lipid interactions and surface activity in the pulmonary surfactant system. *Chemistry and Physics of Lipids*, 141(1):105–118.

Simoni, M. D., Sanchez-Vila, X., Carrera, J., and Saaltink, M. W. (2007). A mixing ratios-based formulation for multicomponent reactive transport. *Water Resources Research*, 43(7).

Sole-Mari, G. and Fernàndez-Garcia, D. (2018). Lagrangian modeling of reactive transport in heterogeneous porous media with an automatic locally adaptive particle support volume. *Water Resources Research*.

Steefel, C., Depaolo, D., and Lichtner, P. (2005). Reactive transport modeling: An essential tool and a new research approach for the earth sciences. *Earth and Planetary Science Letters*, 240(3-4):539–558.

Steefel, C. I. and Lasaga, A. C. (1994). A coupled model for transport of multiple chemical species and kinetic precipitation/dissolution reactions with application to reactive flow in single phase hydrothermal systems. *American Journal of Science*, 294(5):529–592.

Tartakovsky, A., Tartakovsky, G., and Scheibe, T. (2009). Effects of incomplete mixing on multicomponent reactive transport. *Advances in Water Resources*, 32(11):1674–1679.

Taylor, G. (1953). Dispersion of soluble matter in solvent flowing slowly through a tube. In *Proceedings of the Royal Society of London A: Mathematical, Physical and Engineering Sciences*, volume 219, pages 186–203. The Royal Society.

Van Loon, L. and Glaus, M. (1997). Review of the kinetics of alkaline degradation of cellulose in view of its relevance for safety assessment of radioactive waste repositories. *Journal of Environmental Polymer Degradation*, 5(2):97–109.

Villermaux, E. (2012). Mixing by porous media. *Comptes Rendus Mécanique*, 340(11-12):933–943.

Villermaux, E. and Duplat, J. (2003). Mixing as an aggregation process. *Physical Review Letters*, 91(18):184501.

Weller, H. G., Tabor, G., Jasak, H., and Fureby, C. (1998). A tensorial approach to computational continuum mechanics using object-oriented techniques. *Computers in Physics*, 12(6):620–631.

Willingham, T. W., Werth, C. J., and Valocchi, A. J. (2008). Evaluation of the effects of porous media structure on mixing-controlled reactions using pore-scale modeling and micromodel experiments. *Environmental Science & Technology*, 42(9):3185–3193.

Willmann, M., Carrera, J., Sanchez-Vila, X., Silva, O., and Dentz, M. (2010). Coupling of mass transfer and reactive transport for nonlinear reactions in heterogeneous media. *Water Resources Research*, 46(7):n/a–n/a.

Wintsch, R., Christoffersen, R., and Kronenberg, A. (1995). Fluid-rock reaction weakening of fault zones. *Journal of Geophysical Research: Solid Earth*, 100(B7):13021–13032.

Zhang, Y., Papelis, C., Sun, P., and Yu, Z. (2013). Evaluation and linking of effective parameters in particle-based models and continuum models for mixing-limited bimolecular reactions. *Water Resources Research*, 49(8):4845–4865.

Zhou, J., Qian, S., Ye, G., Copuroglu, O., van Breugel, K., and Li, V. C. (2012). Improved fiber distribution and mechanical properties of engineered cementitious composites by adjusting the mixing sequence. *Cement and Concrete Composites*, 34(3):342–348.